FINAL TECHNICAL REPORT

CONTRACT NO. NAS8-21067

# EXPERIMENTAL ANALYSIS OF LOW PROFILE FLANGE CONNECTIONS



By

W. K. Kubitza

and

G. L. Hearne

Prepared for

National Aeronautics and Space Administration
George C. Marshall Space Flight Center
Huntsville, Alabama

Research Institute, University of Alabama in Huntsville
Huntsville, Alabama

March, 1969

FINAL TECHNICAL REPORT

CONTRACT NO. NAS8-21067

# EXPERIMENTAL ANALYSIS OF LOW PROFILE FLANGE CONNECTIONS

By

W. K. Kubitza

and

G. L. Hearne

Prepared for

National Aeronautics and Space Administration
George C. Marshall Space Flight Center
Huntsville, Alabama

Research Institute, University of Alabama in Huntsville
Huntsville, Alabama

March, 1969

# EXPERIMENTAL ANALYSIS OF LOW PROFILE FLANGE CONNECTIONS

By

W. K. Kubitza

and

G. L. Hearne

Research Institute, University of Alabama in Huntsville

Huntsville, Alabama

## ABSTRACT

A comprehensive experimental investigation of a low profile bolted flange connection is described. The investigation includes a qualitative examination of surface stresses using brittle lacquer and photoreflective techniques, a three-dimensional photoelastic analysis of an epoxy model using the stress-freezing method, and a strain gage analysis at selected points on the model. The techniques employed for casting and fabrication of the model are described in some detail. The experimental results are compared with theoretical values calculated for both the flange and adjacent pipe section, and in general, show good agreement.

The conclusion reached is that the low profile flange is a basically sound design, showing very low levels of stress concentration, except in the areas immediately beneath the bolt heads. The combination of flange depth and bolt spacing used, provide an even distribution of stress at the flange to gasket interface. The design and flexibility of the gasket are found to have a significant effect on the stress distribution in both the flange and pipe sections.

TABLE OF CONTENTS

TABLE OF CONTENTS (Concluded)

LIST OF ILLUSTRATIONS

LIST OF ILLUSTRATIONS (CONT.)

## DEFINITION OF SYMBOLS

| Symbol | | Definition | |
|---|---|---|---|
| $\tau_{max}$ | = | Maximum shear stress | (psi) |
| p, q | = | Secondary principal stresses | (psi) |
| n | = | Fringe order | |
| F | = | Model stress fringe value | (psi/fringe) |
| E | = | Youngs modulus | (psi) |
| $M_o$ | = | Discontinuity moment | (lb in/in) |
| $V_o$ | = | Discontinuity shear | (lb/in) |
| $M_x$ | = | Bending moment | (lb in/in) |
| $V_x$ | = | Shear force | (lb/in) |
| $S_1$ | = | Meridional stress | (psi) |
| $S_2$ | = | Hoop stress | (psi) |
| $\beta$ | = | $\sqrt[4]{\frac{3(1-\nu^2)}{r^2 \tau^2}}$ | (1/in) |
| $\epsilon_1$ | = | Meridional strain | (in/in) |
| $\epsilon_2$ | = | Hoop strain | (in/in) |
| P | = | Internal pressure | (psi) |
| a | = | Inner flange radius | (in) |
| b | = | Outer flange radius | (in) |
| r | = | Radius of any fiber of ring | (in) |
| h | = | Flange height | (in) |
| w | = | Flange width | (in) |
| R | = | Radius to centroid of flange | (in) |
| D | = | $\frac{E \tau^3}{12(1-\nu^2)}$ | (lb in) |
| $\tau$ | = | Thickness | (in) |
| $\delta$ | = | Deflection | (in) |
| $\theta$ | = | Slope | vadians |

# EXPERIMENTAL ANALYSIS OF LOW PROFILE FLANGE CONNECTIONS

## SUMMARY

The low profile flange was developed at the George C. Marshall Space Flight Center to withstand the severe conditions of space flight, and by an improved distribution of material, to provide a higher strength-to-weight ratio than is found in conventional pipe flanges.

This report describes an experimental investigation of a low profile flange, including a qualitative examination of stresses in the model assembly using brittle lacquer and the photoreflective technique, electric resistance strain gage measurements at selected points on an epoxy model and a three-dimensional photoelastic analysis using the stress-freezing method. A description of the technique for casting and assembling the model is given. The results obtained during the experimental investigation are compared with theoretical stresses calculated in the appendices.

Based on the results of this investigation it is concluded that the low profile flange is a basically sound design, showing low levels of stress concentration except in the area immediately below the flange bolt heads. Flange depth and bolt spacing are sufficient to provide an even distribution of stress at the flange-to-gasket interface. The geometric design and the flexibility of the gasket have a significant effect on the stress distribution in both the flange and the pipe section.

Stress concentrations under the bolt heads of the flange connection could be reduced by shaped washers or separate bolting rings.

# I. INTRODUCTION

The low profile flange connection was developed at the Marshall Space Flight Center, primarily to meet the special requirements of space flight vehicles. The structural integrity of these flange connections, under the extreme conditions of temperature, pressure, and vibration, is of vital importance to the successful completion of space missions.

Analytical methods are available to predict the stress levels in the cylindrical shell elements adjacent to the flanges. These are generally of the linear discontinuity type, using combinations of idealized ring and shell elements. Although such methods are adequate for design purposes, they do not indicate the location and magnitude of areas of high stress concentration. Furthermore, it is extremely difficult to predict the three dimensional state of stress at points within the flange cross section in the presence of bolt holes and their spot facings and the influence of the joint gasket. Although these stress concentrations may not cause immediate failure of the component, they may initiate fatigue cracks.

The experimental program reported in this paper has the following objectives: (a) To provide a qualitative investigation of the surface stresses and stress concentrations in a scale model of the flange connection. The information gained from this study will be used to locate electrical resistance strain gages, and to indicate areas requiring a more detailed examination in subsequent tests. (b) To conduct a three-dimensional photoelastic investigation of the scale model, using the stress-freezing technique. This investigation will be used to evaluate the stresses caused by internal pressure and flange bolt assembly loads at preselected points in the model and to evaluate areas of high stress concentration. (c) To determine the magnitude of internal and external surface stresses using electrical strain gages. The measured strains will be used to establish a check and correlation of the stresses found by the photoelastic analysis. (d) To compare the experimental results with available analytical methods for bolted flange connections.

A detailed description of the model casting and fabrication techniques is given in the hope that it will be of use in future investigations of this type.

# II. CASTING MOLD

The casting mold was made in four separate parts (Ref. Figure 1): (a) A cylindrical outer section, (b) a central metallic core, (c) a circular base plate, and (d) a flexible sleeve. The thick walled cylindrical outer section, which was machined from 2024-T4 aluminum, has an inside profile contoured to form the outside surface of the model. The hollow cylindrical central core has a slight taper on the inside diameter to facilitate easy separation from the flexible sleeve. This is also

machined from 2024-T4 aluminum. The base plate was made from 3/4 in. thick aluminum and has concentric grooves machined in order to receive and accurately locate the inner and outer sections of the mold.

The flexible sleeve was cast in a mold (Ref. Figure 2) from Dow Corning Silastic RTV 501 and fits over the central core. This sleeve forms the inside contour of the model and accommodates the shrinkage of the Epoxy resin that occurs during the polymerizing cycle. The dimensions of the casting mold and the mold used for casting the flexible sleeve are given in Figures 3 and 4 respectively.

### A. Preparation of Mold for Casting

All extraneous material was removed from the mold components, and the contact surfaces carefully cleaned with acetone. All surfaces which come in contact with the liquid casting material were then coated with a thin film of silicon grease. This serves the dual purpose of acting as a mold release agent and a final seal between the mold components and the base plate. The mold components were assembled, as shown in Figure 1, using a generous amount of silicon grease in the base-plate grooves. As a final precaution, a thin film of grease was applied to the junction of the mold components and the base-plate. This same procedure was followed for each new casting.

## III. MODEL MATERIALS

### A. Solithane 113

Solithane 113 is a soft urethane rubber material which has a high photoelastic sensitivity, and a very low modulus of elasticity. The material exhibits little mechanical or optical creep, and time-edge effects are negligible. Consequently, models may be stored for many years. It is easily cast, but machining at room temperature presents some problems because of the distortion under very low cutting forces. An acceptable finish may be obtained using high speed routing equipment but other machining operations require that the material be frozen at liquid nitrogen temperatures to obtain dimensional accuracy. This material was selected as being the most suitable for the qualitative and quantitative investigation of surface stresses, using the brittle laquer and photoreflective techniques. A mixture of equal parts of resin and catalyst were used in this application giving the following properties:

Young's Modulus 450-600 psi
Material Fringe Value 0.9 psi/fringe
Poisson's Ratio 0.46

### B. Epoxy Resins

In recent years epoxy resins have become the predominant material for two and three dimensional photoelastic stress analysis. They possess a number of important advantages

over other polymeric materials. The chemical reaction between the basic resin and the curing agent converts the basic resin into a chemically and mechanically strong polymer by building the largest possible molecular units.

The material is readily cast, and machined preferably with carbide tipped tools. Complicated models may be assembled by bonding several cast or machined components together. Photoelastic sensitivity is good and the figure of merit is high. The time edge effects exhibited by most epoxies can be eliminated by storage for a short period of time at constant humidity. Shrinkage occurring during polymerization is small and uniform, and the exothermic reaction during gelation is very mild.

Reference 1 contains a comprehensive investigation of the photoelastic properties of epoxy resins using both acid anhydride and amine curing agents. From the results of this investigation, it is concluded that the photoelastic properties of the polymerized resins are virtually independent of the basic epoxy , but depend, to a large extent, on the amount and type of curing agent used. Furthermore, the acid anhydride curing agents are considered to yield a superior photoelastic material. Two combinations of resin and hardener were used in the present investigation. They are as follows:

| | |
|---|---|
| Epoxy No. 1 | 100 parts by weight---ERL 2774 Resin |
| | 42 parts by weight---Phthalic Anhydride |
| | 20 parts by weight---Hexahydrophthalic Anhydride |

The addition of the HEX-anhydride to the mix reduces the degree of exothermic reaction, thereby retarding the gelation rate and reducing casting stresses. This slow gelation rate allows entrapped air bubbles more opportunity to escape. The range of frozen stress properties given in Reference 1 for this mixture is:

| | |
|---|---|
| Critical temperature | $T_{cr} = 162^{\circ} - 175^{\circ}$ C |
| Youngs Modulus | $E_{eff} = 5,300 - 6,500$ psi |
| Material Fringe Value | $f_{eff} = 2.48 - 2.84$ psi/fringe/in |
| Figure of Merit | $Q = 2,100 - 2,450$ |

The following weights of material were sufficient to make one casting and produce enough additional resin to make a calibration specimen:

| | |
|---|---|
| ERL 2774 Resin | 3.945 lb. |
| Phthalic Anhydride Flakes | 1.661 lb. |
| HEX - Anhydride | 0.782 lb. |

The first investigations were carried out with models cast from Epoxy No. 1. They revealed several disadvantages of having to work at the rather high critical temperature of 175°C. The performance of a carefully executed stress-freezing cycle required almost 14 days since the heating and cooling rate must not exceed 1.5°C/hour. At this critical temperature, it is very difficult to perform any necessary adjustments on the model should a leak occur. Beyond that, gasket

material and the pressurizing fluid showed signs of degradation. A search was conducted for another epoxy with a lower critical temperature, but with equally satisfactory photoelastic characteristics. This material is designated as Epoxy No. 2.

C. Epoxy No. 2 Consists of 50 parts by weight---ERL 2774 Resin
50 parts by weight---ERL 2795 Resin
20 parts by weight---ZZL 0803 Hardener

The range of frozen stress properties given in Reference 2 for this mixture are:

| | |
|---|---|
| Critical Temperature | 74° - 79° C |
| Youngs Modulus | 1770-2, 100 psi |
| Material Fringe Value | 1.43 - 1.50 psi/in/fringe |
| Figure of Merit | 1240 - 1400 |

The following weights of material were sufficient to make two castings and several calibration specimens:

| | |
|---|---|
| ERL 2774 Resin | 6.0 lb. |
| ERL 2795 Resin | 6.0 lb. |
| ZZL 0803 Hardener | 1.5 lb. |

D. Adhesives

Since it was decided to cast the model elements to final form in order to minimize machining, a suitable adhesive had to be selected to cement the elements together so that the assembly could be subjected to the stress-freezing cycle. For this purpose, a cement had to be found which maintained its strength at elevated temperatures. Since a good dependable cement has proven to be of critical importance in stress-freezing work, a number of recommended adhesives were tested for a strength of 60 psi at temperatures up to 5° C above the critical temperature of 165° C. Eastman 910 and W. T. Bean BAP-1 and BR-600 which were recommended as high temperature strain gage cements failed to satisfy the requirements. Stycast 2651, an Emerson & Cumming, Inc. product, maintained the required strength at 170°C, but because it is available only as a black epoxy, it could not be used where its presence interferred with optical requirements. The most satisfactory results were obtained with the clear BR-104 strain gage adhesive which was recently brought on the market by W. T. Bean. It was used whenever a clear joint was desirable.

## IV. CASTING PROCEDURES

A. Solithane 113

At room temperature the basic resin is too viscous for convenient handling. It is, therefore, necessary to heat the resin and catalyst. Equal quantities of Solithane 113 resin and C 113-300 catalyst were carefully measured and heated individually to a temperature of 65° C. This temperature was sufficient to reduce the viscosity for

easy pouring without fear of degradation of the basic materials. The heated catalyst was then added to the Solithane resin and the mixture stirred vigorously for approximately three minutes. The stirring action entrapped large quantities of air and it was therefore necessary to degas the mixture before casting. This was accomplished by placing the mixture under a large bell jar and applying a vacuum for approximately 15 minutes until most of the entrapped air had been forced to the surface.

The mixture was immediately cast into the prepared mold, which had previously been placed in the constant temperature cabinet, in order to prevent sudden cooling of the material when it comes in contact with the mold. The temperature in the cabinet was slowly raised to 80° C and allowed to remain at this temperature for a period of twelve hours to complete the polymerization.

B. Epoxy No. 1

The assembled mold was placed in a constant temperature cabinet and leveled to insure an even filling. The temperature in the cabinet was slowly raised to 92° C before the casting mixture was poured into the mold. A carefully measured quantity of ERL 2774 resin was poured into a steel container, and the temperature was raised to 120° C. At the same time, the HEX anhydride was heated above its melting point (75° C) to 100° C and was poured into the resin. The phthalic anhydride flakes, which had been preheated to approximately 92° C, were added to the mixture. The mixture was then thoroughly stirred and heated to a temperature of 115° C until all ingredients had dissolved. Protective masks were worn during this operation to avoid inhalation of the noxious fumes given off by the mixture.

The dissolved mixture was poured into the mold using a length of preheated rubber tubing, and all visible air bubbles were allowed to escape to the surface. The casting was then allowed to gel for a period of two days at a temperature of 92° C. During this gelation period the temperature was held within ± 1° C to avoid precipitation of the anhydrides or highly exothermic reactions. After initial gelation the temperature was slowly raised to 100° C and then slowly lowered to room temperature. The casting was then removed from the mold and placed in the oven. The oven temperature was raised to 100° C at the rate of 6° C per hour and then further increased to 150°C at 2° C per hour. The casting was held at this temperature for a period of eight days and then slowly cooled to room temperature to complete the polymerization. This very slow rate of temperature increase and decrease is necessary to prevent thermal residual stresses in the casting and to avoid cracking of the casting.

C. Epoxy No. 2

The carefully measured quantities of ERL 2774 and ERL 2795 resin were placed in separate containers and heated to a temperature of 60° C. At this temperature the two resins were mixed, thoroughly stirred, and deaerated using a bell jar and vacuum pump. The mixture was then cooled to 32° C by partially immersing the container in a bath of iced water. During this operation the mixture was again stirred to ensure even cooling.

The ZZL 0803 hardener was slowly heated to a temperature of 32° C and carefully added to the resin. The resulting mixture was thoroughly stirred and de-aerated The two molds were partially immersed in a water bath which had been placed in the constant temperature cabinet. The molds were leveled to ensure an even filling, and water was added to the hollow core of the mold. The water bath provided a heat sink to absorb the exotherm from the epoxy and maintain an even temperature distribution.

The prepared epoxy was then cast into the molds and kept at a temperature of 32° C for a period of 48 hours. At this stage the epoxy has the consistency of a hard rubber and must be kept in the mold to avoid distortion during the second phase of polymerization. For the second phase, the complete molds were transferred to the stress-freezing oven and the temperature raised to 76° C at a rate of 2.5°C per hour. The molds were held at this temperature for a period of 72 hours and then slowly brought down to room temperature at a rate of 1°C per hour. The models were easily separated from the molds.

Subsequent examination of the models revealed some residual stresses. These appeared in several small regions of the model and seem to have been caused by adhesion of the model and mold and resulted from irregularities in the parting compound film. The unavoidable creep during the polymerization process then induced the local casting stresses.

## V. ASSEMBLY OF EPOXY MODELS

The mating flanges of all castings were machined square, and 18 equally spaced 5/16 in. dia. holes were drilled on a 9.812 pitch circle diameter. All holes were spotfaced 19/32 in. dia. to insure good bolt seating. The ends of the cylindrical sections of both the upper casting and end closure were machined square, and two shallow concentric grooves were cut on one edge to form a glue trap at the mating surface. A 1/16 in. deep rebate was machined on the end closure plate for the lower half of the model. This rebate accurately located the endplate and provided a good bonding surface.

The RB 104 adhesive and hardener were prepared and mixed according to the manufacturer's instructions. The bonding surfaces were lightly roughened using a coarse abrasive cloth and then thoroughly cleaned with acetone. An even coating of cement was applied to both the upper casting and the end closure sections. The cylinderical sections were carefully brought together starting at one point and gradually closing the joint until the complete circumference was in contact. This procedure minimized the entrapment of air bubbles. A similar procedure was followed in bonding the closure endplates to the model assembly. The assemblies were placed in the constant temperature cabinet, and curing of the adhesive was completed.

The flange gasket was made from 1/16 in. thick silicon rubber. This material was selected after tests had shown that Hysol rubber begins to melt under prolonged exposure

to the combined effects of compressive stress at the required temperature of 165°C. A pressure fitting was inserted in the top endplate as shown in Figure 5. A 3 in. wide strip of aluminum paint was applied to the inside of the model in the longitudinal direction, which enabled observations to be made during the test with the large field photostress meter.

A large weighted Solithane insert, covered with a curved aluminum plate, was placed inside the lower half of the model. The insert was intended to take up most of the volume, thereby reducing the amount of total energy stored in the compressed air during the test. The aluminum plate acted as a secondary reflector for observing photoelastic fringe patterns during the stress-freezing cycle by the reflective photoelasticity method. With the rubber gasket in place, the two parts of the model assembly were fastened together with 1/4 in. dia. steel bolts and helical coil springs as shown in Figure 6. The coil springs were used to apply an even, accurately measured bolt force to the flange connection. The force required to completely compress each spring was measured and the spring identified. The average closing force was found to be about 50 lb.

The assembled model was placed in a loading frame and a load of 42.5 lb. was applied to each bolt using a lever-and-weight jig. The applied load compressed the coil spring allowing the nut to be tightened by hand to take up the slack. Subsequent examination with the large field polariscope showed an even fringe pattern in the flange between each bolt. The model was connected to the air supply, and the bleed valve was closed. A pressure of 3 psi was applied, and the model was immersed in water to test for air leaks. Some very small leaks were noted at three of the bolt locations. It was considered that these leaks were relatively insignificant and that in all probability the slight softening of the gasket at the test temperature would preclude further leakage. The average flange contact stress due to a bolt load of 42.5 lb. is calculated at approximately 22 psi. The corresponding bolt load for the model cast from Epoxy 2 was 22 lb. per bolt and the contact stress was 11.35 psi.

## VI. SOLITHANE MODEL

After initial experimentation with models cast from Epoxy No. 1, it was found to be desirable to make exploratory investigations on a model which would respond to small internal pressure and permit experimentation at room temperature. This model was used to establish a satisfactory experimental procedure and check qualitatively the photoelastic response of the model to internal pressure and pressure from the connecting bolts simulating the conditions existing during the stress-freezing process.

### A. Systems Model

A complete model assembly consisting of three flange units and two end closure plates was cast from Solithane 113. The parts were cemented together using Solithane as the bonding material after all contact surfaces have been treated with emory cloth and thoroughly cleaned. A special jig was constructed for the machining of the flange

surfaces and for the drilling of the bolt holes in the flanges. This jig was necessary because the material deforms easily under the pressure of machining. The complete assembly is shown in Figure 6.

The initial experimentation was aimed at developing a functional pressurizing system to study the rate of pressure to be applied and the accuracy of controlling pressure during the period in which readings were taken. Several gasket materials were tried and their effect on the flange connection was investigated. When the flange connection was made by using 1/4 in. steel bolts and nuts, it was found difficult and time consuming to adjust the bolt tension evenly in all 18 bolts, since a small difference in the thread friction caused a significant difference in the pressure exerted on the flange. This difficulty was overcome by using spring-loaded bolts, which proved to be easy to adjust by means of a lever so that the same tension in each bolt could be measured. The final Solithane assembly was used without a gasket. Air tightness was achieved by applying a thin coat of silicon grease to the machined surfaces of the flanges. The internal pressure was held within 1 to 2 psi in order to prevent excessive deformations in the model.

B. Reflecting Polariscope

Experimentation with the Solithane model for the stress-freezing investigations proved particularly helpful since this material responds photoelastically at room temperature approximately in the manner as Epoxy 1 and Epoxy 2 at stress-freezing temperatures. By coating the inside surfaces with aluminum paint, the model could be observed with the reflective polariscope, and areas of probable stress concentrations and their fringe patterns could be evaluated at different internal pressures. Based on these studies, the internal pressure of 1.5 psi at stress-freezing temperatures for Epoxy 2 was selected to produce sufficiently clear fringe patterns without introducing large strains. The study also clearly showed that the influence of the bolt pressure on the flanges is limited to a zone of about 1-in. width in the adjoining pipe section.

C. Investigation by Stresscoat

Further use of this Solithane model was made by carrying out a stresscoat investigation. As shown in Figure 6 a part of the model was covered with a brittle coating. After hardening of the coating during a period of 20 hours, the assembly was pressurized in increments of 0.1 psi. The developing cracks were observed and etchant was applied to make the crack pattern visible, indicating the principal tensile stress directions for photographic recording.

D. Mechanical Strain Measurements

An attempt was made to make strain measurements with the Huggenberger extensometer at selected points and compare measured and computed strains. However, the results of these measurements were highly inaccurate because the pressure necessary to bring the extensometer in proper contact with the surface of

the model induced local deformations, which influenced the strain measurements and prevented accurate readings.

### E. Results

Although the investigations carried out were mostly exploratory, they showed satisfactory accord with the results obtained from the simplified numerical analysis. The stresscoat investigation clearly indicated the direction of maximum principal stress as shown in Figure 6. The first longitudinal crack appeared between 0.1 and 0.2 psi, and the complete pattern was developed between 0.5 and 0.7 psi. It will be noticed that in a narrow region approximately 1.5 in. from either flange, the pattern has a crazed appearance. This crazed pattern is caused by the bending that is occurring close to the flange.

## VII. STRAIN GAGE TEST OF EPOXY MODEL

### A. Model Assembly

Strain gages were applied to the upper half of the model in accordance with the manufacturer's recommended procedure using Eastman 910 cement. The gage locations are shown in Figure 7. A large Solithane insert was placed inside the lower half of the model prior to assembly to reduce the stored energy during the test. The upper and lower halves of the model were assembled using a 1/4 in. Hysol gasket and 18-1/4 in. diameter steel bolts. The assembled model was then connected to the air supply by an inlet control valve and a pressure gage. The strain gages were connected to a Budd switch and balance unit and a strain indicator. A diagram of the general arrangement is given in Figures 5 and 8.

### B. Pressure Test

The strain indicator was set for a quarter bridge circuit and a gage factor of 2.05. All gages were zeroed on the switch and balance unit allowing at least one minute for heating up the circuit. A pressure of 15 psi was applied to the model and held for a period of five minutes to allow for any creep in the epoxy material. A reading was taken of each gage in turn, again allowing a minute for heating of the circuit. The procedure was repeated for a pressure of 25 psi and all readings noted. The pressure was subsequently released and all zeroes checked.

### C. Flange Bolt Loading Test

Additional strain gages, numbers 19 and 20, were added to the upper half of the model. The locations are given in Figure 9. Each of the 1/4-in. diameter bolts was generously lubricated with silicon grease to insure an even friction during torquing. The model was then reassembled, using the 1/4-in. thick Hysol gasket and the bolts finger-tightened only.

The strain indicator was set for a quarter bridge circuit and a gage factor of 2.05. All gages were zeroed on the switch and balance unit, and one minute allowed for heating of the circuit. Bolt torques were applied using a sensitive torque wrench having a range of zero to 120 in-lb. A torque was applied to diametrically opposite bolts around the complete flange until each bolt showed an even torque of 10 in-lb. (equivalent to axial load of 258 lb.). A delay of five minutes was allowed before taking any readings to permit any creep to take place in either the epoxy model or the Hysol gasket. Readings were then taken of each gage in turn, allowing an interval of one minute between readings for heating of the circuit. The procedure was repeated for bolt torques of 20 and 40 in-lb. The bolt loads were subsequently released and the zeroes checked.

### D. Results

The measured strains and calculated stresses due to bolt loading and bolt loading with internal pressure are given in Figures 8 through 11. Plots of longitudinal and circumferential stress and strain versus distance from flange are given in Figures 11 through 17, and are compared with the theoretical values calculated in Appendix A. The results of the flange bolt loading test are given in Figure 9. Longitudinal and circumferential strains are plotted against distance from flange in Figures 18 and 19. Plots of flange strain versus bolt torque for gages 9 through 20 are given in Figures 20 and 21.

## VIII. EPOXY MODEL (STRESS FREEZING)

### A. The Test Set-Up

A diagram of the test set-up is shown in Figure 22. The air supply was connected by a rubber hose and a tee joint to a pressure accumulating cylinder and a mercury manometer. Air pressure was transmitted by stainless steel tubing from the accumulator outlet through the exhaust vent of the oven to a flexible pipe connected to the model. Hand operated valves were inserted in the system such that either the model or the air supply could be isolated. A special adaptor plate was made to close off the exhaust vent of the oven. All tube connections were checked for leakage, using either a soap solution or total immersion in water.

### B. Procedure

The assembled model was placed in the oven with the painted aluminum strip facing the observation window. The air supply was connected to the model and the bleed valve was closed. The connection was then checked for leakage. A folded metal sheet was placed around the model leaving just the region containing the painted strip exposed. This was done as a precaution to prevent uneven temperature distribution caused by the forced air circulation within the oven.

The oven was closed and the wide field reflection polariscope was placed opposite the observation window. The temperature in the oven was slowly raised at approximately 1.5° C/hour. The rate of change of the temperature is achieved by cam controlled program, which was designed for this requirement. The temperature was allowed to rise at this extremely low rate for approximately two days until the critical temperature of 175°C was reached. Observation with the reflection polariscope continued through the stress freezing process.

At the critical temperature the pressure was applied in the following manner: Valve "B" connecting the model to the pressure accumulator was closed, and valve "A" was opened. The pressure supply tap was opened until 0.5 psi registered on the manometer. Valve "A" was then closed, and valve "B" was slowly opened. The change in fringe pattern was observed in the cylindrical section of the model at a point approximately 1.5 in. below the glued joint. The color sequences were noted, and the fringe order was estimated. This procedure was repeated at 0.5 psi increments in five minute intervals until a maximum of 3 psi was reached.

At this time the temperature and pressure were held constant for a short period while the program cam was changed to reverse the temperature cycle. During this period, a sudden drop in pressure was observed, and subsequent examination revealed that this was caused by several large cracks in the model at the junction of the lower end plate and the cylinderical section. Two attempts were made at stress freezing using models cast from Epoxy No. 1, but both of these were abandoned when cracks appeared at or near discontinuities in the model.

At this point a search was conducted for an alternative epoxy material with a lower critical temperature, but with equally satisfactory photoelastic properties. A suitable material, designated Epoxy No. 2, was found (Ref. 2 and 3) which had double the sensitivity of Epoxy No. 1, and would, therefore, work at a much lower temperature and pressure to give the same results.

A similar test procedure was followed for the model cast from Epoxy No. 2. During this test the temperature was raised at the rate of 1°C/hour until the critical temperature of 75° was reached. At this point, the internal pressure was applied in increments of 0.5 psi to a maximum of 1.5 psi. The temperature and pressure were held steady for a period of four hours. At the end of this period, the program cam was reversed and the temperature lowered at approximately 0.6°C/hour until room temperature was reached. The pressure was held constant at 1.5 psi during the down cycle. At this point, the stress freezing oven was switched off, and examination with the wide field reflection polariscope confirmed that a successful stress freezing test had been achieved.

The model was then removed from the oven and disassembled. An examination of the model revealed no outward signs of cracking or excessive distortion. Eight slices were removed from the model. The location of these are given in Fig. 23. All slices were carefully sawed to a thickness of 7/16 in., and then the surfaces machined, using a fly-cutter to give a final thickness of 3/8 in. A thin film of silicon grease was applied

to the machined surfaces and the slice mounted in the polariscope. Photographs of the isochromatic patterns were taken using a Nikon "F" camera in conjunction with a telemicroscope.

C. Results

Figures 24 through 28 are photographs of the isochromatic fringe patterns obtained for the various slices, the locations of which are given in Figure 23. Figures 29 through 32 are drawings of these fringe patterns in which the fringe orders are identified. In most cases the fringe order was accurately determined by means of a frozen stress compensating strip.

The isochromatic fringes are directly proportional to the maximum shear stresses:

$$\tau_{max} = \frac{p - q}{2} = n F \quad \text{----------} \quad (1)$$

in which

$\tau_{max}$ = maximum shear stress

p, q = secondary principal stresses

n = fringe order

F = model stress - fringe value/psi/fringe

The differences of secondary principal stresses ( p - q ) are therefore obtained directly from the photoelastic fringe patterns, by placing a suitable grid overlay on the photograph and reading the fringe order at the various grid points. In order to complete the analysis and separate the stresses, values for the sum of the secondary principal stresses (p + q) must be established. In the case of free boundaries, for example, at the outside surface of the model, one of the stresses is zero; the other may be obtained directly from equation 1. For the remaining boundaries, the theoretical stresses apply. For example, at the inner boundary of slices 1 and 3, for internal pressure of 1.5 psi the stress optic law (equation 1) gives

$$p - (-1.5) = 2 n F$$

$$p = 2 n F - 1.5$$

and

$$p + q = (2 n F - 1.5) + (-1.5)$$

$$= 2 n F - 3.0.$$

Once the boundary values for each slice are determined, the value of (p + q) at the interior points are obtained by applying an iterative solution of the Laplace equation.

$$\frac{\partial^2 U}{\partial x^2} + \frac{\partial^2 U}{\partial y^2} = 0$$

Since there are a considerable number of interior points in the network, the evaluation becomes somewhat laborious and time consuming. A computer program was, therefore, written to perform the necessary iterations.

The values of $(p - q)$ and $(p + q)$, together with the separated principal stresses are given in Figures 33 through 46. Examination of the isochromatics for slice No. 7 shows a high stress gradient caused by the local bolt pressure. In this region, the mesh size was halved to give a more accurate determination of the stresses. These results are given in Figures 41 through 44.

For the evaluation of slices 1 and 3, which have curvilinear boundaries, it is convenient to use polar coordinates in place of the ordinary cartesian coordinates. The equations and calculations of the conformal transformation required are given in Appendix C.

Finally, Figure 47 is a side view of the flange, and shows the isochromatic fringe pattern between bolt holes due to bolt loading only. Although there is some distortion due to the curvature of the specimen, the photograph shows that the stress induced in the pipe section by the flange bolt loadings, is confined to about a 1-in. zone. The photograph also shows how the stress distribution in the flange beneath the bolt head spreads out to form a pressure cone.

# IX. DISCUSSION OF RESULTS

The results derived from the experimental investigation reflect the distribution stress and strain in the model which was designed to simulate the prototype flange connection. Although the overall dimensions of the model were chosen to be those of the prototype, some conditions of the prototype could be simulated only in a qualitative sense.

The most important of these conditions is the interaction between gasket and flange. The gasket material used in the model assembly was somewhat softer than the material of the flange, while in the prototype connection, gasket and flange material have about the same moduli of elasticity. The gasket of the model is flat and has the same width as the machined surface of the flange, while three different gasket configurations are in use for the prototype connections. The choice of material and form of the model gasket represents an economical compromise in an effort to simulate the prototype conditions.

A softer gasket permits a greater angular rotation of the flange under applied internal pressure and bolt load than would occur with a stiffer gasket material. On the other hand, a wide gasket will restrain the rotation of the flange more than an o-ring type gasket. These differences in form and material of the gasket will result in somewhat different stress distribution in the flange and the zone of the pipe adjoining the flange.

Another necessary compromise in the design of the model is the number of bolts used in the flange connection. The number chosen for the model was limited by the fact that the epoxy material is very brittle at room temperature, and did not allow a closer spacing of bolt holes without risking cracking of the model during machining operations, or employing special and costly machining procedures. The prototype with a greater number of bolt holes represents a less severe loading condition since the stress concentration in the flange immediately under the washer will be reduced and a more uniform stress distribution will result at the flange-gasket interface.

The experimental values of stresses and strains for the cylindrical section of the model obtained during the strain gage pressure test, are compared with the theoretical values calculated in Appendix A (Ref. Figures 12, 13, 15 and 16). The stresses and strains induced by the bolt loading are shown separately for comparison. The theoretical values do not include the influence of flange bolt loading, gasket deflection, and the stiffening effect of the fillet between flange and pipe section. The most significant of these factors appears to be the influence of the gasket, resulting in a reduction of the bending moment acting on the flange. The resulting internal longitudinal stress is higher and the external stress is lower than the theoretical stresses as shown in Figures 15 and 16. The corresponding circumferential stresses (Ref. Figures 14 and 17) are 25 to 30% higher than the theoretical values.

The initial tightening of the flange bolts causes a rotation of the flange which is resisted by the adjoining pipe section. This action induces local bending stresses in the pipe section (Ref. 18 and 19). The degree of bending will depend to a great extent on the dimensions of the flange, the fillet radius and the stiffness and configuration of the gasket. The rotation or rolling of the flange produces some bending in the plane of the flange as shown by gages No. 12 and 20.

In evaluating stresses and strains from isochromatic patterns, points in the flange are selected which are located in areas of maximum and minimum stress representing the upper and lower limits of stresses in the flange connection. Since these points are located in planes of symmetrical stress patterns, the secondary principal stresses obtained from the photoelastic stress evaluation have been used to describe the state of stress at these chosen points in the model.

The isochromatic fringe patterns obtained from the stress freezing experiment (Ref. Figures 24 through 28) clearly show the areas of stress concentration. They are mainly confined to the area adjacent to the flange bolt holes. The bolt holes in slices 1 and 3 (Ref. Figures 24 and 26) cause only minor local disturbances in the fringe patterns and their effect on the overall flange stress calculations may be neglected. The low stress concentration at the fillet between flange and pipe section (Ref. Figure 27) indicates that the fillet radius is adequate in providing a smooth transition from flange to pipe section. The major stress concentration in the flange is located immediately below the bolt head and the spot facing for the washer (Ref. Figure 28 and 47). The patterns show that the stresses induced by the bolt load rapidly spread out in the form of a pressure cone in the first half of the flange depth, resulting in a fairly uniform stress distribution at the flange-to-gasket contact surfaces.

A comparison of flange stresses obtained from the photoelastic evaluation of slices 1 and 3 (Ref. Figures 35 and 38) and those calculated in Appendix B indicates higher experimental stresses at the inner radius and lower stresses at the outer radius of the flange.

## X. CONCLUSIONS AND RECOMMENDATIONS

The casting technique and the assembly of the model described in this report gave satisfactory experimental results. However, a close control of the heating and cooling rates during casting and stress freezing and careful preparation of the mold before casting is necessary for obtaining stress-free castings.

Easier handling of the epoxy during casting, its lower critical temperature, and substantial saving of time during the polymerization and stress freezing cycle recommend Epoxy No. 2 as the most satisfactory material used for the fabrication of the photoelastic model.

The low profile flange is basically a sound design. The only significant stress concentrations were observed in the area immediately beneath the spot facing for the washers of the bolt heads. These stress concentrations could lead to problems in a fatigue environment but could be reduced by using either shaped washers or a separate bolting ring, which would make spot facing unnecessary. The depth of the flange and the bolt spacing provide an acceptable distribution of stress at the contact surface with the gasket.

The stiffening effect of the fillet between flange and pipe section cannot be accurately evaluated from this investigation. However, its size is sufficient to reduce the stress concentration in this transition zone. The geometric design and flexibility of the gasket has a significant effect on the stress distribution in both the flange and the adjoining pipe section.

Although a complete simulation of the prototype conditions was not attainable at reasonable costs, the results obtained in this investigation allow the conclusion that the low profile flange satisfies the structural requirements of a reliable flange connection.

Since the model dimensions are large compared to the deformations occurring under load, the scale effect is minimized, and the results of this investigation may be extrapolated for larger prototype dimensions. It is recommended that design tables or charts be developed to simplify the design of such flange connections.

# APPENDIX A

## MODEL IDEALIZATION FOR INFLUENCE COEFFICIENT PROGRAM

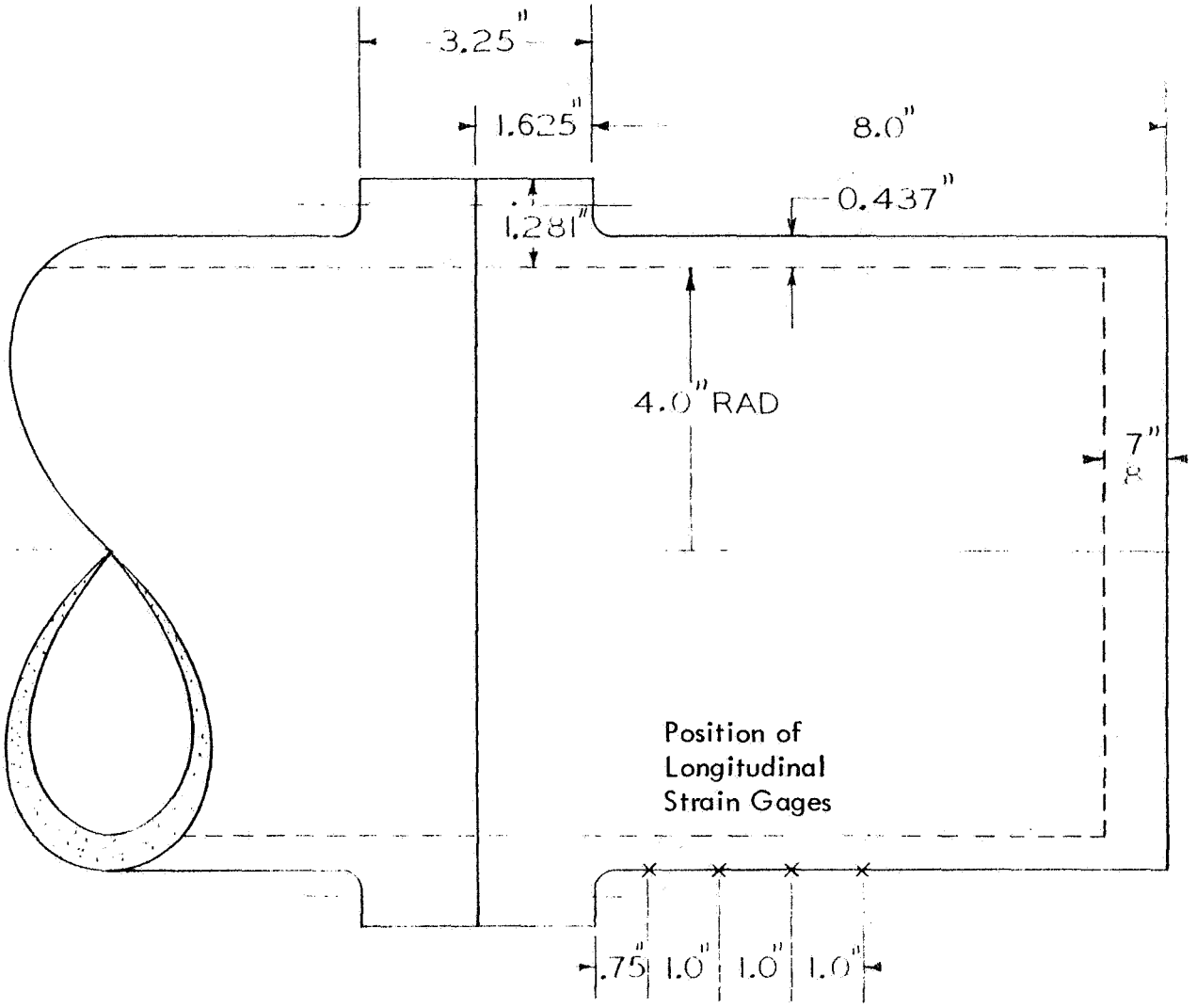


P = 100 Psi

E = 500 x $10^3$

$\mu$ = .35

Influence Coefficients For Long Cylinder

Input Data

Element Number = 1
Radius = 4.2180
Length = 7.5500
Thickness = 0.43700
E of Element = 0.50000 E 06
Poisson Ratio = 0.350
Option = 0

Beta*L - 2.*PI = 0.80026E 00

E Norm = 0.50000E 06
E Ratio = 0.10000E 01

Influence Coefficients Times E Norm

| | | | |
|---|---|---|---|
| 0.76394E 02 | 0.71673E 02 | 0.00000E 00 | 0.00000E 00 |
| 0.71673E 02 | 0.13448E 03 | 0.00000E 00 | 0.00000E 00 |
| 0.00000E 00 | 0.00000E 00 | -0.76394E 02 | 0.71673E 02 |
| 0.00000E 00 | 0.00000E 00 | 0.71673E 02 | -0.13448E 03 |

Influence Coefficients For Ring

Input Data

Element Number = 2
Radius at 0 = 4.21800
Radius at C = 4.64050
Radius at L = 4.21800
E0 = 1.62500
EL = 1.62500
Area = 4.16330
E = 0.50000E 06
Moment of Inertia = 3.66450

E Norm = 0.50000E 06
E Ratio = 0.10000E 01

Influence Coefficients Times E Norm

| | | | |
|---|---|---|---|
| 0.18806E 02 | 0.86798E 01 | 0.94032E 01 | -0.53414E 01 |
| 0.86798E 01 | 0.47014E 01 | 0.86798E 01 | -0.53414E 01 |
| -0.94032E 01 | -0.86798E 01 | -0.18806E 02 | 0.86798E 01 |
| 0.86798E 01 | 0.47014E 01 | 0.86798E 01 | -0.53414E 01 |

Influence Coefficients For Long Cylinder

Input Data

Element Number = 3
Radius = 4.2180
Length = 100.0000
Thickness = 0.43700
E of Element = 0.50000E 06
Poisson Ratio = 0.350
Option = 0

Beta* L - 2. * P I = 0.87537E 02

E Norm = 0.50000E 06
E Ratio = 0.10000E 01

Influence Coefficients Times E Norm

| | | | |
|---|---|---|---|
| 0.76394E 02 | 0.71673E 02 | 0.00000E 00 | 0.00000E 00 |
| 0.71673E 02 | 0.13448E 03 | 0.00000E 00 | 0.00000E 00 |
| 0.00000E 00 | 0.00000E 00 | -0.76394E 02 | 0.71673E 02 |
| 0.00000E 00 | 0.00000E 00 | 0.71673E 02 | -0.13448E 03 |

*Coefficient Matrix*

C ( 1, 1 ) = -0.95200E 02
C ( 2, 1 ) = 0.62993E 02
C ( 3, 1 ) = -0.94032E 01
C ( 4, 1 ) = 0.86798E 01

C ( 1, 2 ) = 0.62993E 02
C ( 2, 2 ) = -0.13919E 03
C ( 3, 2 ) = -0.86798E 01
C ( 4, 2 ) = 0.47014E 01

C ( 1, 3 ) = -0.94032E 01
C ( 2, 3 ) = -0.86798E 01
C ( 3, 3 ) = -0.95200E 02
C ( 4, 3 ) = -0.62993E 02

C ( 1, 4 ) = 0.53414E 01
C ( 2, 4 ) = 0.53414E 01
C ( 3, 4 ) = -0.62993E 02
C ( 4, 4 ) = -0.13983E 03

Solution of Redundant Shears and Moments Using Gaussian Elimination

Input Data

```
-0.952E 02  0.629E 02-0.940E 01  0.534E 01  0.270E 04
 0.629E 02-0.139E 03-0.867E 01  0.534E 01  0.000E 00
-0.940E 01-0.867E 01-0.952E 02-0.629E 02-0.270E 04
 0.867E 01  0.470E 01-0.629E 02-0.139E 03  0.000E 00
```

Output Data

```
Redundant Shear     ( 1 ) = -0.55320E 02
Redundant Moment    ( 1 ) = -0.29693E 02
Redundant Shear     ( 2 ) =  0.56332E 02
Redundant Moment    ( 2 ) = -0.29810E 02
```

Check

| Input Constant | Calculated | Difference |
|---|---|---|
| 0.27071E 04 | 0.27070E 04 | 0.24414E-02 |
| 0.00000E 00 | -0.40769E-04 | 0.40769E-04 |
| -0.27071E 04 | -0.27070E 04 | -0.97656E-03 |
| 0.00000E 00 | -0.31280E-03 | 0.31280E-03 |

## Discontinuity Stresses For Epoxy Model

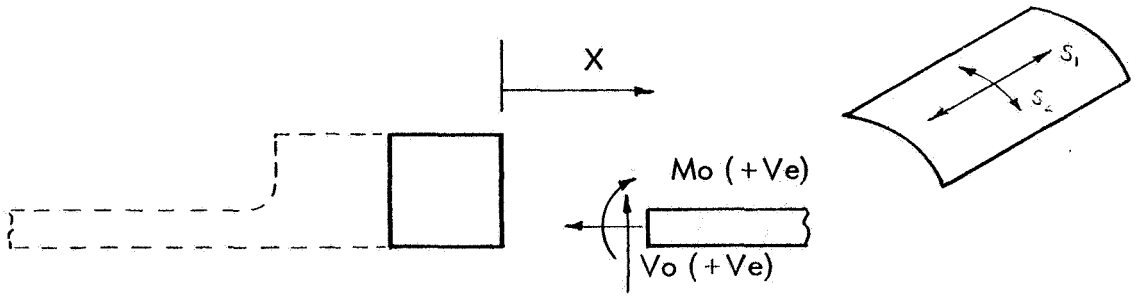


## Stresses Due to Radial Shear Vo

$$M_x = \frac{1}{\beta} \; Vo \; e^{-\beta x} \sin \beta x \qquad \text{(lbs ins)}$$

$$V_x = Vo \; e^{-\beta x} \; (\cos \beta x - \sin \beta x) \quad \text{(lbs)}$$

Meridional bending stress $S_1 = \frac{6 M_x}{t}$

Hoop Stress $S_2 = \frac{-2 Vo}{t} \; (\beta \; R \; e^{-\beta x} \cos \beta x)$

$$\beta = \sqrt[4]{\frac{3 (1 - V^2)}{R^2 t^2}} = \sqrt[4]{\frac{3 (1 - .35^2)}{4.218^2 \times .437^2}}$$

$$= 0.938$$

$$\beta^2 = 0.938^2 = 0.88$$

| Position X ins | $\beta x$ | $e^{-\beta x}$ | Sin $\beta x$ | Cos $\beta x$ | $e^{-\beta x} \sin \beta x$ | Cos $\beta x$ - Sin $\beta x$ |
|---|---|---|---|---|---|---|
| 0.75 | .704 | .494 | .6468 | .7627 | .3190 | .1159 |
| 1.75 | 1.64 | .192 | .998 | -.0645 | .1915 | -1.0625 |
| 2.75 | 2.58 | .0756 | .5329 | -.8462 | .0403 | -1.3791 |
| 3.75 | 3.52 | .0296 | -.3584 | .9336 | -.0106 | 1.2920 |

| Position X (ins) | Bending Moment Mx | Meridional Stress $S_1^1$ | Hoop Stress $S_2^1$ | Shear Force Vx |
|---|---|---|---|---|
| 0.75 | .340 Vo | 4.67 Vo | -6.82 Vo | .573 Vo |
| 1.75 | .204 Vo | 2.80 Vo | 0.224 Vo | -.204 Vo |
| 2.75 | .043 Vo | .59 Vo | 1.160 Vo | -.104 Vo |
| 3.75 | -.0113 Vo | -.155 Vo | -.50 Vo | .0374 Vo |

Stresses due to Uniform Radial Edge Moment Mo

$$Mx = Mo\ e^{-\beta x}\ (\cos \beta x + \sin \beta x) \qquad \text{(lbs ins)}$$

$$Vx = 2\beta\ Mo\ e^{-\beta x}\ \sin \beta x \qquad \text{(lbs)}$$

Meridional Bending Stress $S_1^1 = \dfrac{6Mx}{t}$

Hoop Stress $S_2 = \dfrac{2\beta^2 R\ Mo\ e^{-\beta x}\ (\cos \beta x - \sin \beta x)}{t}$

| Position X (ins) | $\cos\beta x + \sin\beta x$ | Bending Moment Mx | Meridional Stress $S_1^1$ | Hoop Stress | Shear Force Vx |
|---|---|---|---|---|---|
| 0.75 | 1.4095 | .6963 Mo | 9.559 Mo | .975 Mo | 0.6 Mo |
| 1.75 | .9335 | .1792 Mo | 2.460 Mo | -3.470 Mo | .359 Mo |
| 2.75 | -.3133 | -.02368 Mo | -.325 Mo | -1.770 Mo | .076 Mo |
| 3.75 | .5752 | .0170 Mo | .2334 Mo | .635 Mo | -.0199 Mo |

## Total Stresses

For P = 25 Psi

M = -7.42
V = -13.81
} From Computer Program Output

| | Meridional Stress $S_1$ | | | | | Hoop Stress $S_2$ | | | |
|---|---|---|---|---|---|---|---|---|---|
| sition x (ins) | Membrane | Due to Vo | Due to Mo | Total External | Total Internal | Membrane | Due to Vo | Due to Mo | Total External |
| ).75 | 108.5 | 64.5 | 71 | 244 | -27 | 217 | -94.2 | 7.25 | 130.1 |
| .75 | ↓ | 38.7 | 18.25 | 165.5 | 51.65 | ↓ | 3.1 | -25.8 | 194.3 |
| ?.75 | ↓ | 8.15 | -2.41 | 114.2 | 102.76 | ↓ | 16.05 | -13.15 | 219.9 |
| 3.75 | ↓ | -2.14 | 1.73 | 108.1 | 108.91 | ↓ | -6.91 | 4.71 | 214.8 |

## trains

$$\epsilon_1 = \frac{1}{E}(S_1 - \mu S_2) \qquad \epsilon_2 = \frac{1}{E}(S_2 - \mu S_1)$$

@ Room Temperature $E = 0.5 \times 10^6$ $\mu = .35$

External

| X (ins) | $S_1$ | $S_2$ | $\mu S_1$ | $\mu S_2$ | $\epsilon_1 \times 10^6$ | $\epsilon_2 \times 10^6$ |
|---|---|---|---|---|---|---|
| 0.75 | 244 | 130.1 | 85.4 | 45.5 | 397 | 89.4 |
| 1.75 | 165.5 | 194.3 | 57.9 | 68.0 | 195 | 272.2 |
| 2.75 | 114.2 | 219.9 | 40.0 | 77.0 | 74.4 | 359.8 |
| 3.75 | 108.1 | 214.8 | 37.8 | 75.2 | 65.8 | 354.0 |

Internal

| X (ins) | $S_1$ | $S_2$ | $\mu S_1$ | $\mu S_2$ | $\epsilon_1 \times 10^6$ |
|---|---|---|---|---|---|
| 0.75 | -27 | 130.1 | -9.5 | 45.5 | -145 |
| 1.75 | 51.65 | 194.3 | 18.1 | 68.0 | -32.7 |
| 2.75 | 102.76 | 219.9 | 35.9 | 77.0 | 51.52 |
| 3.75 | 108.91 | 214.8 | 38.0 | 75.2 | 67.42 |

# APPENDIX B

## FLANGE STRESS ANALYSIS

Because of the many variables and unknowns, the work involved in a rigorous theoretical analysis of the flange becomes prohibitive. The following analysis considers only the primary effects inducing flange stresses. These are:

a. Radial extension of the flange due to internal pressure.

b. Stress caused by the radial shear/in at the discontinuity.

c. Rolling of the flange caused by the moment at the discontinuity, plus the moment of the radial shear/in about the flange centroid.

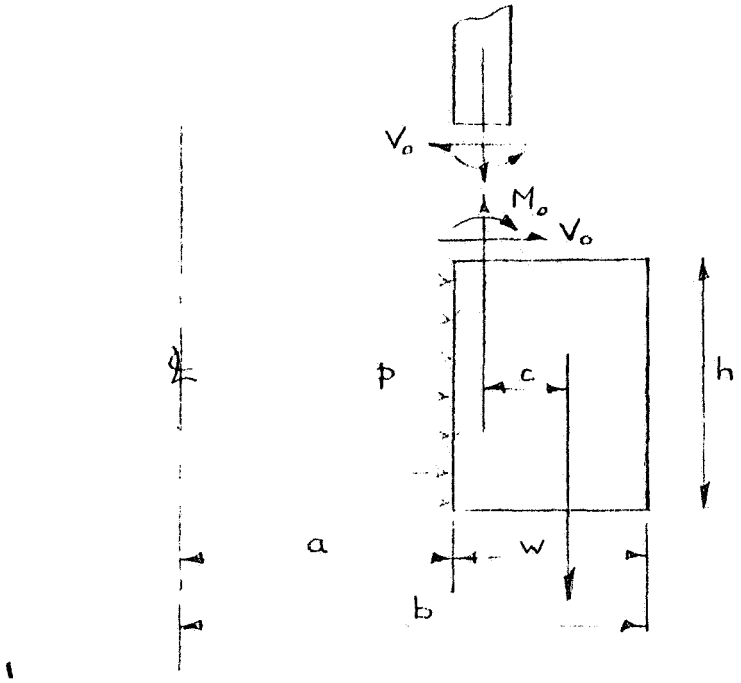


a. Internal Pressure (Using Lamé Equations)

Radial Stress

$$\sigma_r = \frac{p\,a^2}{b^2 - a^2}\left(1 - \frac{b^2}{r^2}\right)$$

Circumferential Stress

$$\sigma_\theta = \frac{p\,a^2}{b^2 - a^2}\left(1 + \frac{b^2}{r^2}\right)$$

Where:

p = internal pressure = 1.5 psi

a & b = inner and outer flange radii

r = radius of any fiber of the ring.

Circumferential Stresses

at $r = a = 4.0$ in

$$\sigma_\theta = \frac{1.5 \times 4.0^2}{5.28^2 - 4.0^2} \left(1 + \frac{5.28^2}{4.0^2}\right) = 5.54 \text{ psi}$$

at $r = b = 5.28$ in

$$\sigma_\theta = \frac{1.5 \times 4.0^2}{5.28^2 - 4.0^2} \left(1 + \frac{5.28^2}{5.28^2}\right) = 4.04 \text{ psi}$$

Radial Stresses

at $r = a$

$$\sigma_r = \frac{1.5 \times 4.0^2}{5.28^2 - 4.0^2} \left(1 - \frac{5.28^2}{4.0^2}\right) = -1.5 \text{ psi}$$

at $r = b$

$$\sigma_r = \frac{1.5 \times 4.0^2}{5.28^2 - 4.0^2} \left(1 - \frac{5.28^2}{5.28^2}\right) = 0$$

b. Discontinuity Shear

Discontinuity shear and moment for a flexible flange gasket are:

$$V_o = -0.43 \text{ lb/in} \quad M_o = -0.465 \text{ lb in/in}.$$

Average stress due to

$$V_o = \frac{V_o a}{h_o w}$$

Where:

$V_o$ = radial shear/in

$a$ = inner flange radius

$h$ = flange height

$w$ = flange width

$$\sigma_\theta = \frac{-0.43 \times 4.0}{1.625 \times 1.28} = -0.825 \text{ psi}$$

c. Flange Rolling Moment

$$\overline{M} = M_o + \frac{V_o h}{2} + \frac{p a . c}{2}$$

$$= -0.465 - \frac{0.43 \times 1.625}{2} + \frac{1.5 \times 4 \times 0.5}{2} = 0.685 \text{ lb in/in}$$

Flange Bending Stress

$$\sigma_m = \pm \frac{12 \overline{M} R y}{h^3 r \log_e b/a} \quad \text{(Ref. 4)}$$

Where:

R = radius to flange centroid

y = distance from flange neutral axis.

At r = a $y = \pm 0.59$ in

$$\sigma_m = \pm \frac{12 \times 0.685 \times 4.64 \times 0.59}{1.625^3 \times 4.0 \log_e 5.28/4.0} = \pm 4.72 \text{ psi}$$

At r = b $$y = \pm \frac{12 \times 0.685 \times 4.64 \times 0.59}{1.625^3 \times 5.28 \log_e 5.28/4.0} = \pm 3.56 \text{ psi}$$

# FLANGE CIRCUMFERENTIAL STRESSES

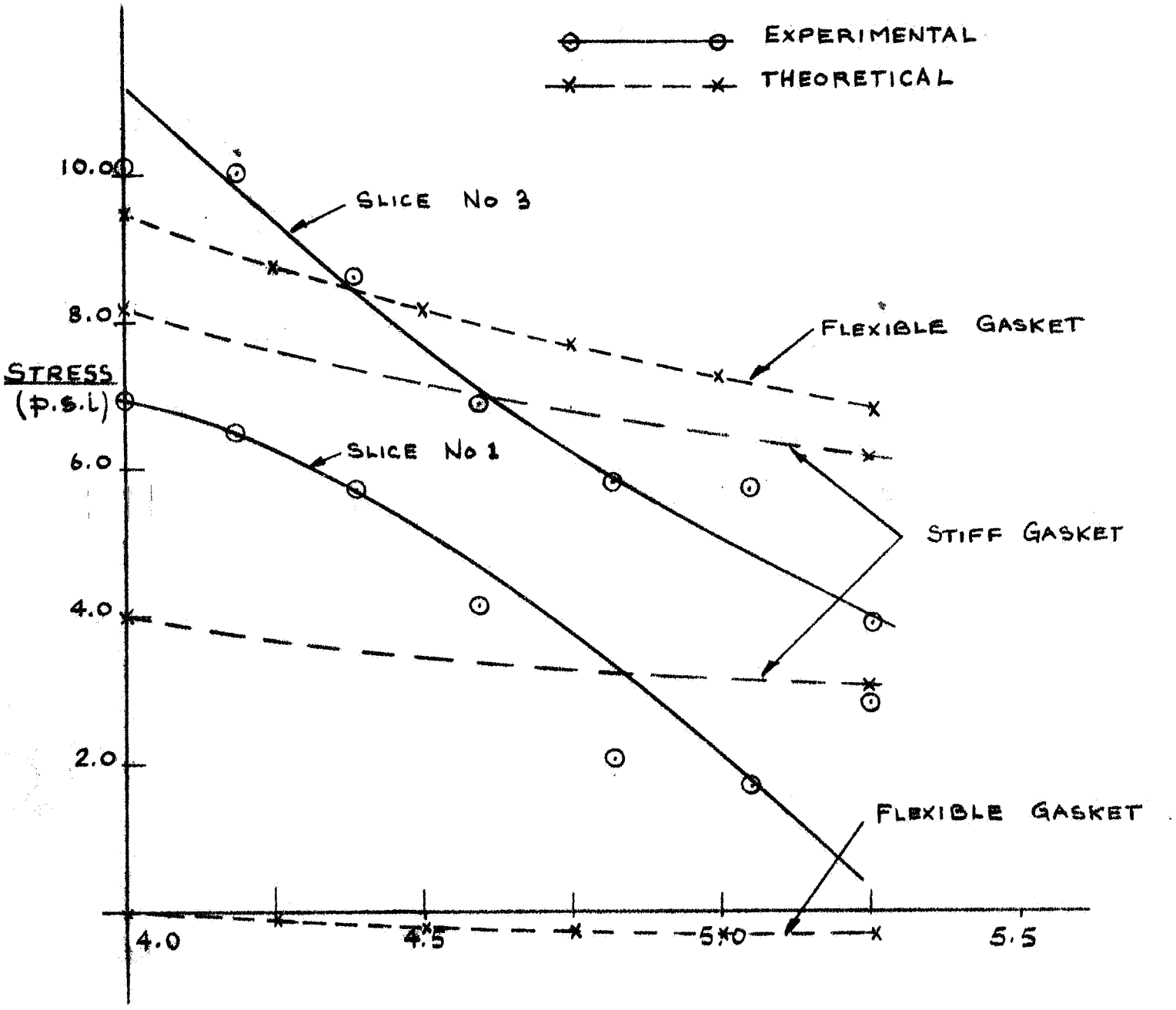

# APPENDIX C

## CONFORMAL TRANSFORMATION TO POLAR COORDINATES

### Photoelastic Evaluation of Slices 1 and 3

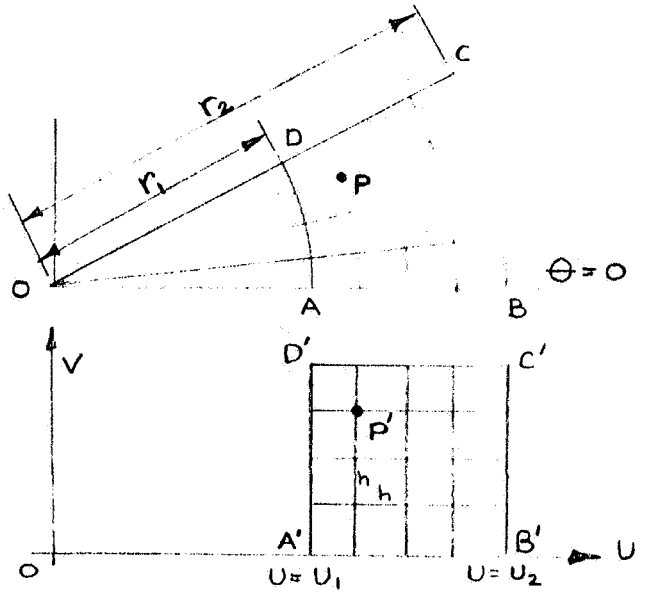


For Polar Coordinates

$w = f(r, \theta) = \ln z$

Where $z = x + iy$

$= r(\cos\theta + i \sin\theta)$

$= \underline{r e^{i\theta}}$

Now $w = u + iv$

$u + iv = \ln r e^{i\theta} = \ln r + i\theta$

Equating real and imaginary parts

$$u = \ln r \quad \text{— — —} \quad A$$

$$v = \theta \quad \text{— — —} \quad B$$

$\Delta v = \Delta\theta = h$ = grid spacing

Also $u_1 = \ln r_1$ and $u_2 = \ln r_2$

$$\frac{u_1 - u_2}{n} = h = \text{grid spacing}$$

From A $r = e^u$

$r_1 = e^{u_1}$ and $r_1 + \Delta r_1 = e^{u_1 + \Delta u}$

$\Delta r = e^{u_1 + \Delta u_1} - e^{u_1} = e^{u_1}(e^{\Delta u} - 1)$

In general $\Delta r = r_1 (e^{\Delta u} - 1)$

For square grid $\Delta v = \Delta\theta = h$

and $h = \frac{u_2 - u_1}{n} = \frac{\ln r_2 - \ln r_1}{n}$

For model $r_1 = 4.''0$ $r_2 = 5.''281$ $\theta = \frac{360}{18} = 20^\circ$

For $n = 6$ $\quad h = \ln(5.281) - \ln(4."0) = .0463$

$$\theta = 20^{\circ} = .3491 \text{ rads}$$

For square grid $\quad n\theta = \frac{.3491}{.0463} = 7.54$

$$\Delta\theta = 20/7.54 = 2.65^{\circ}$$

$$\Delta r_1 = r_2 ( e^{\Delta u} - 1 ) = 4.0 ( e^{.0463} - 1 )$$

| n | $\Delta u = n \Delta u_1$ | $e^{\Delta u}$ | $(e^{\Delta u} - 1)$ | $\Delta r = 4(e^{\Delta u} - 1)$ | $r = 4.0 + \Delta r$ (Model) | r (Photograph) = r Model xK |
|---|---|---|---|---|---|---|
| 1 | .0463 | 1.0473 | .0473 | .189 | 4.189 | 6.65 |
| 2 | .0926 | 1.0968 | .0968 | .387 | 4.387 | 6.95 |
| 3 | .1389 | 1.149 | .1490 | .595 | 4.595 | 7.28 |
| 4 | .1852 | 1.2039 | .2039 | .815 | 4.815 | 7.65 |
| 5 | .2315 | 1.261 | .2610 | 1.045 | 5.045 | 8.0 |
| 6 | .2778 | 1.320 | .320 | 1.280 | 5.280 | 8.37 |

$$K = \frac{r \text{ (Photograph)}}{r \text{ (Model)}} = \frac{6.35}{4.0} = 1.585$$

## REFERENCES


1. Leven, M. M., Epoxy Resins for Photoelastic Use, Photoelasticity, Edited by M. M. Frocht, MacMillan Company, New York, 1963.

2. Sampson, Robert C., A Three-Dimensional Photoelastic Method for Analysis of Differential-Contraction Stresses, Experimental Mechanics, Vol. 3, No. 10, P. 225-237, (Oct. 1963).

3. Durelli, A. J., Parks, V. J., and Del Rio, C. J., Experimental Determination of Stresses and Displacements in Thick-wall Cylinders of Complicated Shape, Experimental Mechanics, Vol. 8, No. 7, P. 319-326, (July 1968).

4. Timoshenko, Stephen, Strength of Materials - Part II, Advanced Theory and Problems, P. 138-140, Third Edition, Van Nostrand Company, Inc.

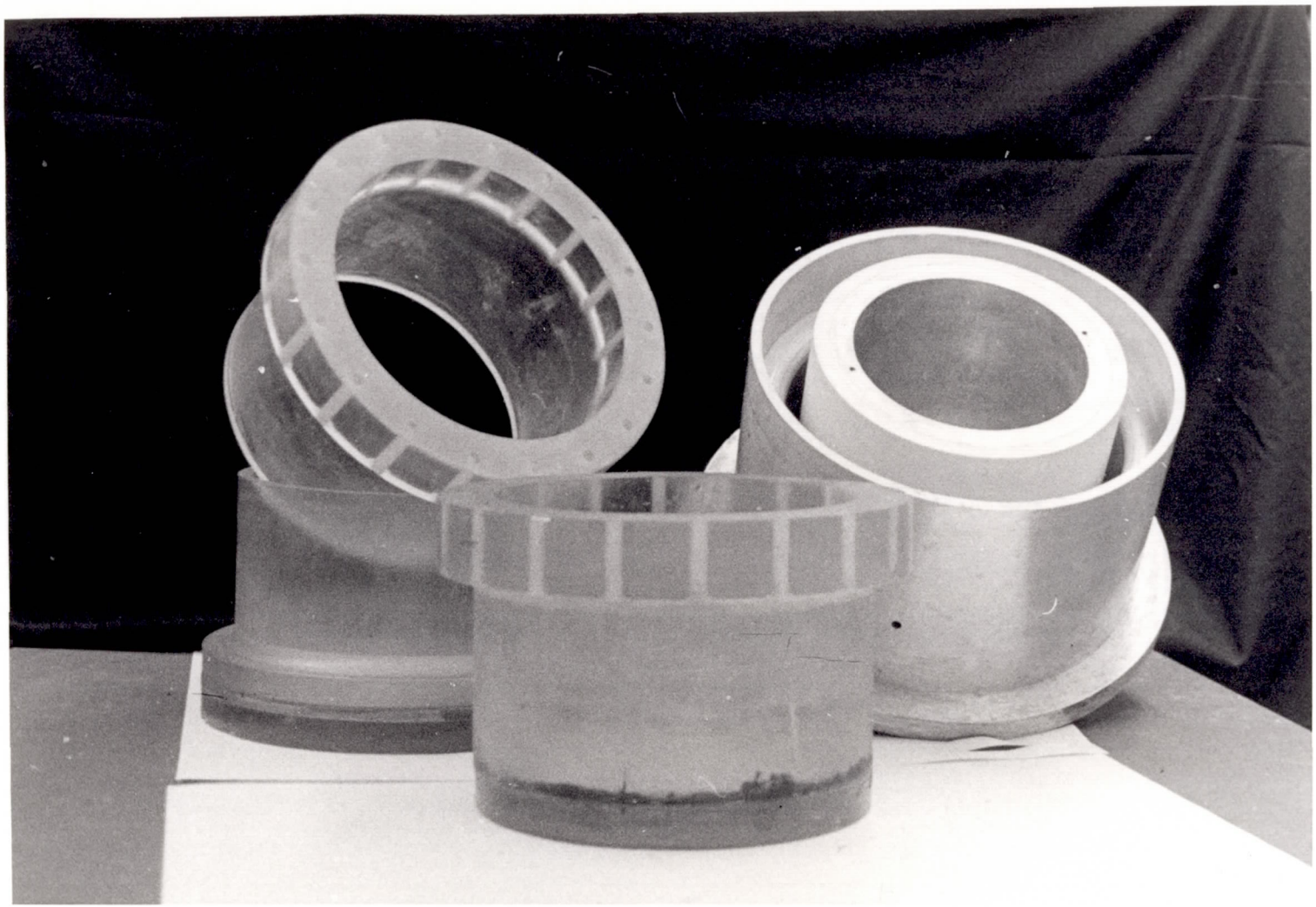

FIGURE 1. ASSEMBLED CASTING MOLD AND MACHINED CASTINGS

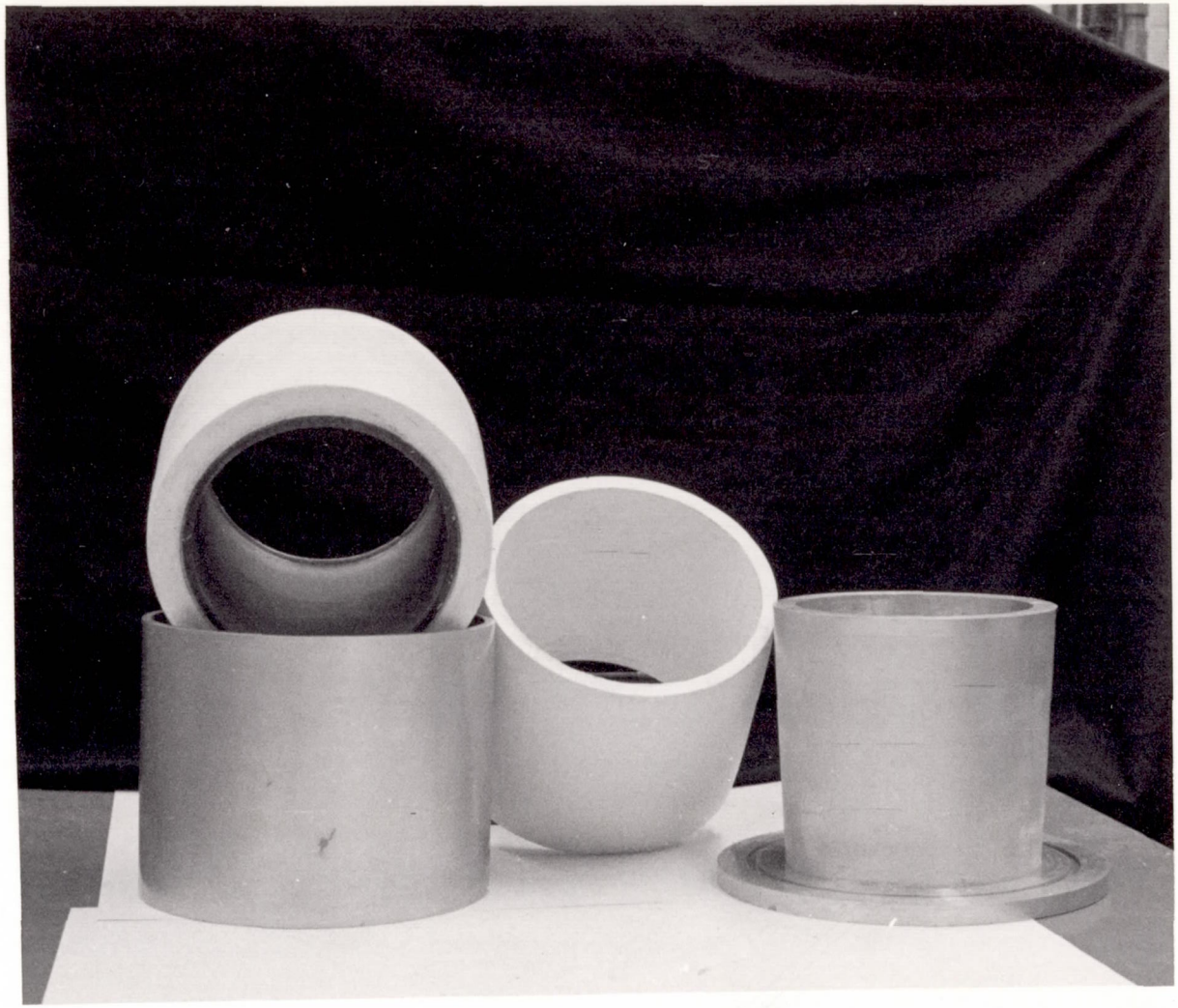

FIGURE 2. CASTING MOLD FOR FLEXIBLE SLEEVE

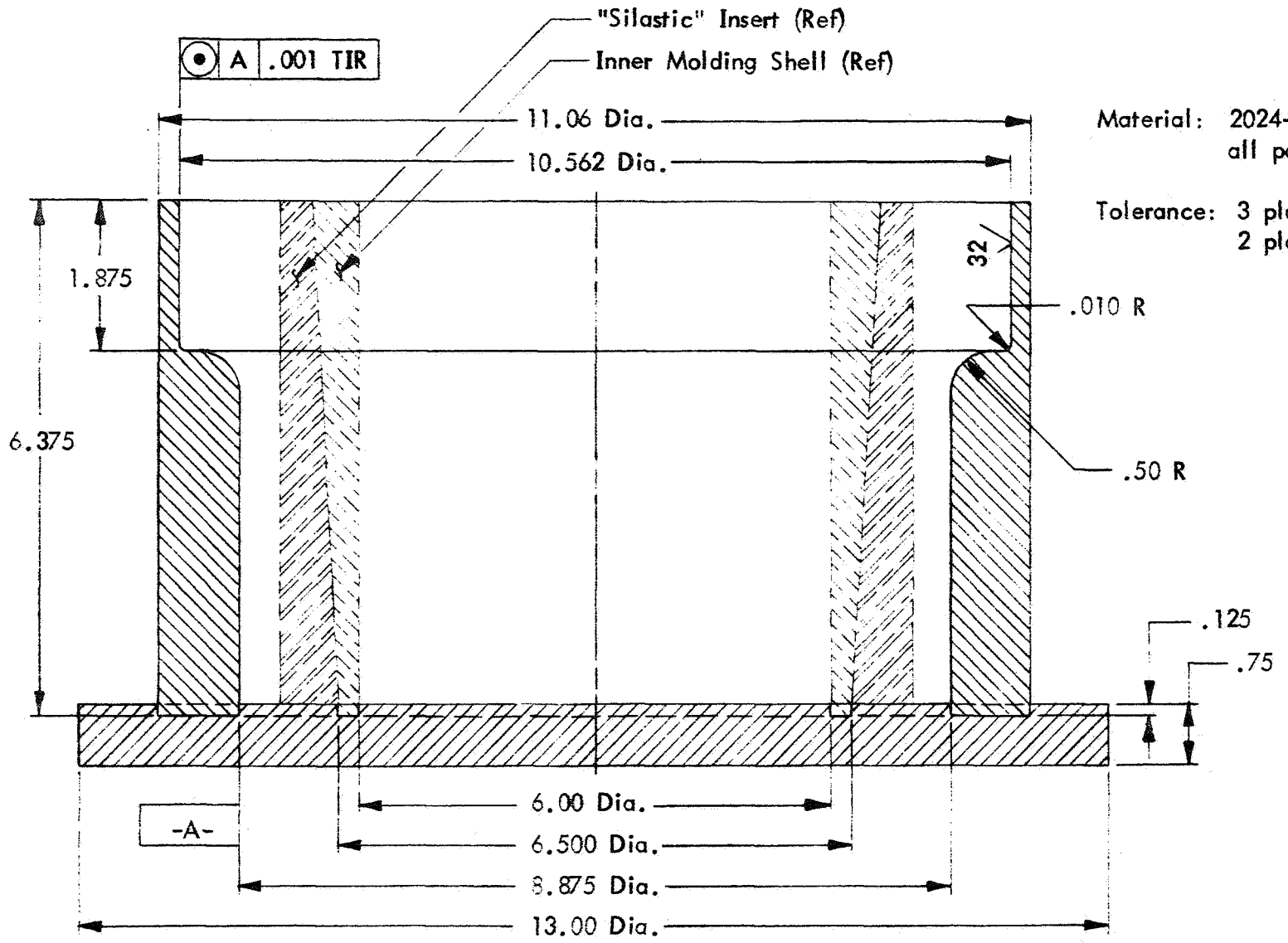


Note: Base plate grooves fit for mating parts .001 to .003 loose

FIGURE 3. CASTING MOLD FOR LOW PROFILE FLANGE

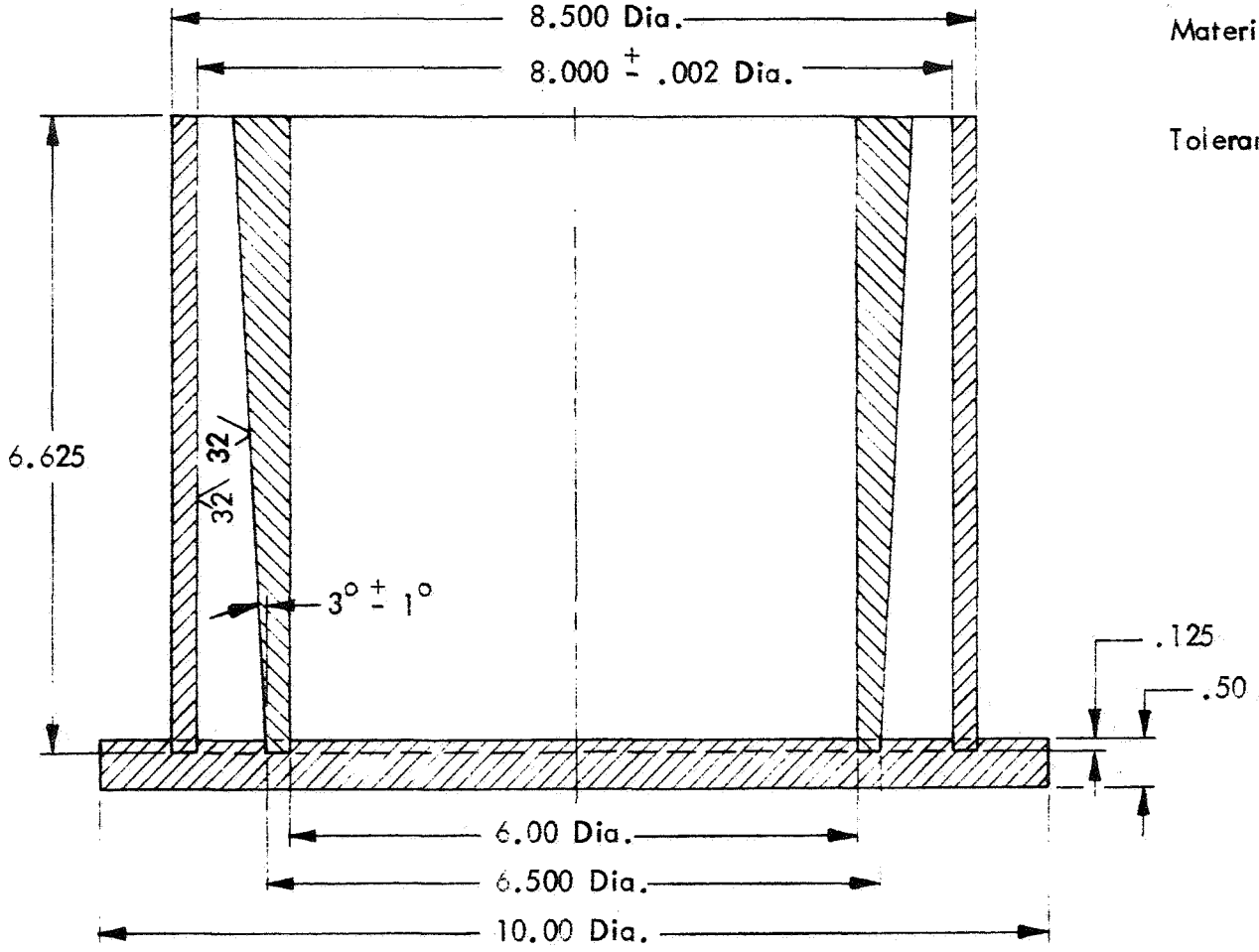


Material: 2024-T4 Aluminum for all parts

Tolerance: 3 place decimals, ± .005
2 place decimals, ± .010

Note: Base plate grooves fit for mating parts .001 to .003 loose

FIGURE 4. MOLDING SHELLS FOR LOW PROFILE FLANGE

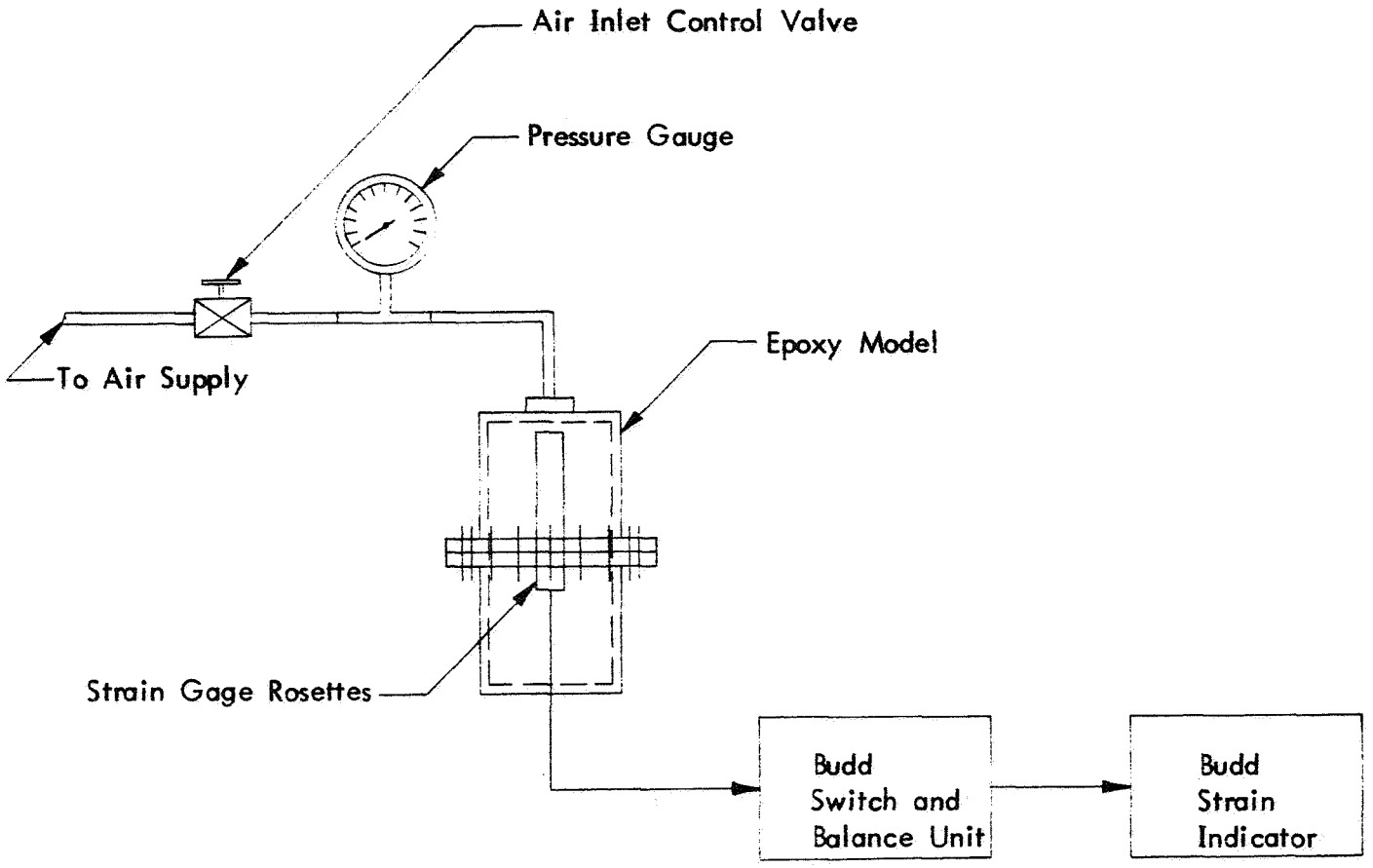


FIGURE 5. GENERAL ARRANGEMENT FOR ROOM TEMPERATURE PRESSURE TEST OF EPOXY MODEL

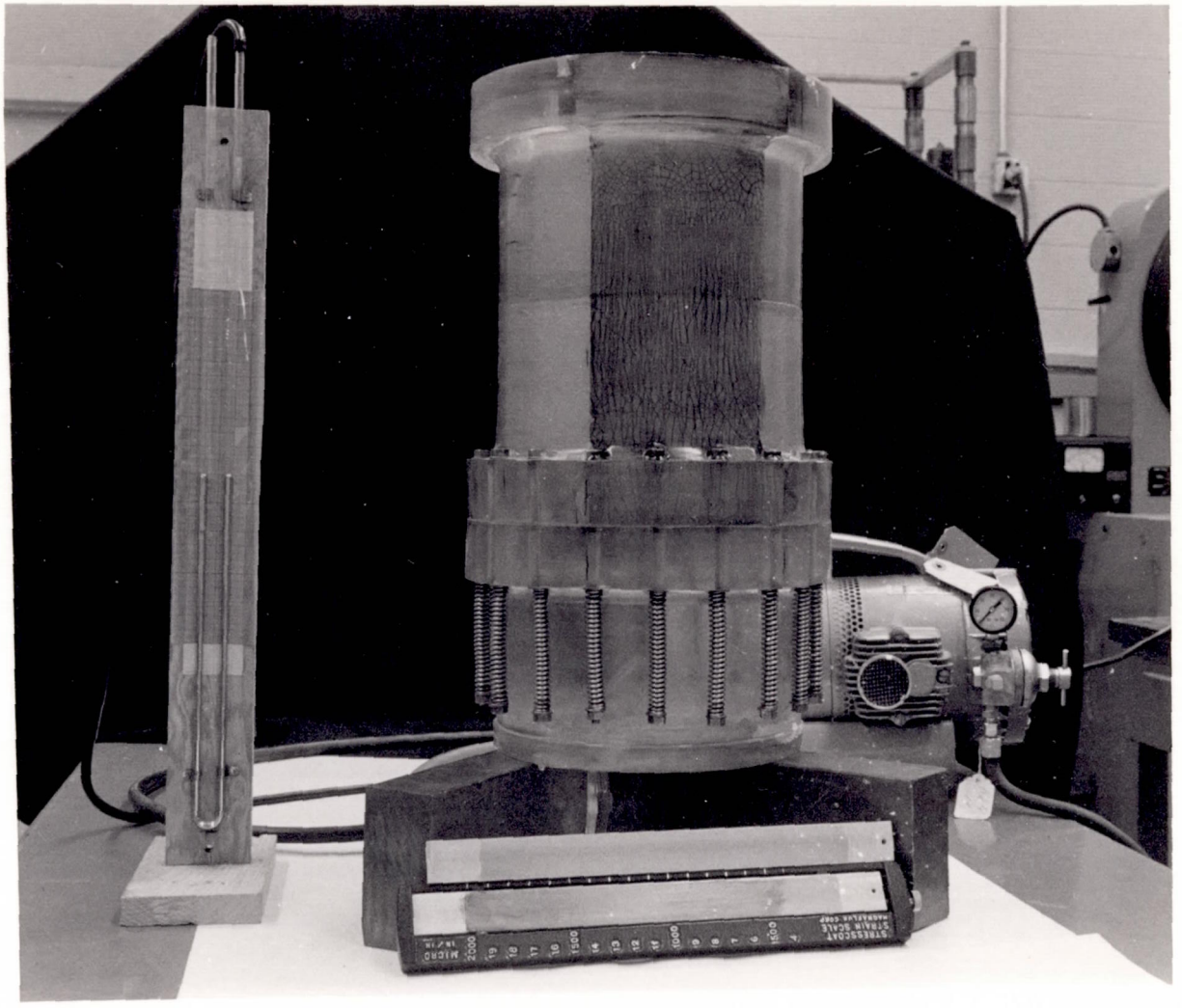


FIGURE 6. MODEL ASSEMBLY SHOWING STRESS COAT PATTERN

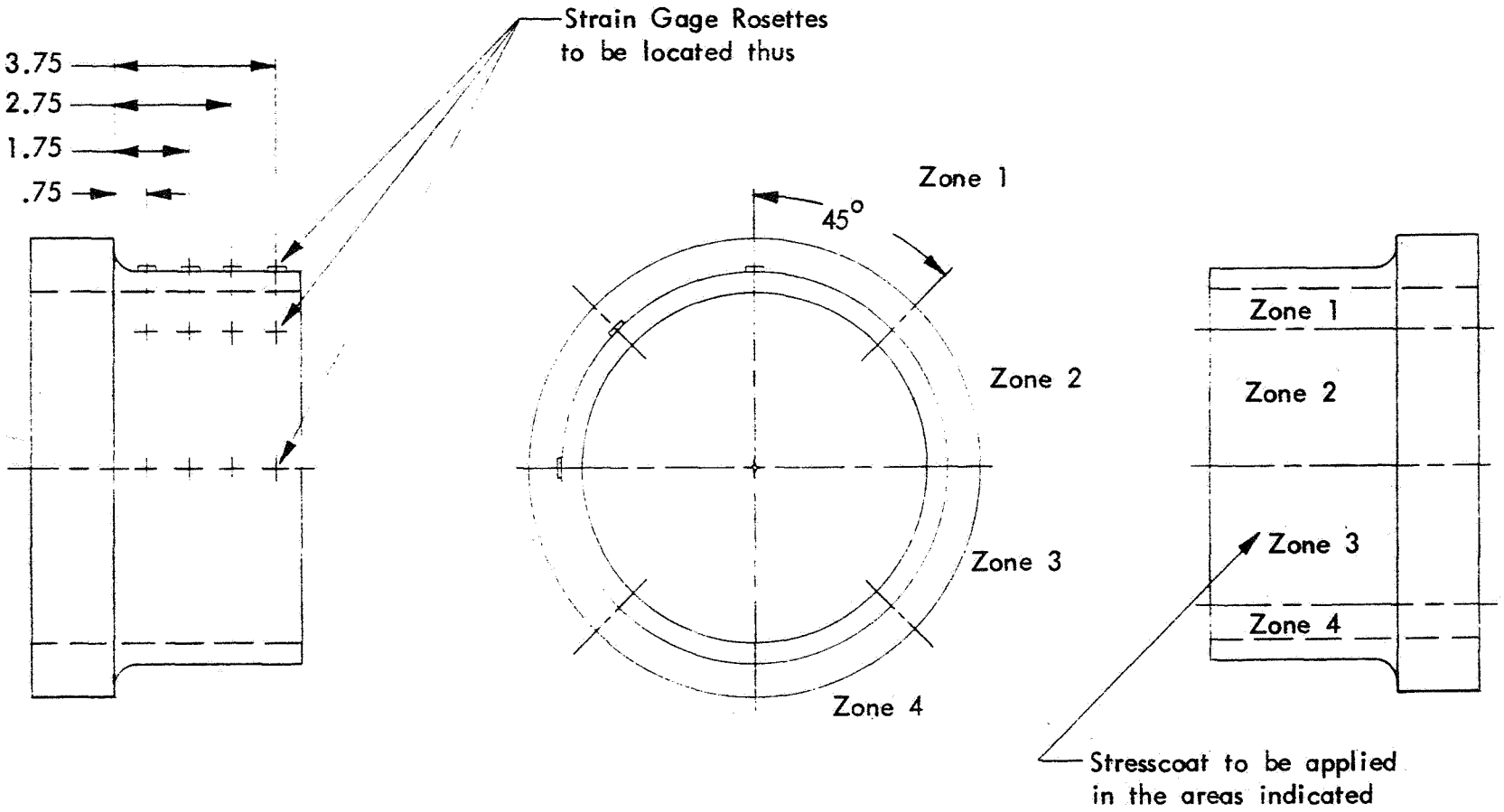


FIGURE 7. APPLICATION OF STRESSCOAT AND STRAIN GAGES TO LOW PROFILE FLANGE

FIGURE 8. STRAIN GAGE LOCATIONS AND RECORDED STRAINS

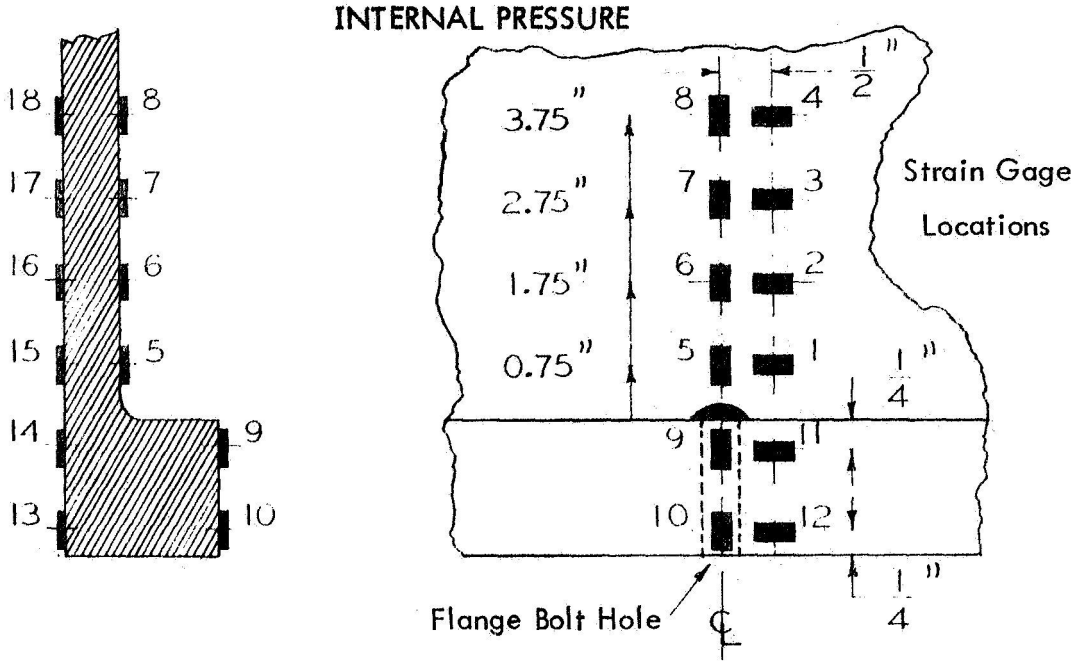


| Gage No. | Gage Factor | Gage Type | Strain Readings * (μ in/in) | | | | |
|---|---|---|---|---|---|---|---|
| | | | 0 Psi | Bolt** Loading | Bolt Loading + Pressure 15 Psi | 25 Psi | 0 Psi |
| 1 | 2.02 | C40-141C | 0 | 49 | 307 | 490 | 50 |
| 2 | 2.02 | " | 0 | -9 | 305 | 487 | -10 |
| 3 | 2.05 | C40-141B | 0 | -55 | 304 | 471 | -60 |
| 4 | 2.05 | " | 0 | -47 | 293 | 478 | -50 |
| 5 | 2.02 | C40-141C | 0 | +42 | 150 | 260 | 46 |
| 6 | ↓ | ↓ | 0 | -58 | 42 | 55 | -60 |
| 7 | | | 0 | -49 | 20 | 13 | -49 |
| 8 | | | 0 | -6 | 47 | 52 | -6 |
| 9 | 2.05 | C40-141B | 0 | -46 | -170 | -262 | -50 |
| 10 | | | 0 | -173 | -188 | -194 | -170 |
| 11 | | | - | -400 | -252 | -154 | -400 |
| 12 | | | - | 100 | 144 | 173 | 100 |
| 13 | | | -2000 | -2268 | -2218 | -2194 | -2258 |
| 14 | | | 0 | -148 | -147 | -158 | -142 |
| 15 | | | 0 | -157 | -288 | -384 | -156 |
| 16 | | | 0 | 10 | 30 | 42 | 12 |
| 17 | | | -2000 | -1973 | -1909 | -1868 | -1972 |
| 18 | ↓ | ↓ | 0 | 10 | 20 | 20 | 10 |

*Corrected for Gage Factor Variations

**Bolt Torque 10 inch-lbs/bolt ( 258 # axial load)

FIGURE 9. STRAIN GAGE LOCATIONS AND RECORDED STRAINS
FLANGE BOLT LOADING

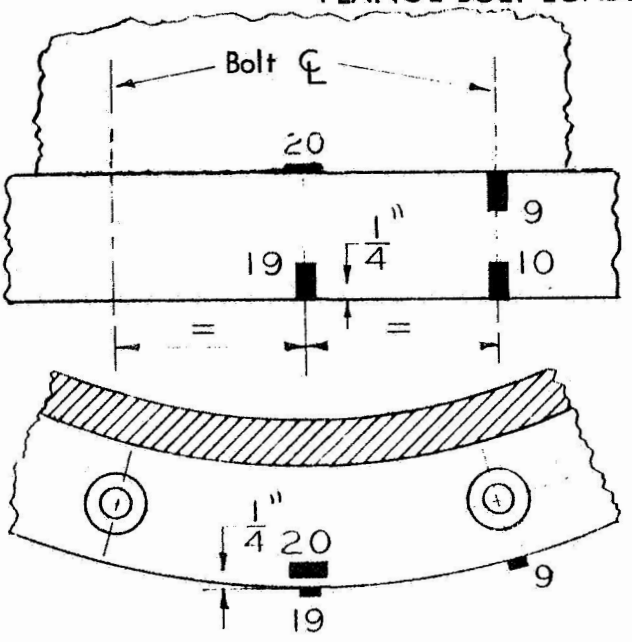


Additional Gage Locations For Bolt Test Only

| Gage No. | Gage Factor | Gage Type | Strains Due to Bolt Loading Only ( μin/in) | | | |
|---|---|---|---|---|---|---|
| | | | Torque : 0 (in lbs.) Axial Load : 0 (lbs.) | 10 258 | 20 516 | 40 1032 |
| 1 | 2.02 | C 40-141C | 0 | 49 | 102 | 332 |
| 2 | 2.02 | " | 0 | -9 | 25 | 127 |
| 3 | 2.05 | C 40-141B | 0 | -55 | -47 | -22 |
| 4 | 2.05 | " | 0 | -47 | -53 | -34 |
| 5 | 2.02 | C 40-141C | 0 | 210 | 133 | 300 |
| 6 | ↓ | ↓ | 0 | 72 | -25 | -75 |
| 7 | ↓ | ↓ | 0 | 49 | -13 | -29 |
| 8 | ↓ | ↓ | 3000 | 3062 | 3055 | 3065 |
| 9 | 2.05 | C 40-141B | 0 | 22 | -88 | -438 |
| 10 | ↓ | ↓ | 0 | -163 | -214 | -430 |
| 11 | ↓ | ↓ | 0 | -46 | -3 | -70 |
| 12 | ↓ | ↓ | 4000 | 3995 | 3970 | 3890 |
| 13 | ↓ | ↓ | -1000 | -1337 | -1416 | -1680 |
| 14 | ↓ | ↓ | 0 | -14 | -186 | -433 |
| 15 | ↓ | ↓ | 0 | -64 | -214 | -560 |
| 16 | ↓ | ↓ | 0 | 93 | 68 | 112 |
| 17 | ↓ | ↓ | -1000 | -905 | -915 | -837 |
| 18 | ↓ | ↓ | 0 | 44 | 40 | 70 |
| 19 | ↓ | ↓ | -4000 | -4154 | -4251 | -4580 |
| 20 | ↓ | ↓ | 0 | 82 | 286 | 792 |

$$S_1 = \frac{E}{(1-\mu^2)} \left[\epsilon_1 + \mu \epsilon_2\right]$$

$$S_2 = \frac{E}{(1-\mu^2)} \left[\epsilon_2 + \mu \epsilon_1\right]$$

$E = 0.5 \times 10^6$ $\mu = 0.35$

EXTERNAL

| X (INS) | $\epsilon_1$ | $\epsilon_2$ | $\mu\epsilon_1$ | $\mu\epsilon_2$ | $S_1$ | $S_2$ |
|---|---|---|---|---|---|---|
| 0.75 | 260 | 490 | 91.0 | 172 | 246.0 | 296 |
| 1.75 | 55 | 487 | 19.3 | 170.5 | 128.5 | 289 |
| 2.75 | 13 | 471 | 4.5 | 165 | 101.5 | 271 |
| 3.75 | 52 | 478 | 18.2 | 167 | 125.0 | 283 |

INTERNAL

| X (INS) | $\epsilon_1$ | $\epsilon_2$ | $\mu\epsilon_2$ | $S_1$ |
|---|---|---|---|---|
| 0.75 | -384 | 490 | 172 | -121 |
| 1.75 | 42 | 487 | 170.5 | 121 |
| 2.75 | 132 | 471 | 165 | 169 |
| 3.75 | 20 | 478 | 167 | 106.5 |

FIGURE 10. EXPERIMENTAL STRESSES - INTERNAL PRESSURE AND BOLT LOADING

EXTERNAL

| X (INS) | $\epsilon_1$ | $\epsilon_2$ | $\mu\epsilon_1$ | $\mu\epsilon_2$ | $S_1$ | $S_2$ |
|---|---|---|---|---|---|---|
| 0.75 | 42 | 49 | 14.7 | 17.15 | 33.7 | 36.3 |
| 1.75 | -58 | -9 | -20.3 | -3.2 | -34.9 | -16.7 |
| 2.75 | -49 | -55 | -17.15 | -19.25 | -38.9 | -41.1 |
| 3.75 | -6 | -47 | -2.1 | -16.45 | -12.8 | -28 |

| X (INS) | $\epsilon_1$ | $\epsilon_2$ | $\mu\epsilon_2$ | $S_1$ |
|---|---|---|---|---|
| 0.75 | -157 | 49 | 17.15 | -79.7 |
| 1.75 | 10 | -9 | -3.2 | 3.9 |
| 2.75 | 27 | -55 | -19.25 | 4.4 |
| 3.75 | 10 | -47 | -16.45 | -3.68 |

FIGURE 11. EXPERIMENTAL STRESSES - BOLT LOADING ONLY

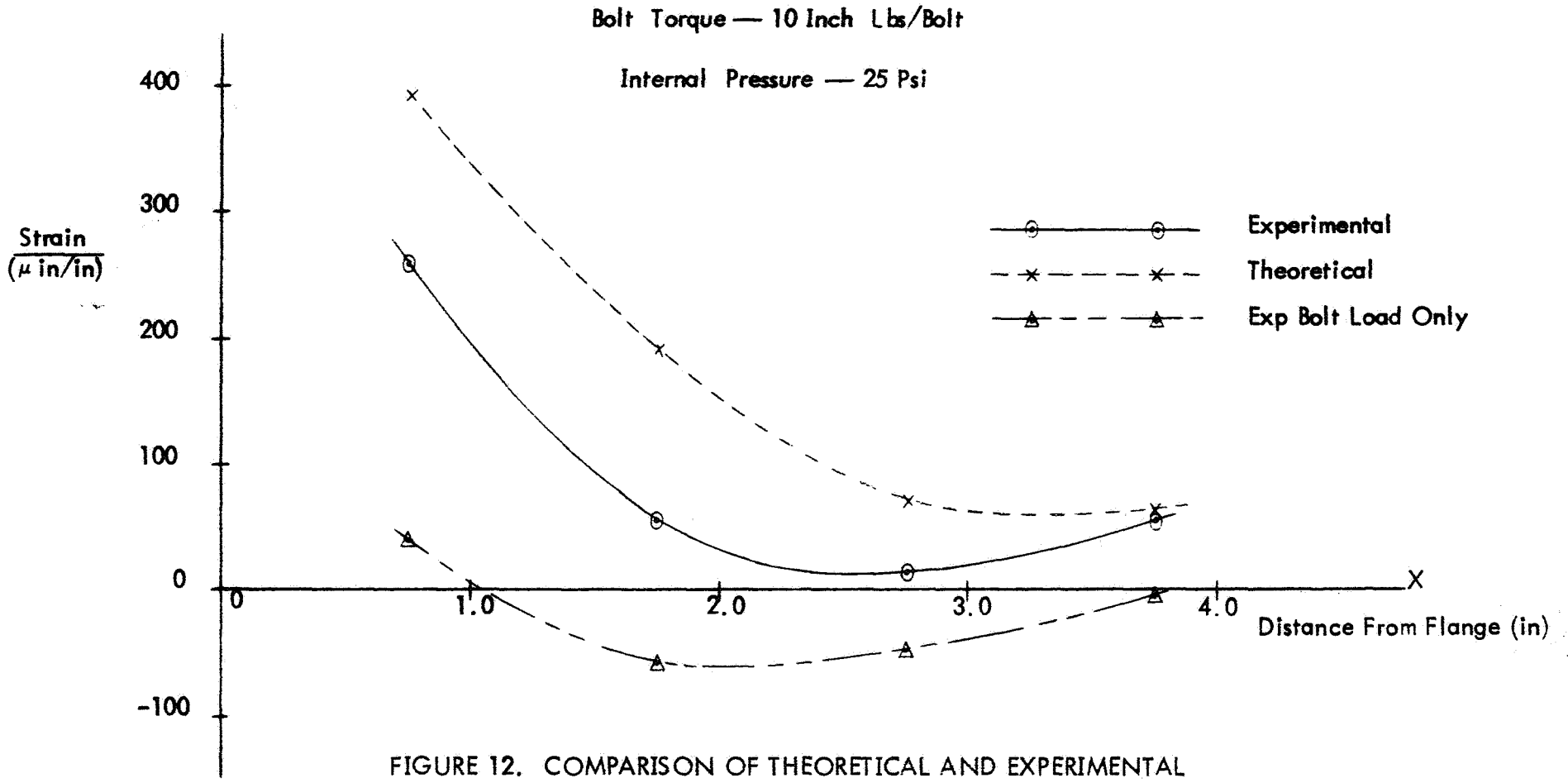


FIGURE 12. COMPARISON OF THEORETICAL AND EXPERIMENTAL LONGITUDINAL STRAIN IN EPOXY MODEL (EXTERNAL)

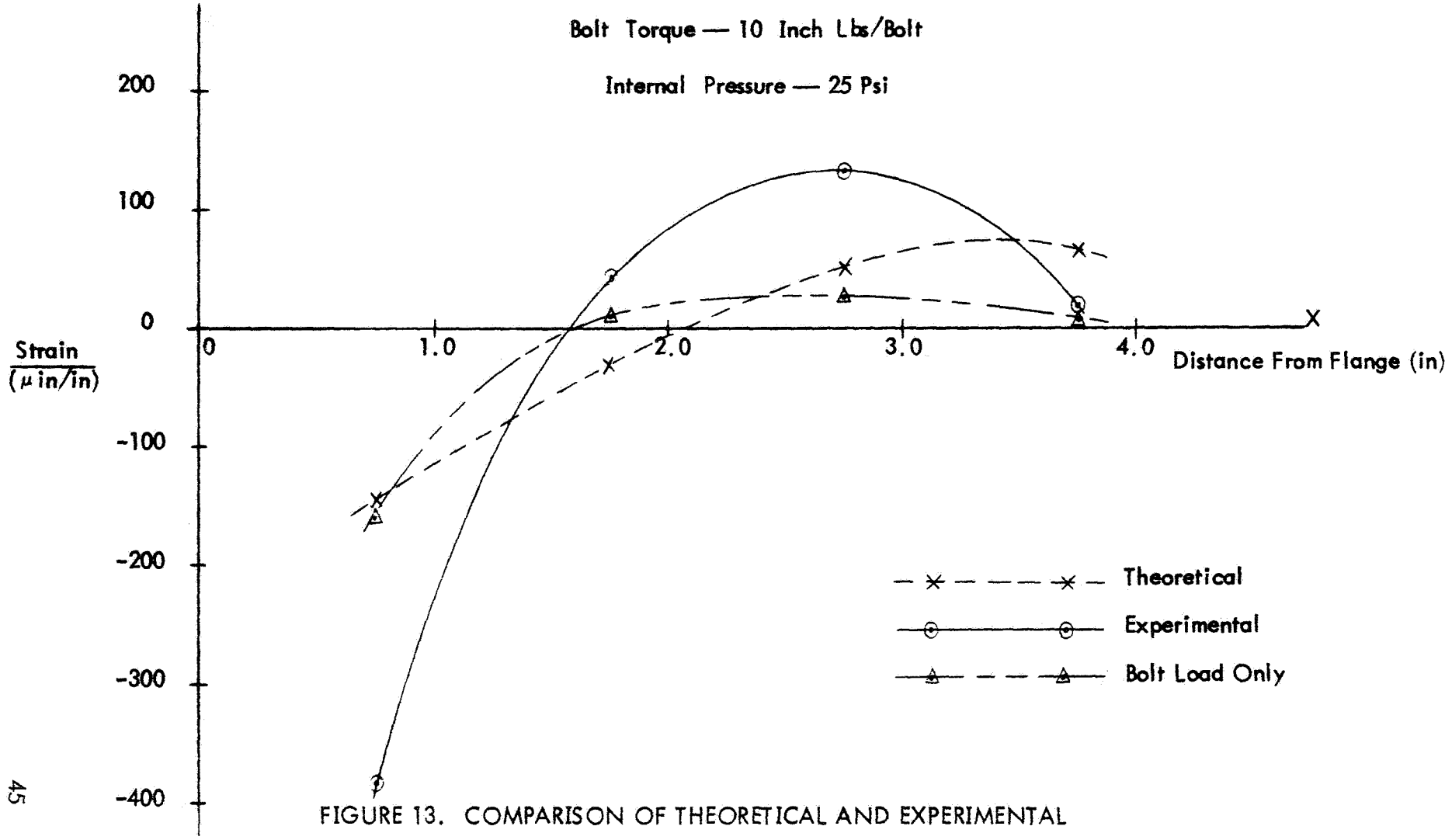


FIGURE 13. COMPARISON OF THEORETICAL AND EXPERIMENTAL LONGITUDINAL STRAIN IN EPOXY MODEL (INTERNAL)

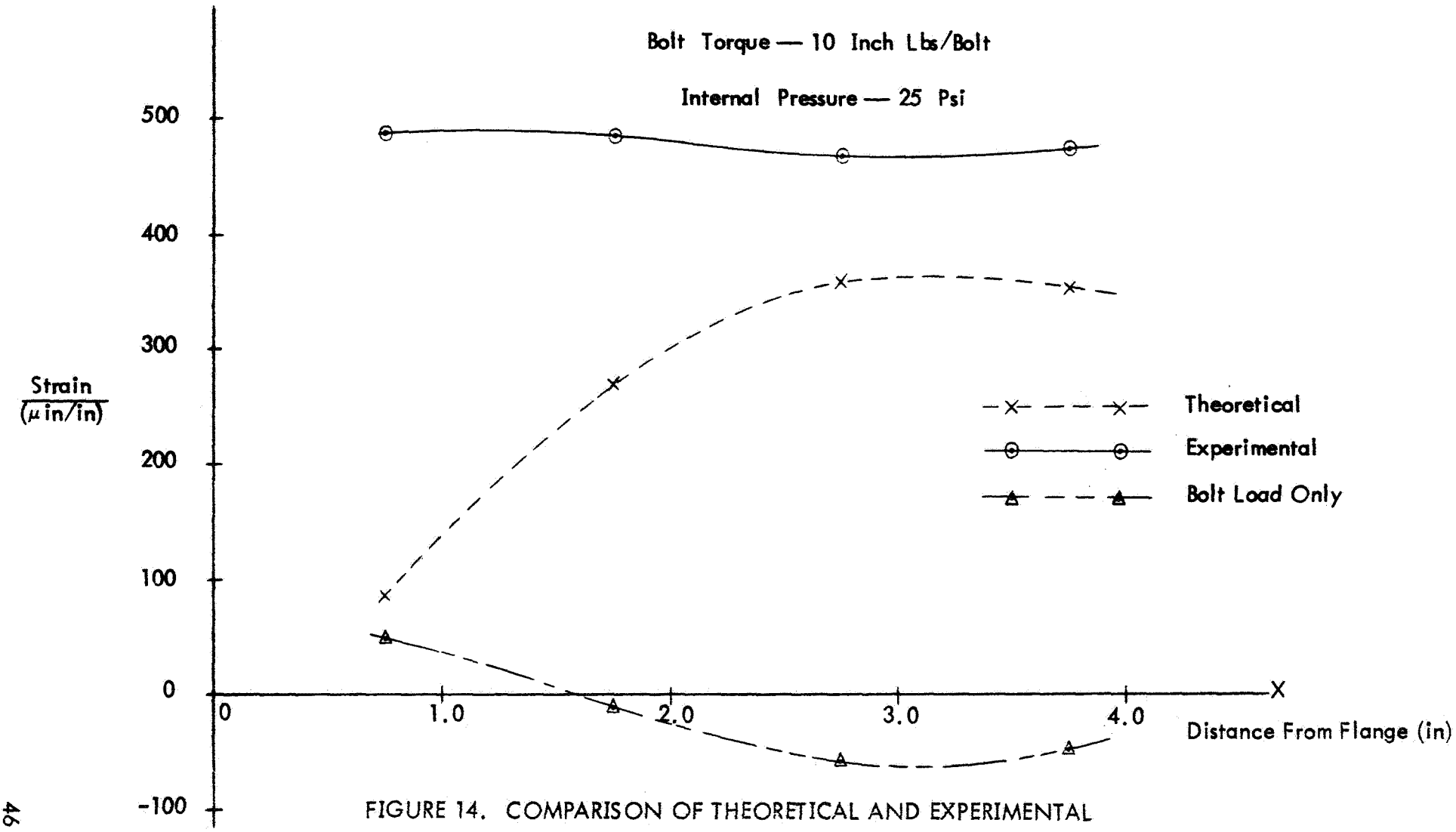


FIGURE 14. COMPARISON OF THEORETICAL AND EXPERIMENTAL CIRCUMFERENTIAL STRAINS IN EPOXY MODEL (EXTERNAL)

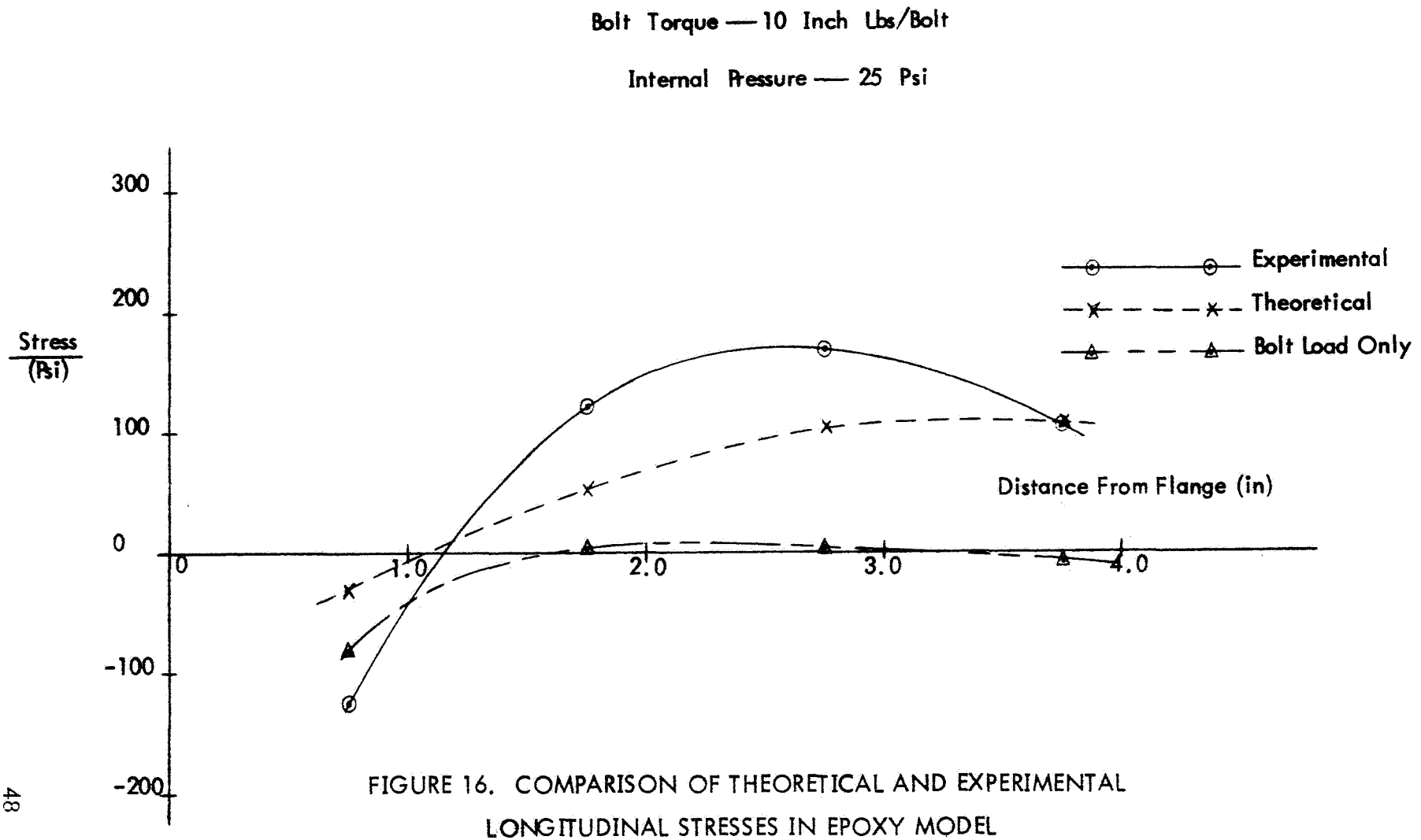


FIGURE 16. COMPARISON OF THEORETICAL AND EXPERIMENTAL LONGITUDINAL STRESSES IN EPOXY MODEL (INTERNAL)

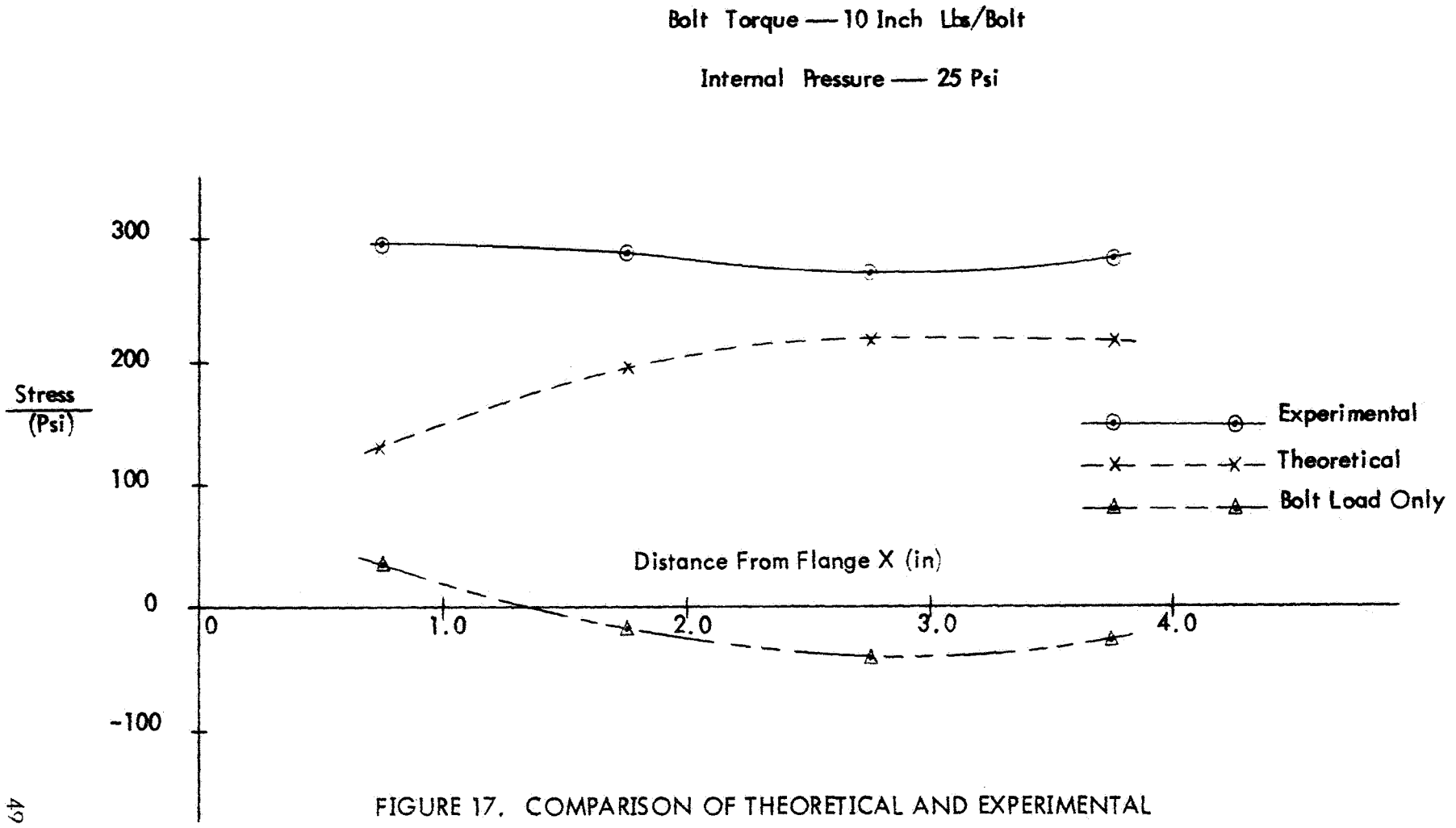


FIGURE 17. COMPARISON OF THEORETICAL AND EXPERIMENTAL CIRCUMFERENTIAL STRESSES IN EPOXY MODEL

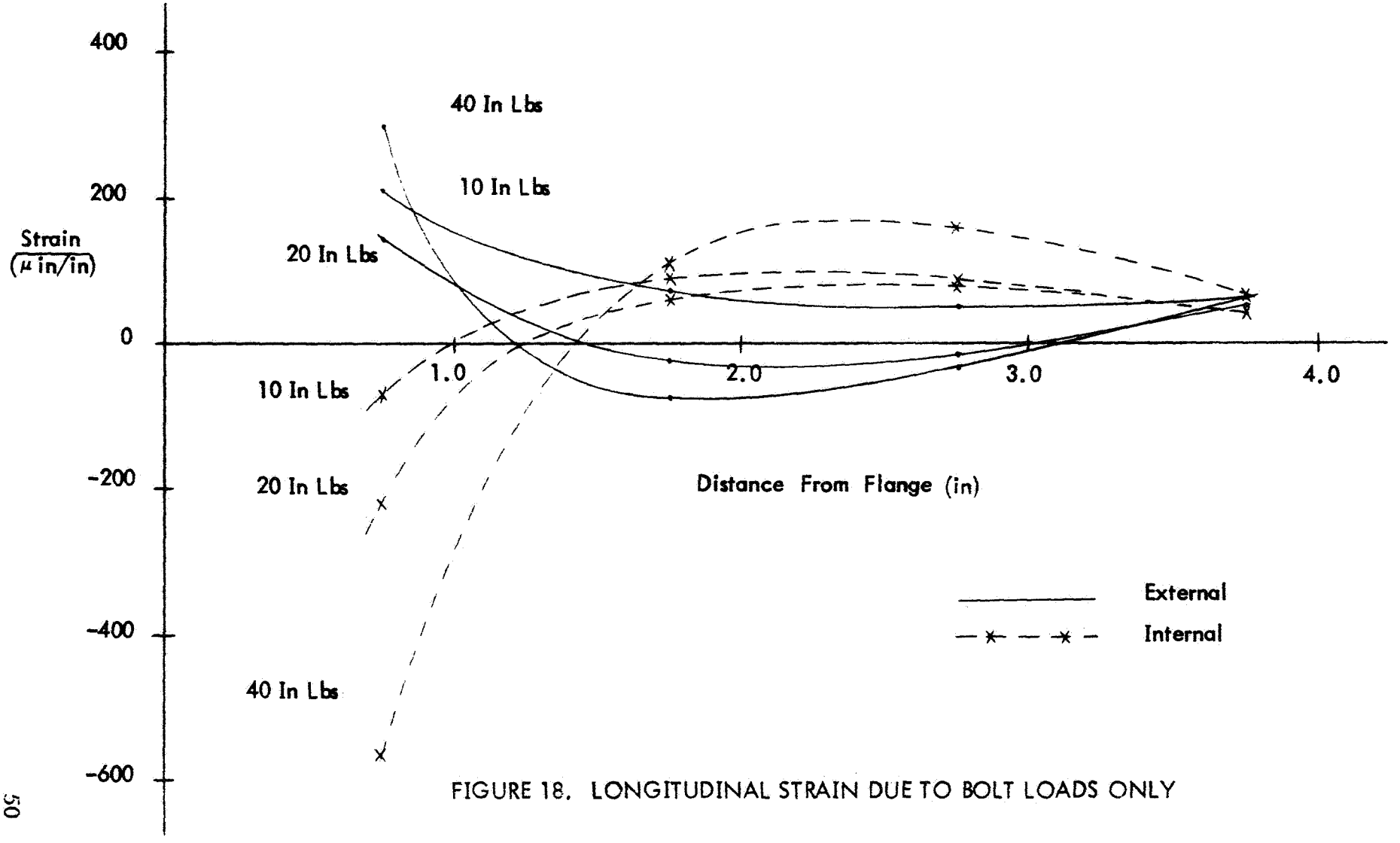


FIGURE 18. LONGITUDINAL STRAIN DUE TO BOLT LOADS ONLY

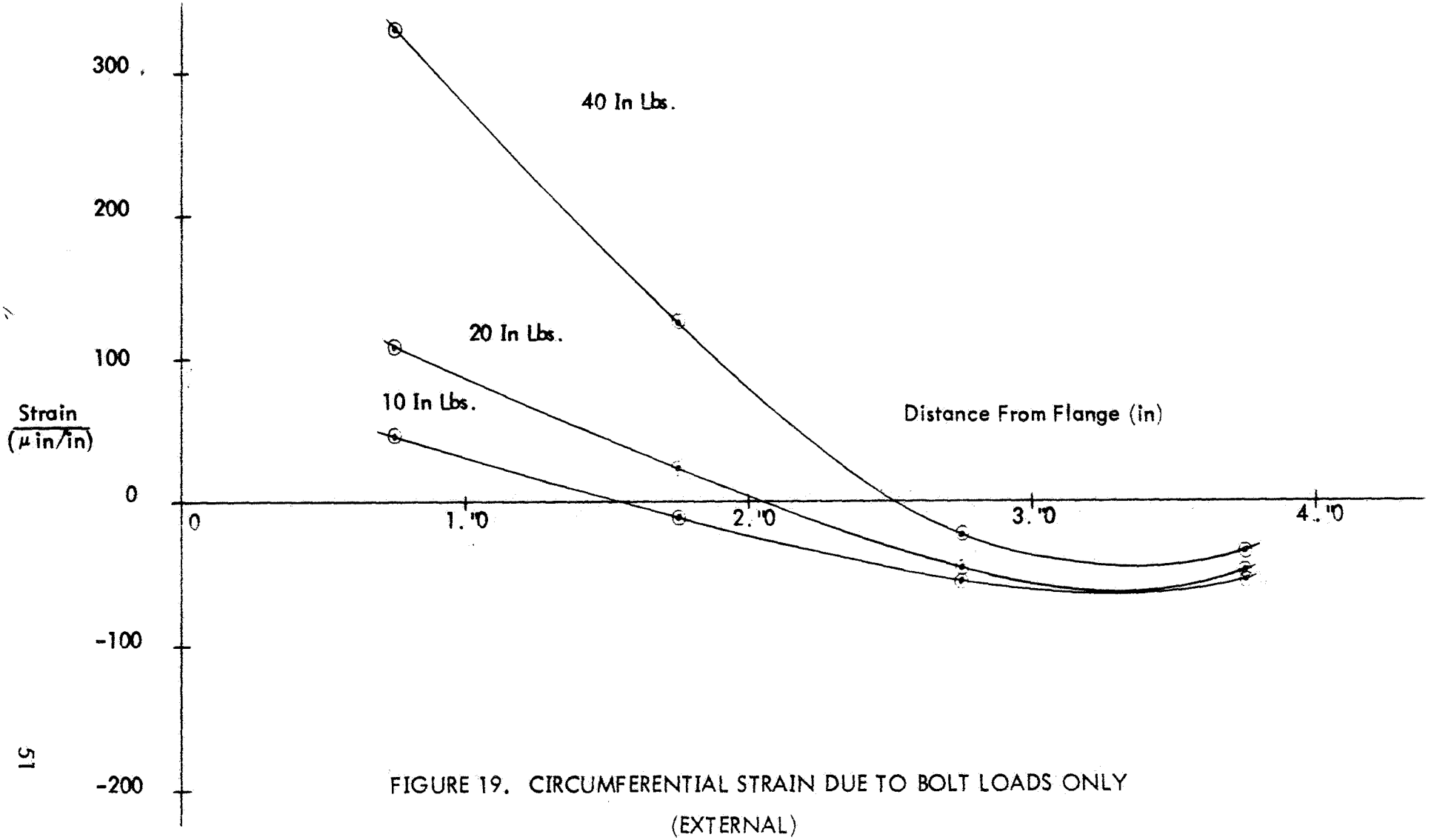


FIGURE 19. CIRCUMFERENTIAL STRAIN DUE TO BOLT LOADS ONLY (EXTERNAL)

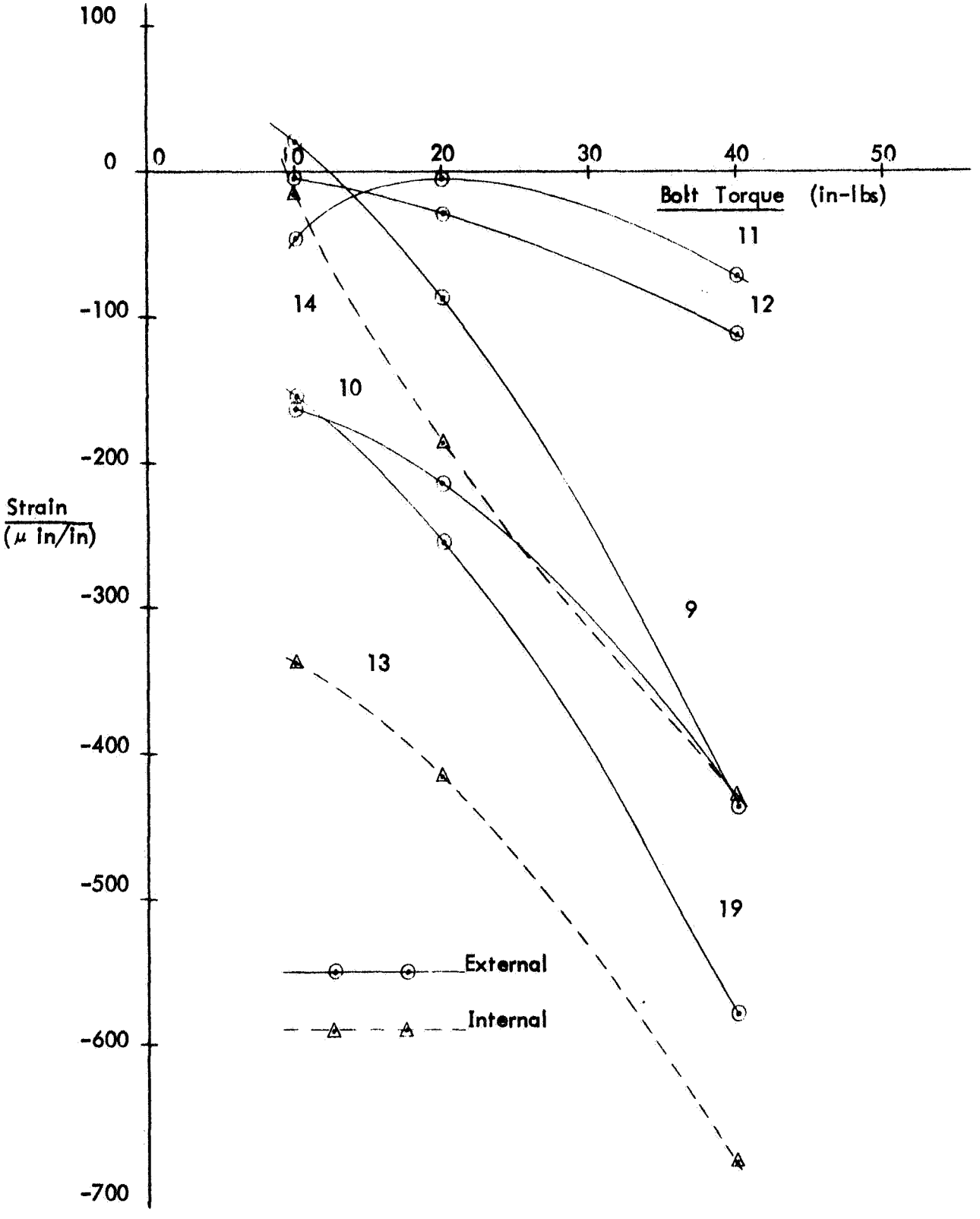


FIGURE 20. FLANGE STRAINS VS BOLT TORQUE

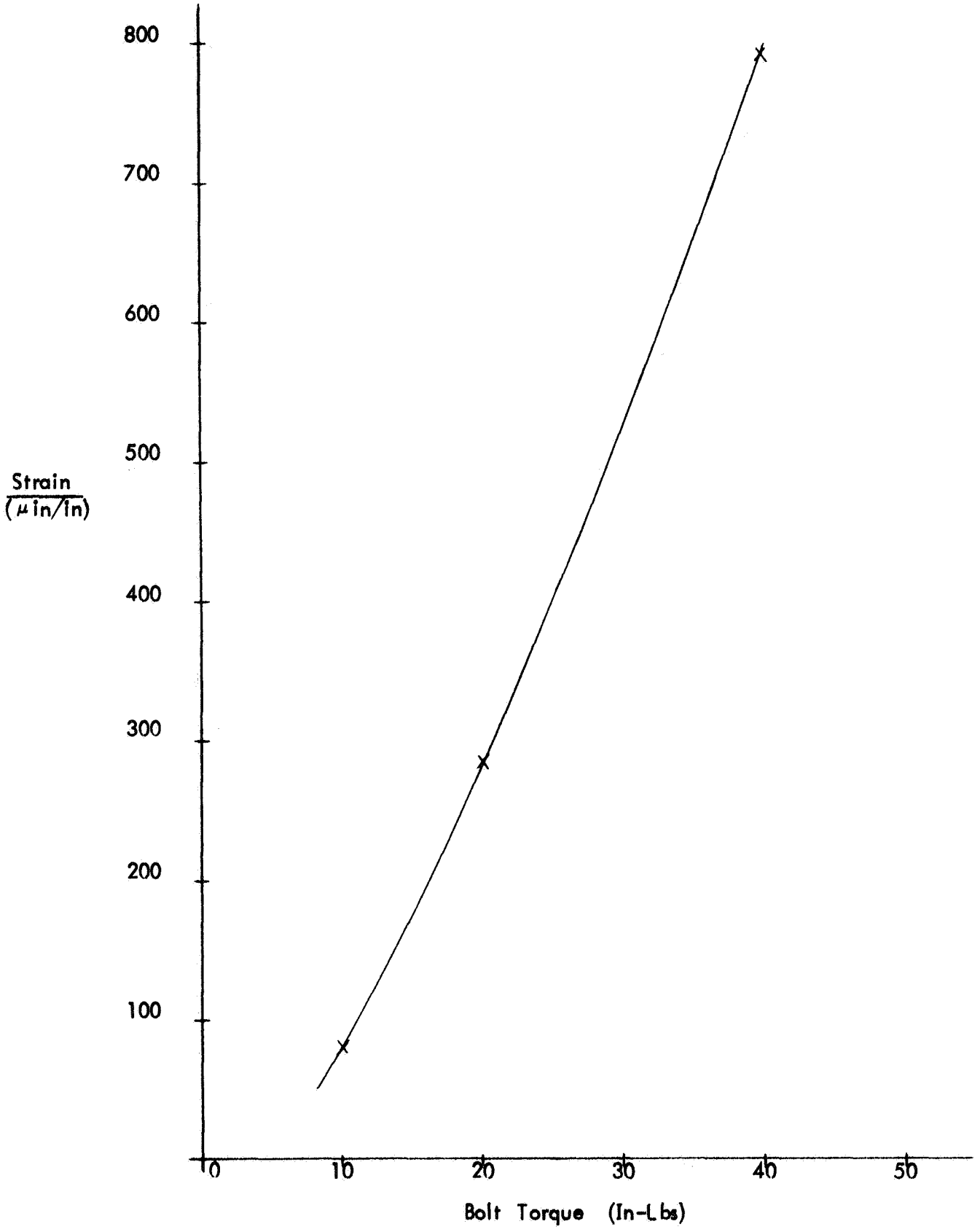


FIGURE 21. FLANGE STRAIN VS BOLT TORQUE - GAGE NO 20

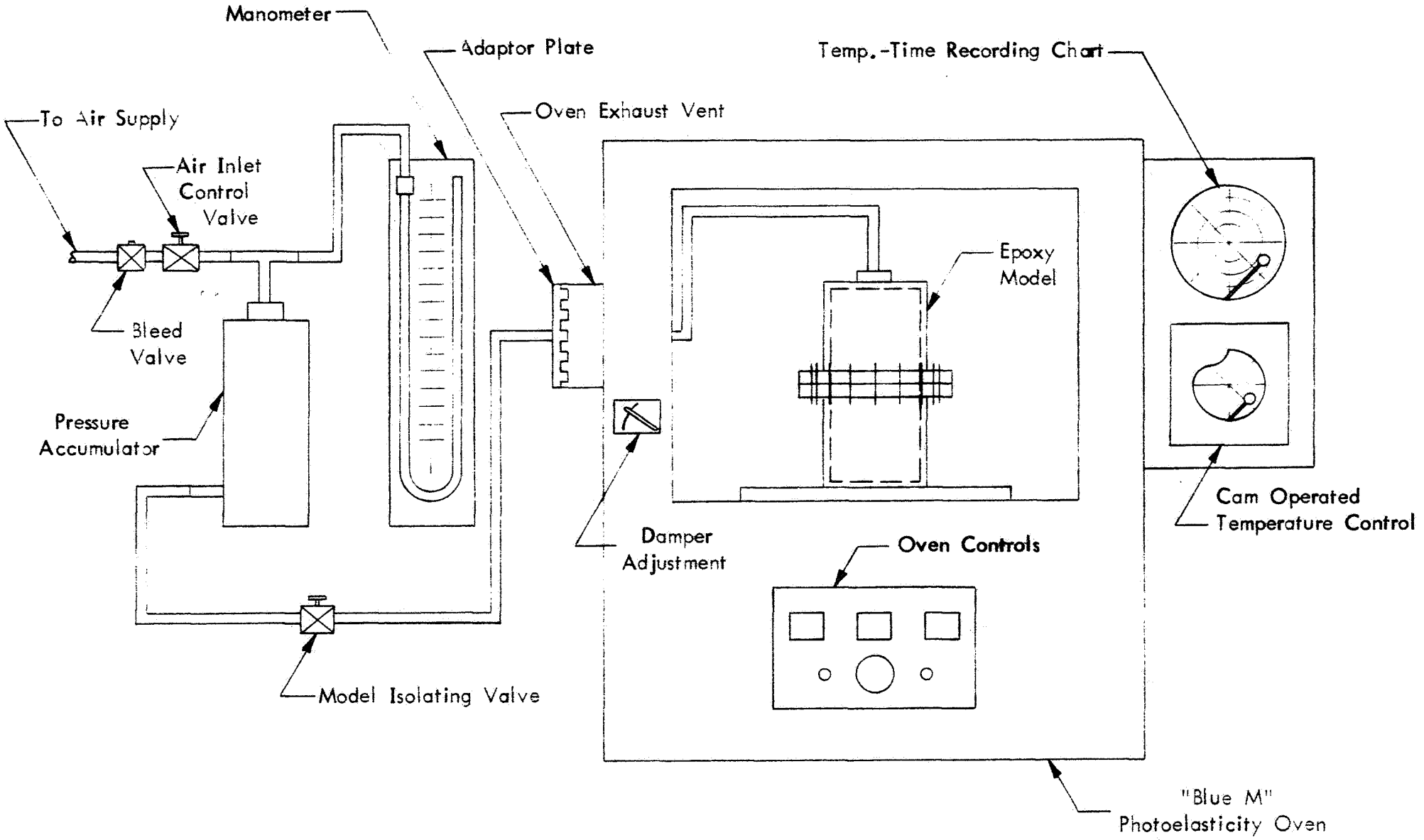


FIGURE 22. GENERAL ARRANGEMENT OF TEST APPARATUS FOR STRESS FREEZING

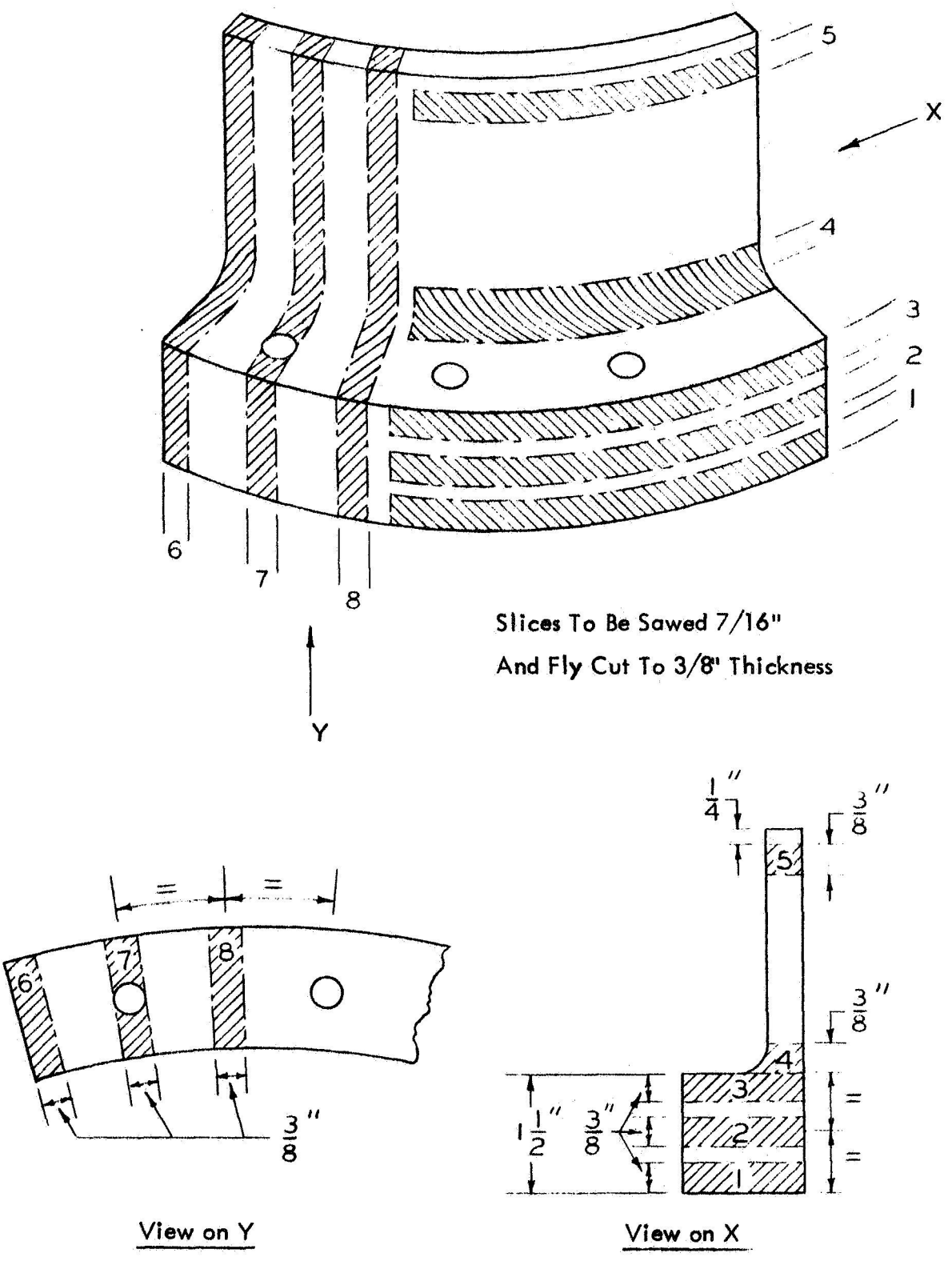


FIGURE 23. LOCATION OF SLICES REMOVED FOR ANALYSIS

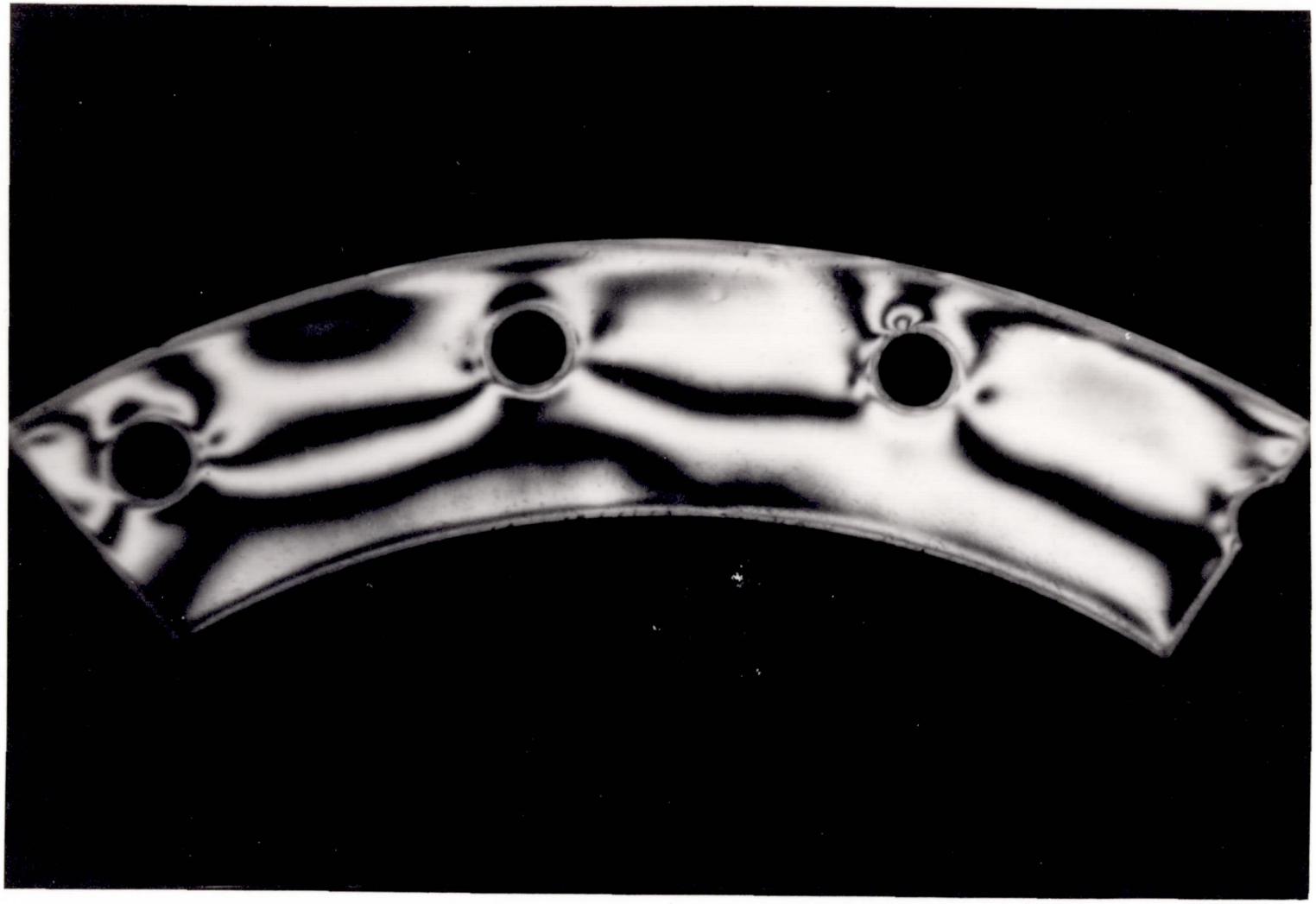

FIGURE 24. ISOCHROMATIC FRINGE PATTERN FOR SLICE NO. 1

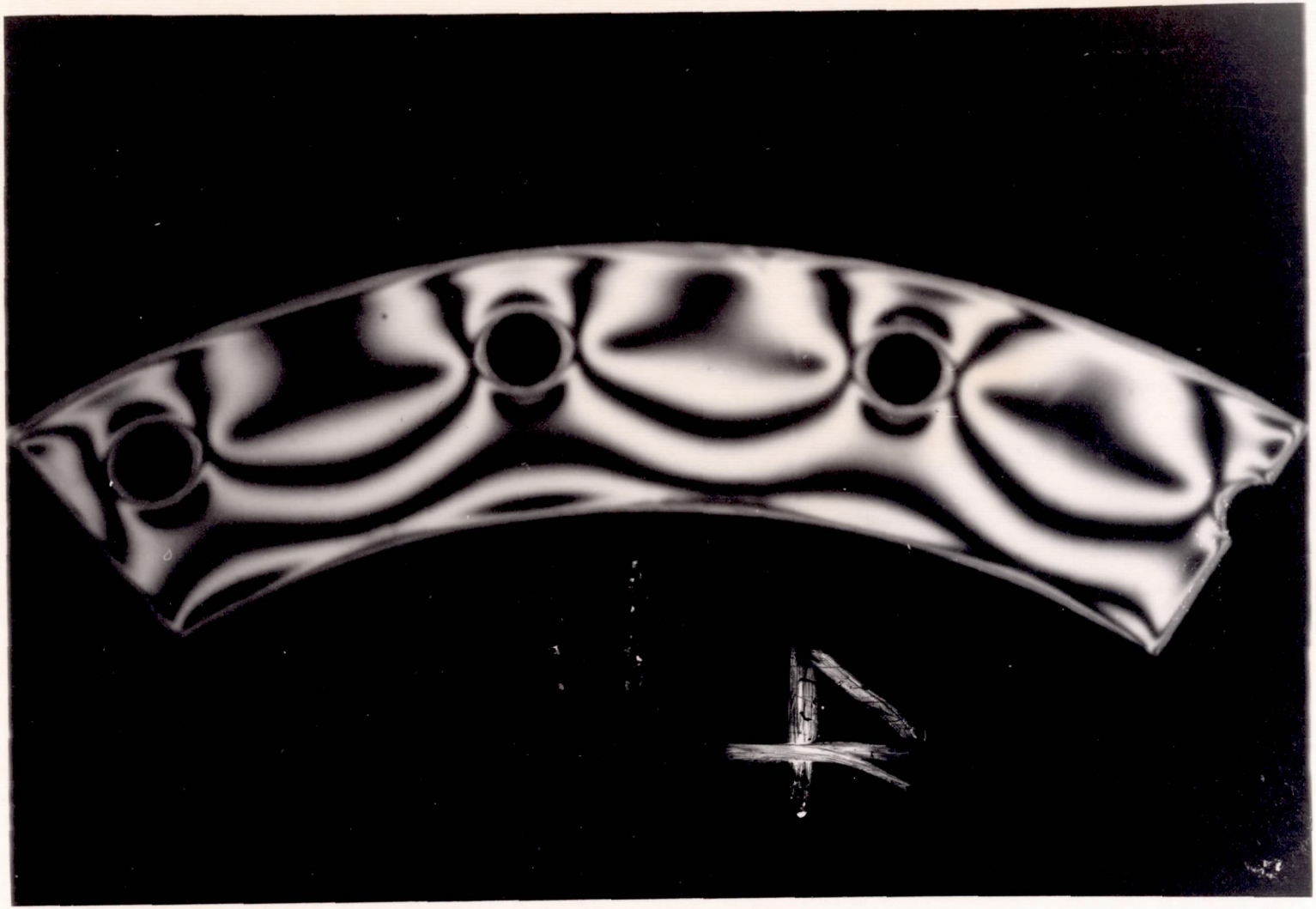

FIGURE 25. ISOCHROMATIC FRINGE PATTERN FOR SLICE NO. 2

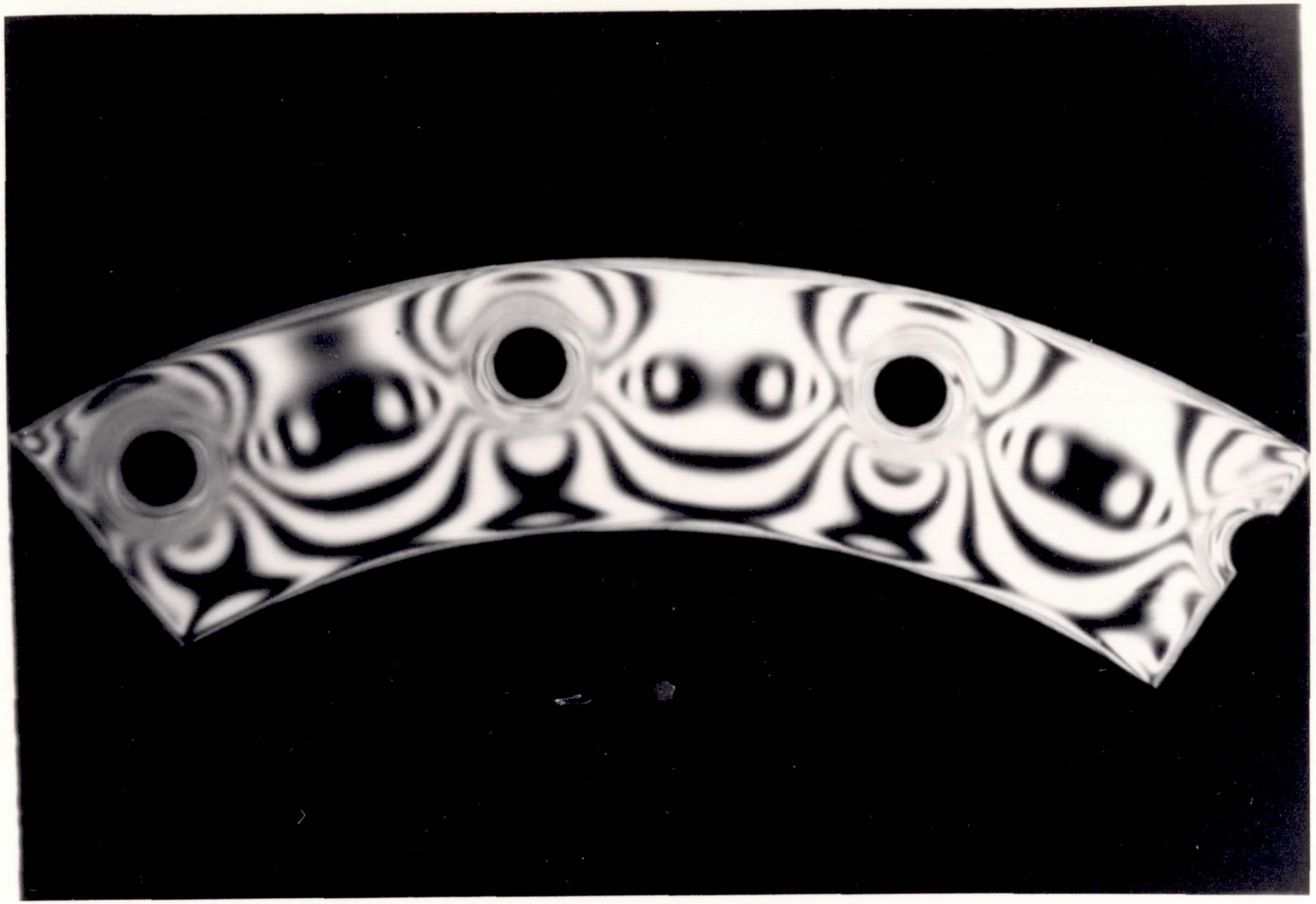

FIGURE 26. ISOCHROMATIC FRINGE PATTERN FOR SLICE NO. 3

FIGURE 27. ISOCHROMATIC FRINGE PATTERN FOR SLICE NO. 8

FIGURE 28. ISOCHROMATIC FRINGE PATTERN FOR SLICE NO. 7

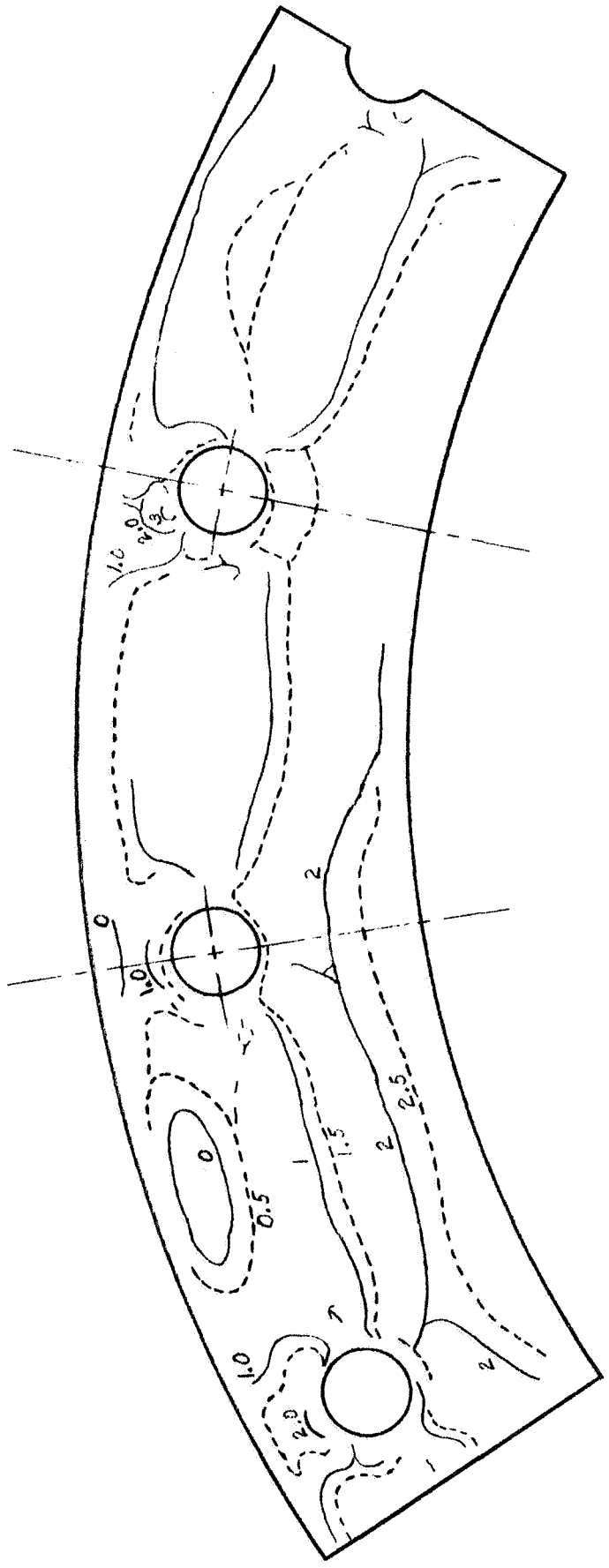


FIGURE 29. SLICE NO. 1 — ISOCHROMATICS

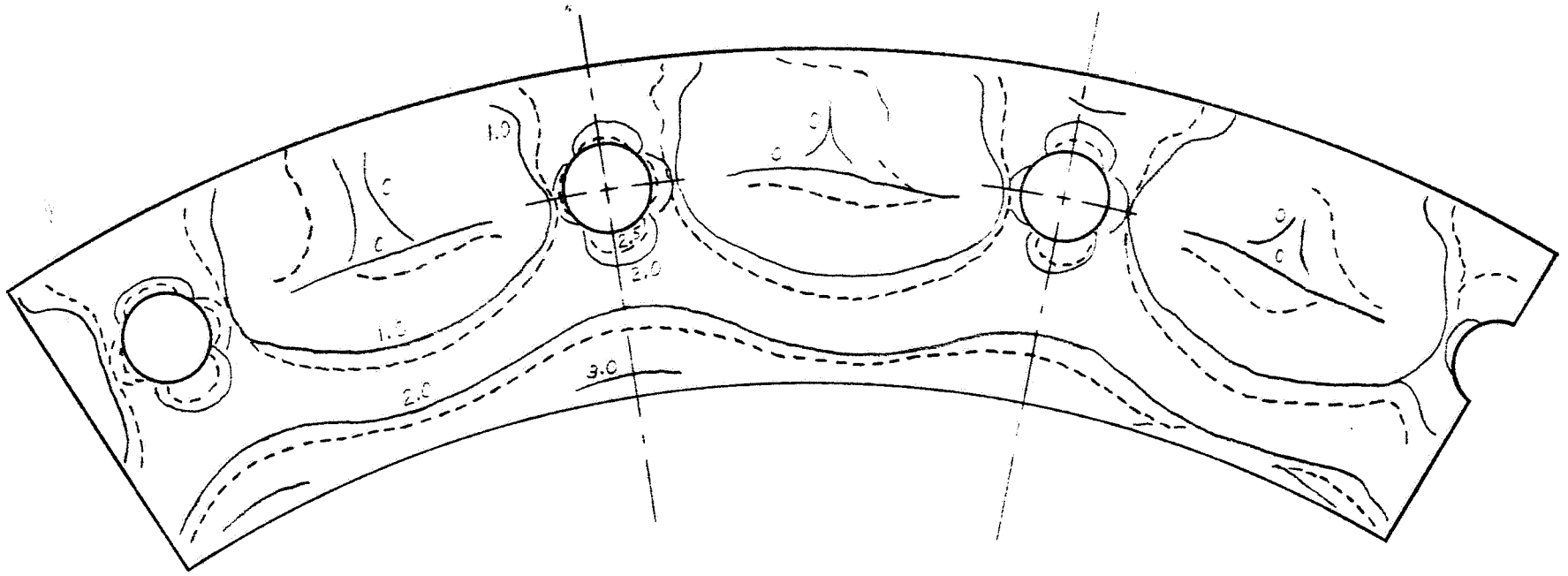


FIGURE 30. SLICE NO. 2 — ISOCHROMATICS

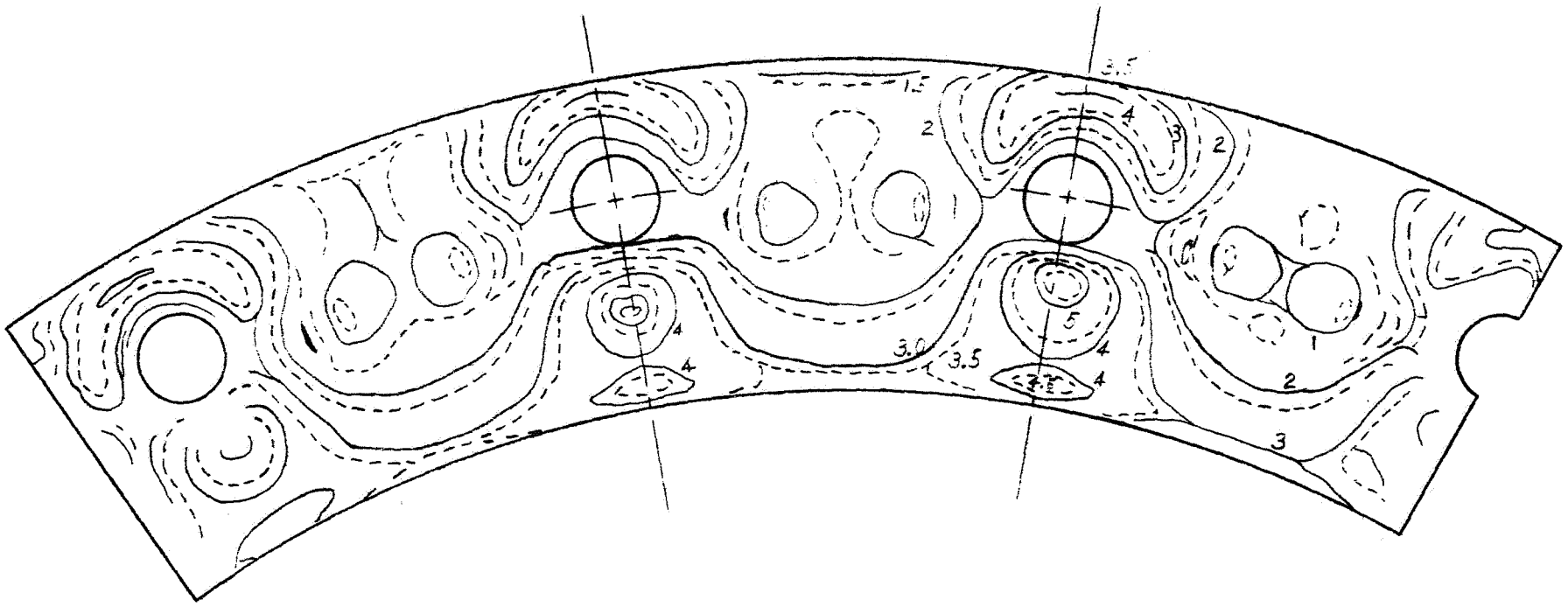


FIGURE 31. SLICE NO. 3 — ISOCHROMATICS

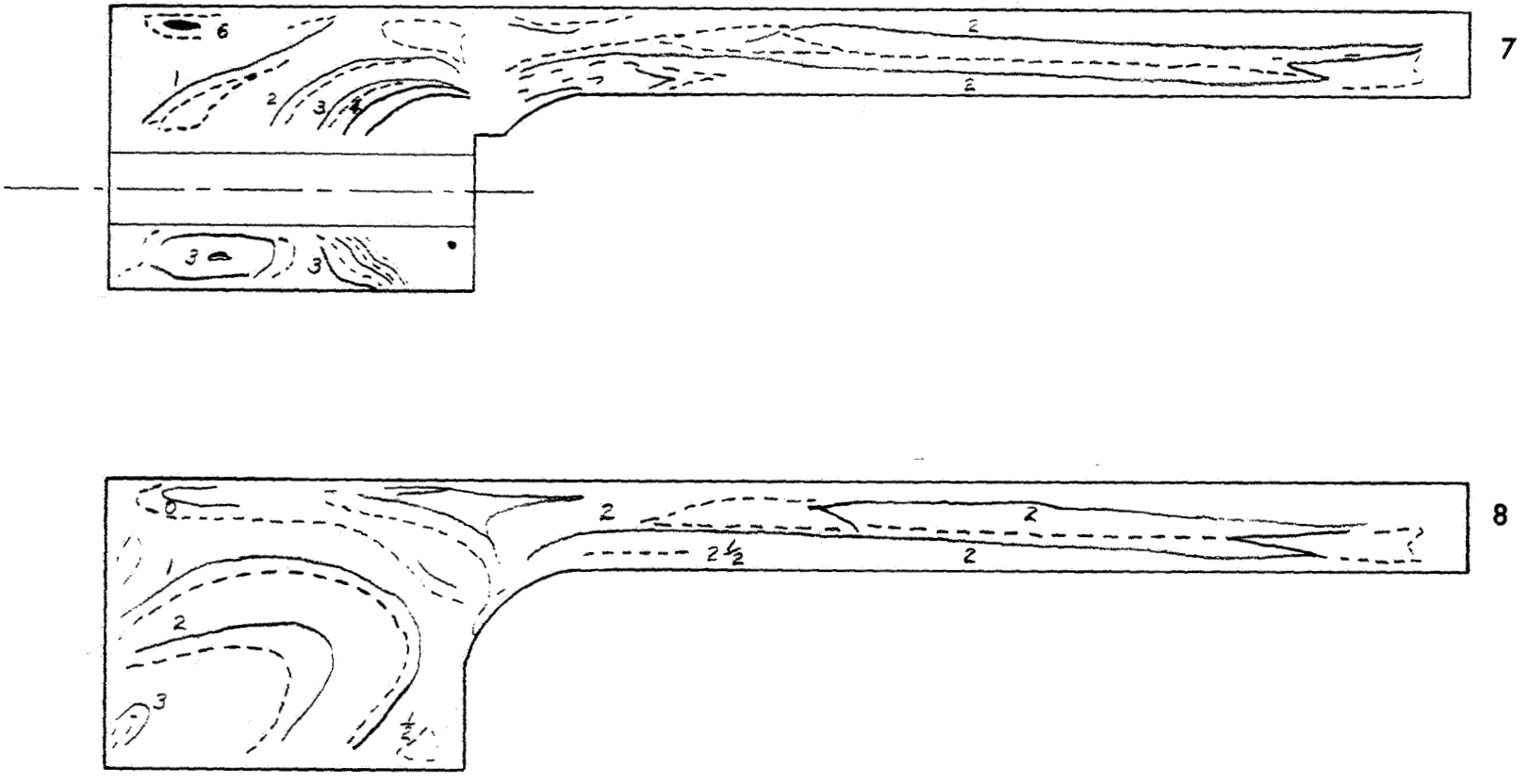


FIGURE 32. SLICES NO. 7 & 8—ISOCHROMATICS

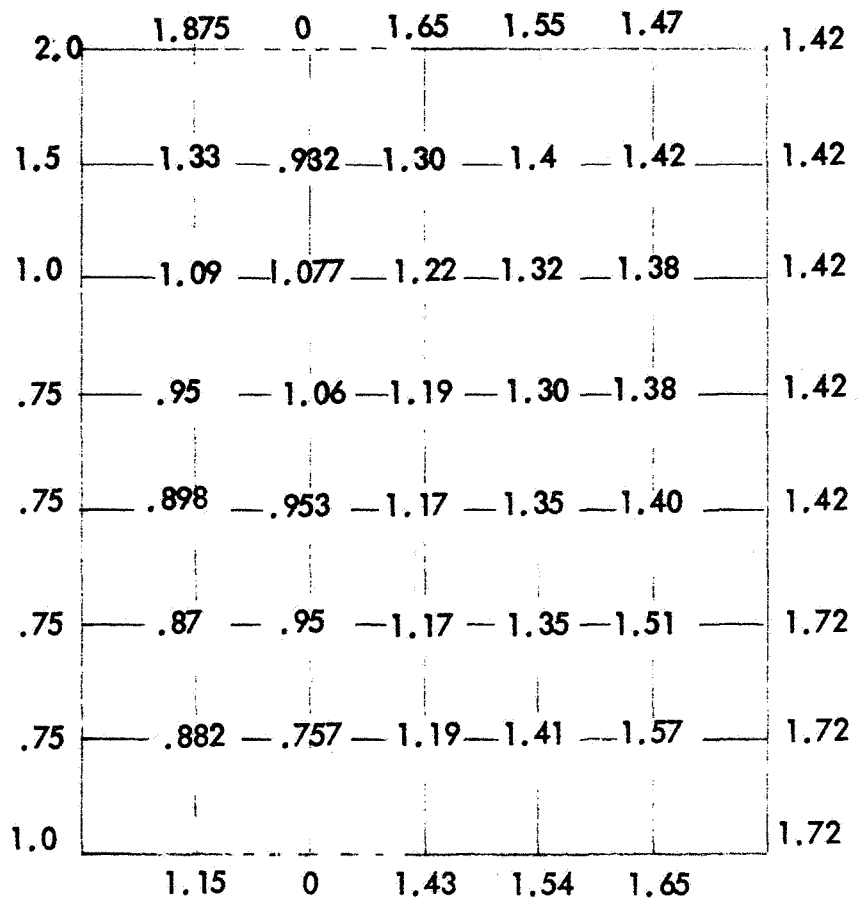


(p +q) Fringes

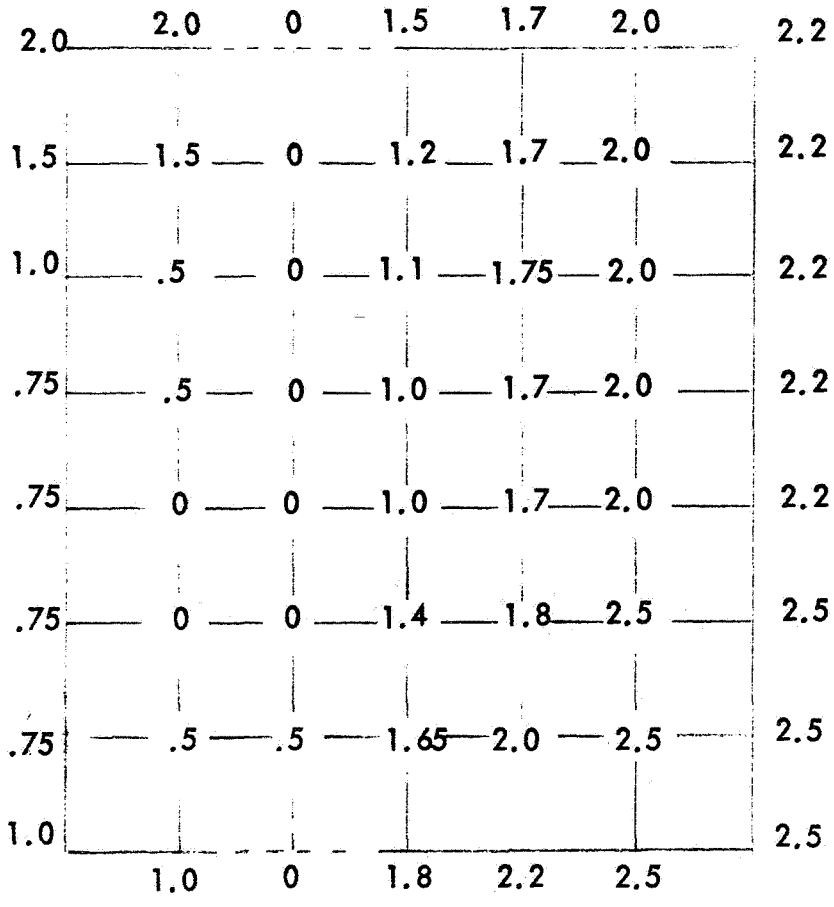


(p – q) Fringes



FIGURE 33. PHOTOELASTIC EVALUATION OF SLICE NO. 1

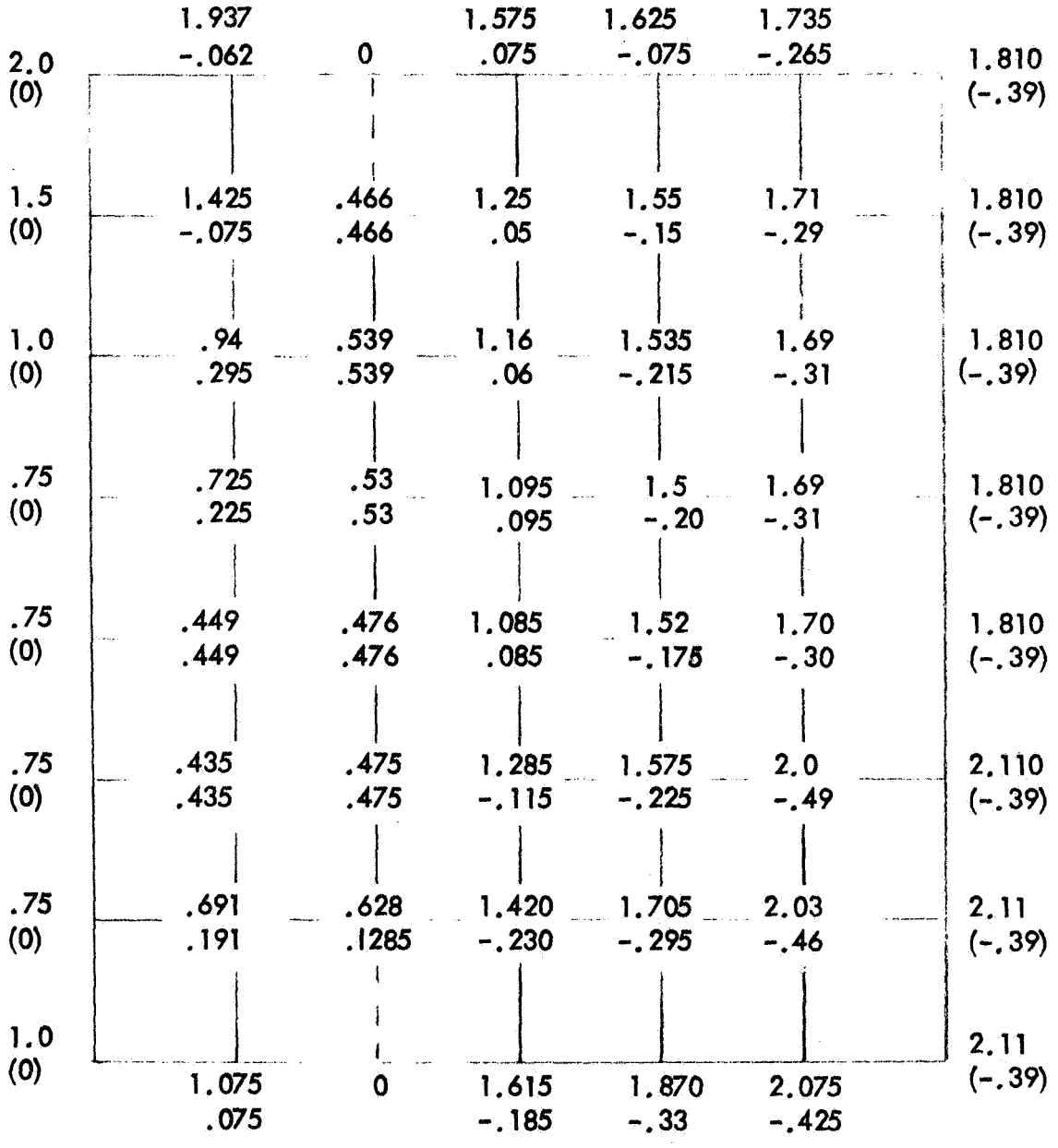


FIGURE 34. SEPARATED STRESSES (FRINGES) FOR SLICE NO. 1

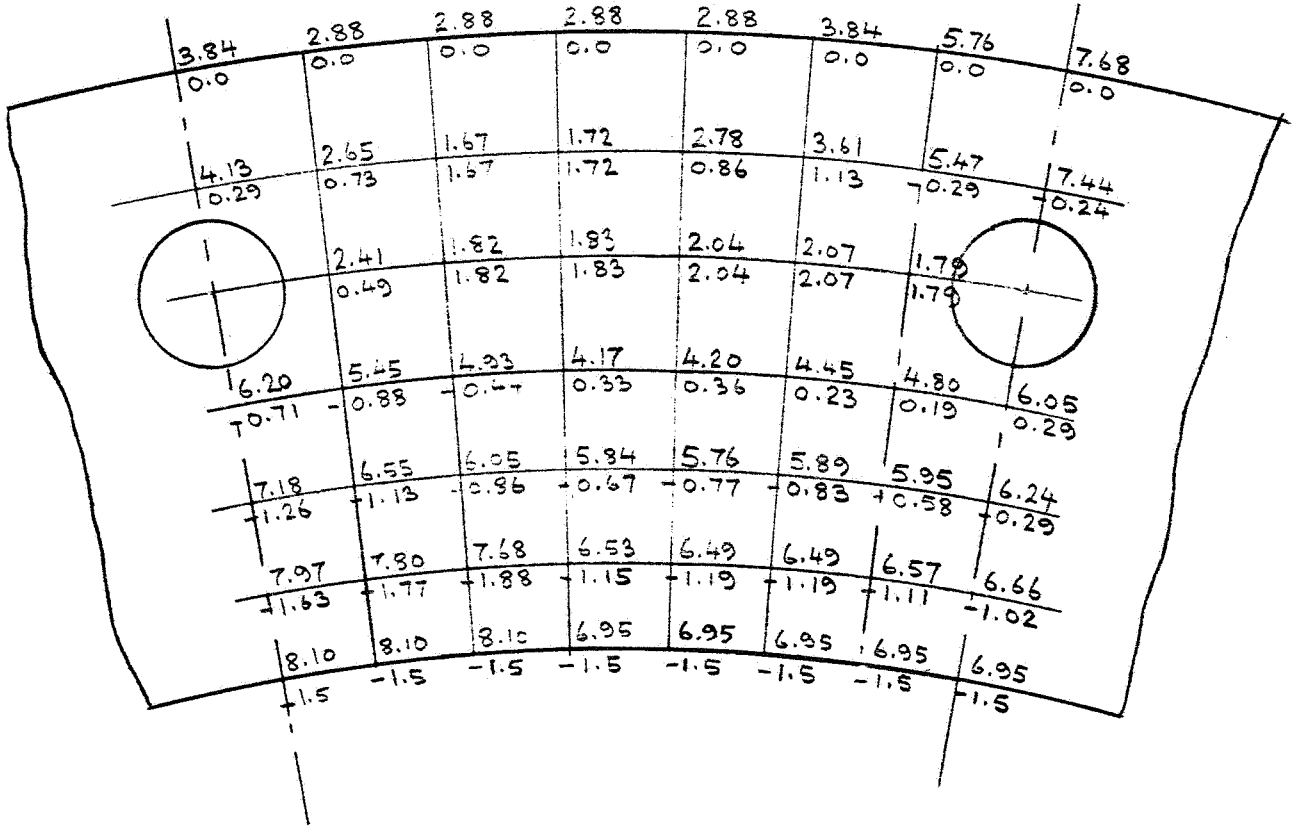


FIGURE 35. SECONDARY PRINCIPAL STRESSES FOR SLICE NO. 1

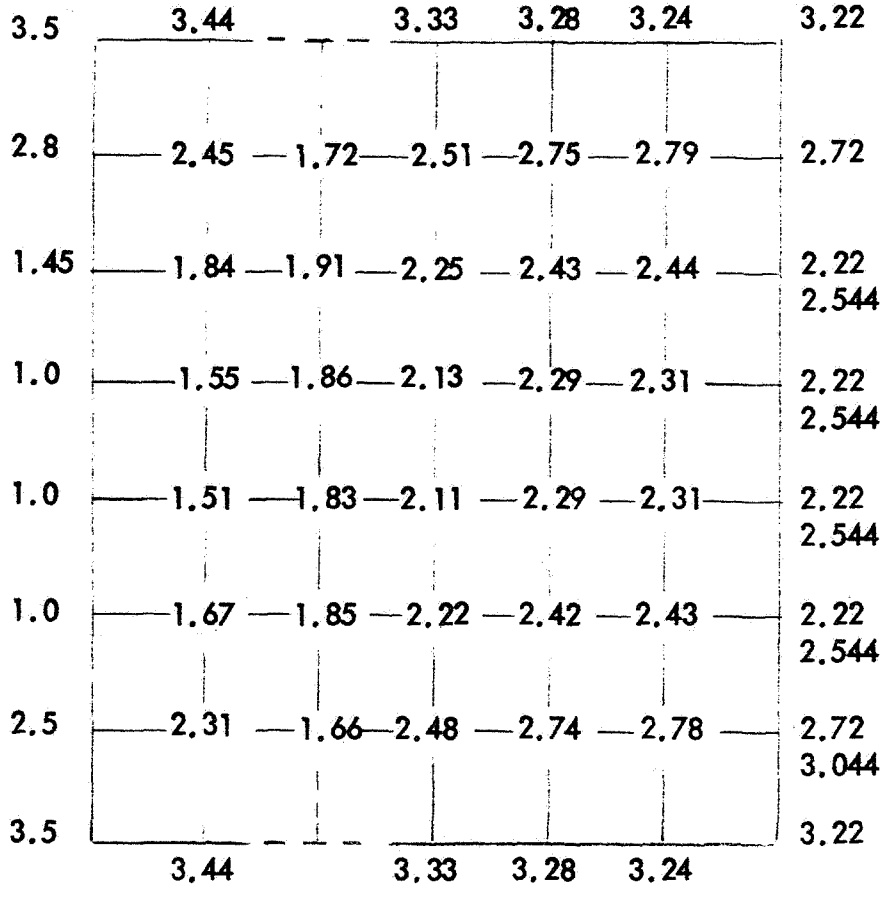


(p + q) Fringes

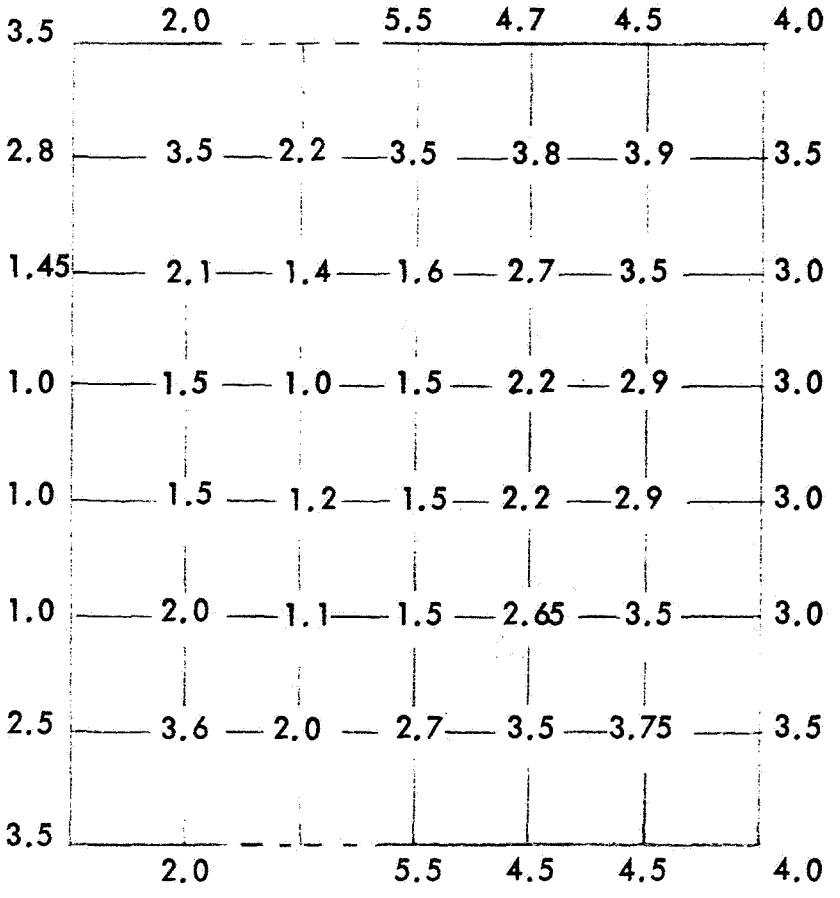


(p - q) Fringes



FIGURE 36. PHOTOELASTIC EVALUATION OF SLICE NO. 3

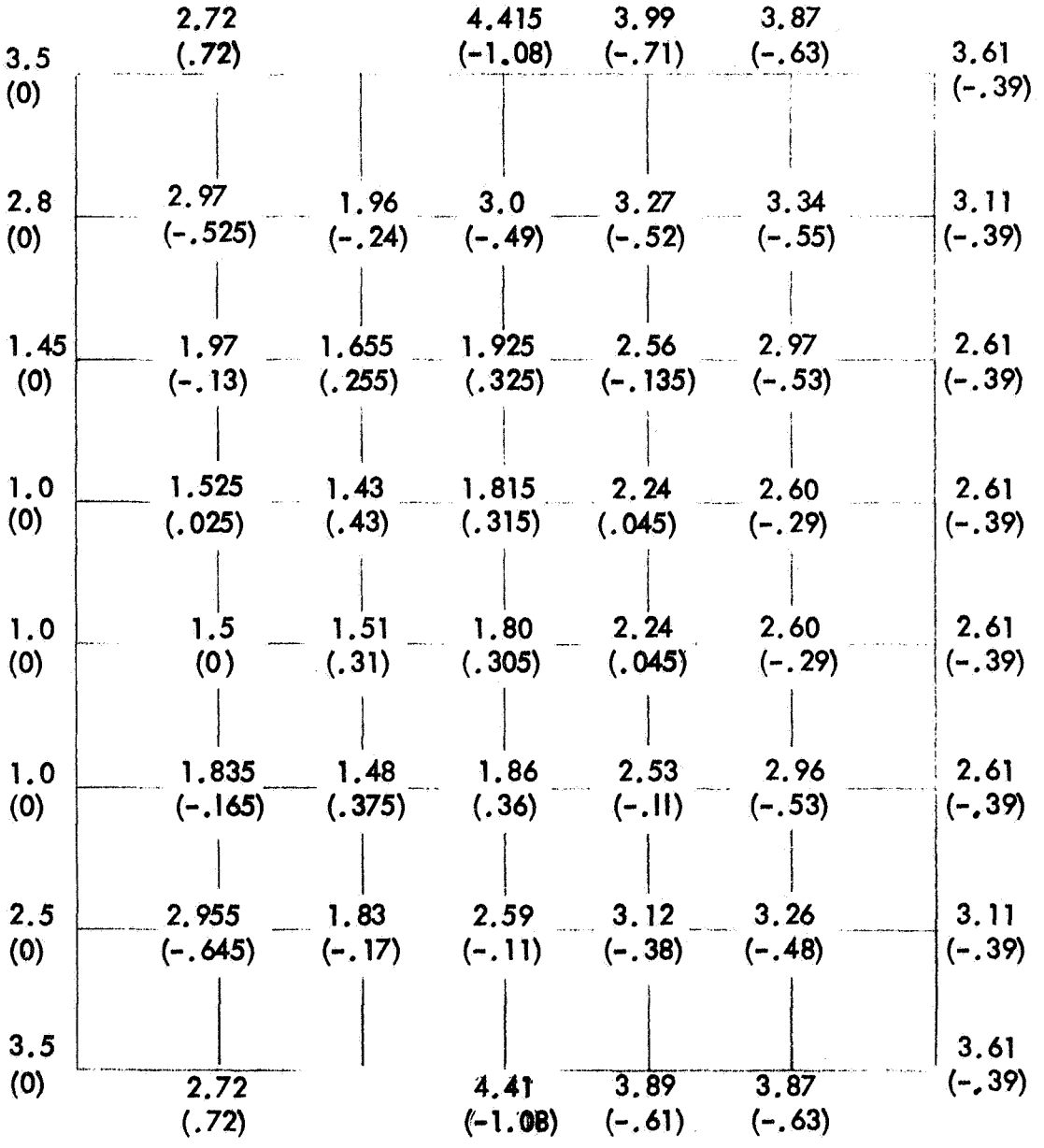


FIGURE 37. SEPARATED STRESSES (FRINGES) FOR SLICE NO. 3

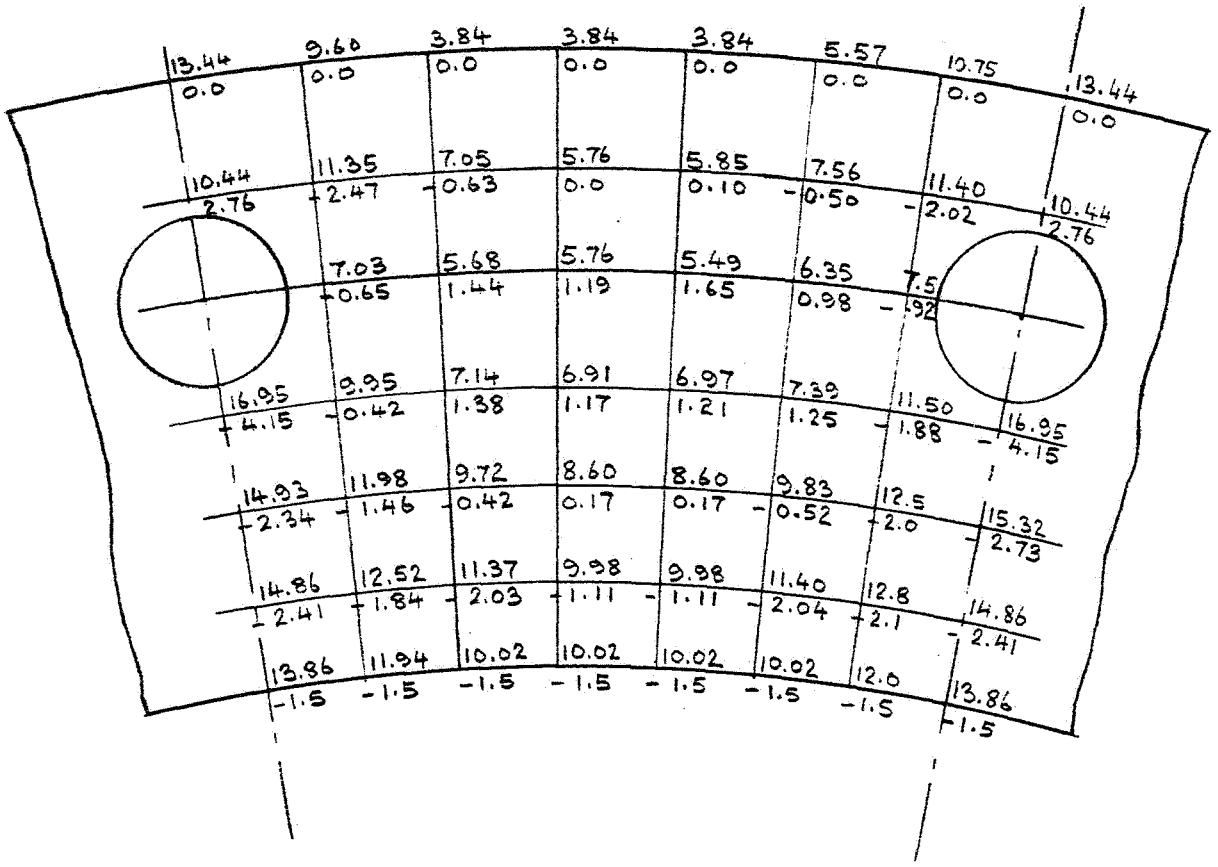


FIGURE 38. SECONDARY PRINCIPAL STRESSES FOR SLICE NO. 3

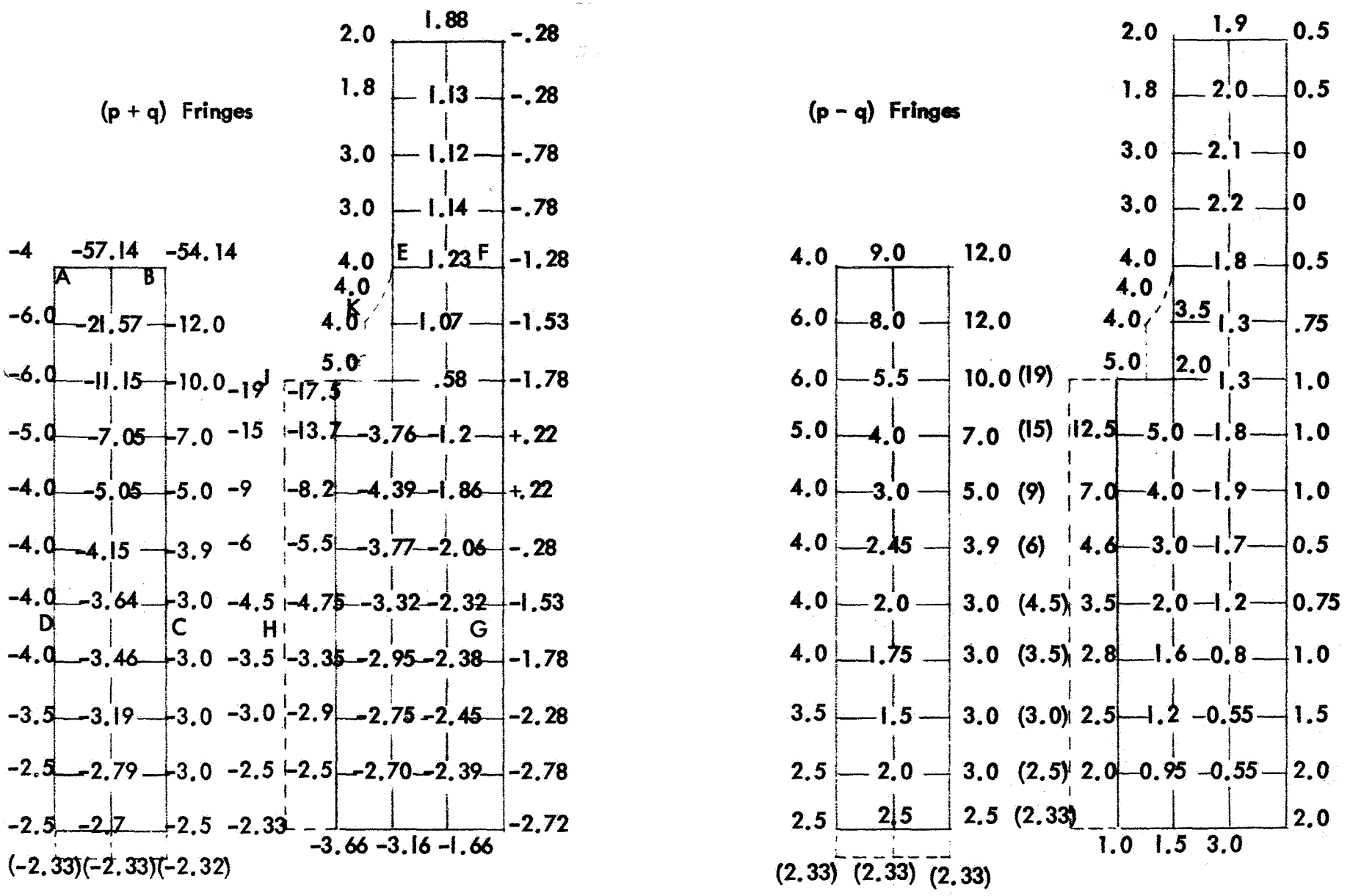


FIGURE 39. PHOTOELASTIC EVALUATION OF SLICE NO. 7

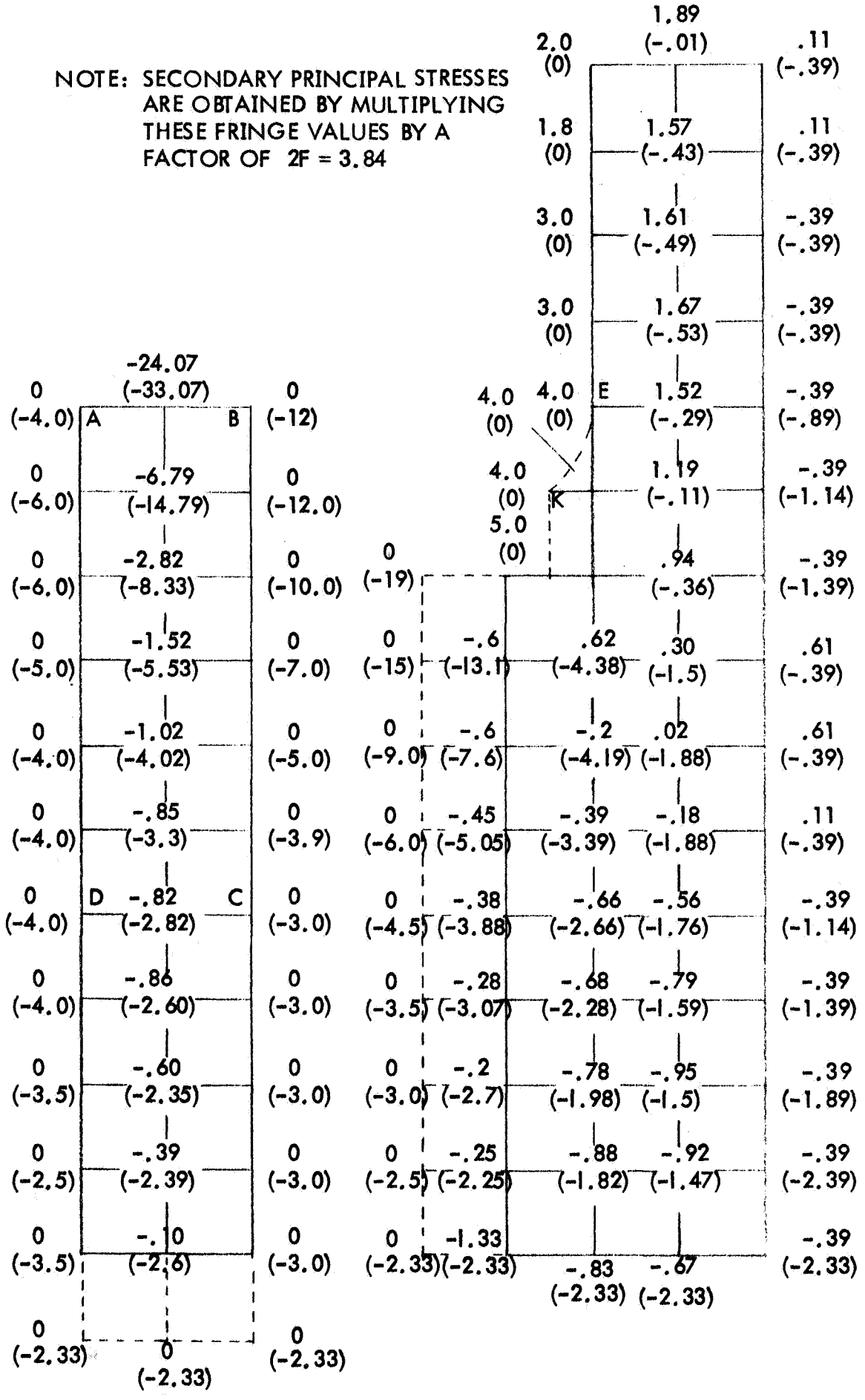


FIGURE 40. SEPARATED STRESSES (FRINGES) FOR SLICE NO. 7

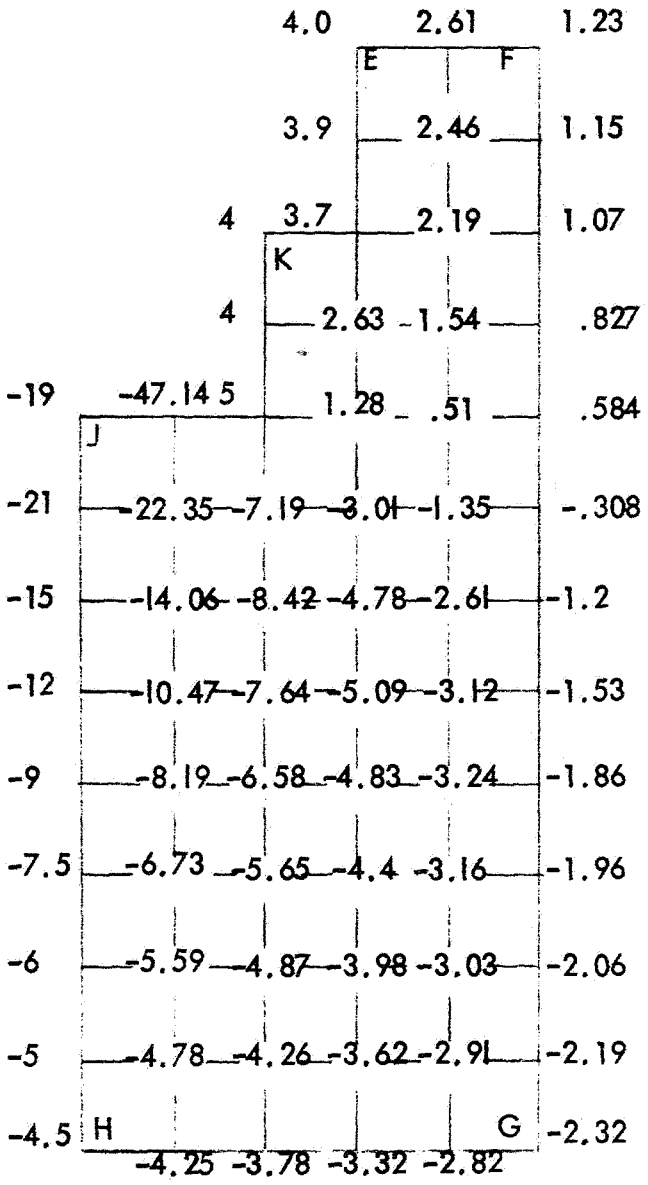


(p + q) Fringes

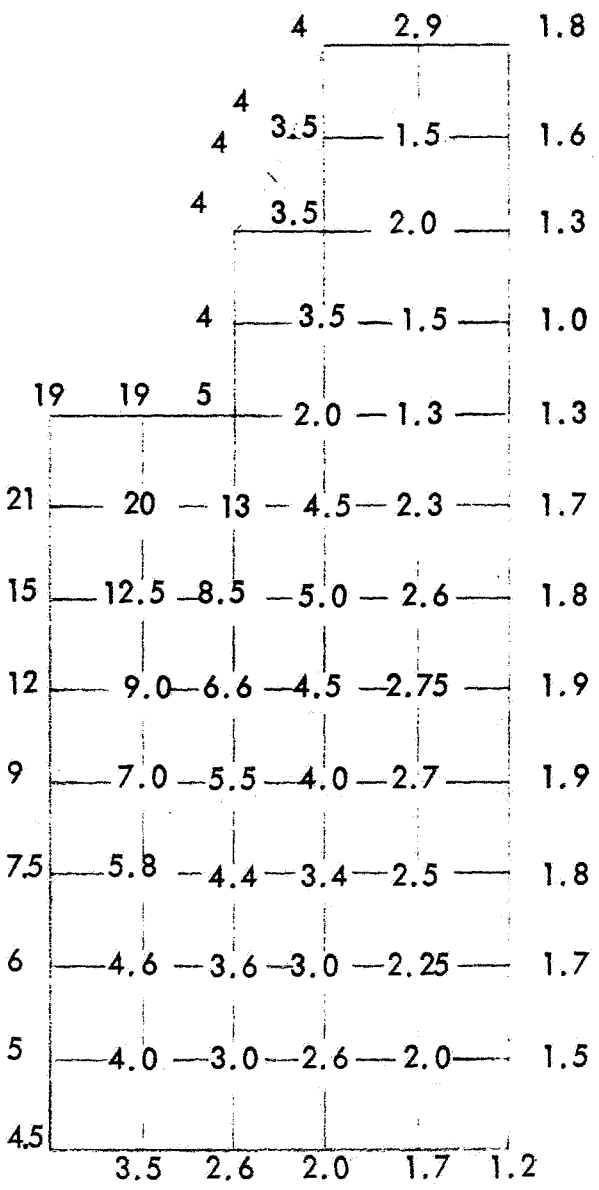


(p - q) Fringes

FIGURE 41. PHOTOELASTIC EVALUATION OF AREA EFGHJK OF SLICE NO. 7 USING FINE GRID

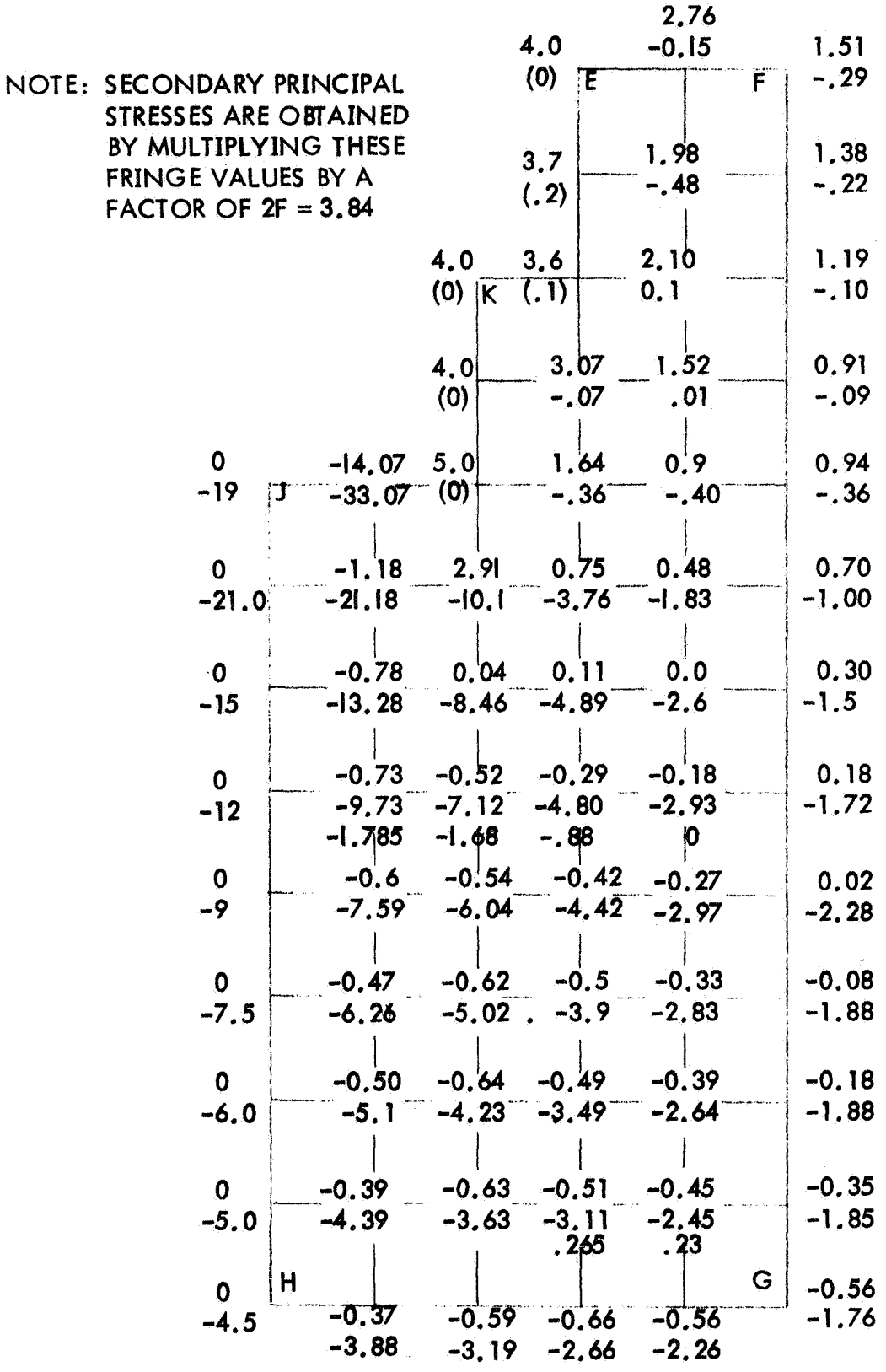


FIGURE 42. SEPARATED STRESSES (FRINGES) FOR AREA EFGHJK OF SLICE NO. 7

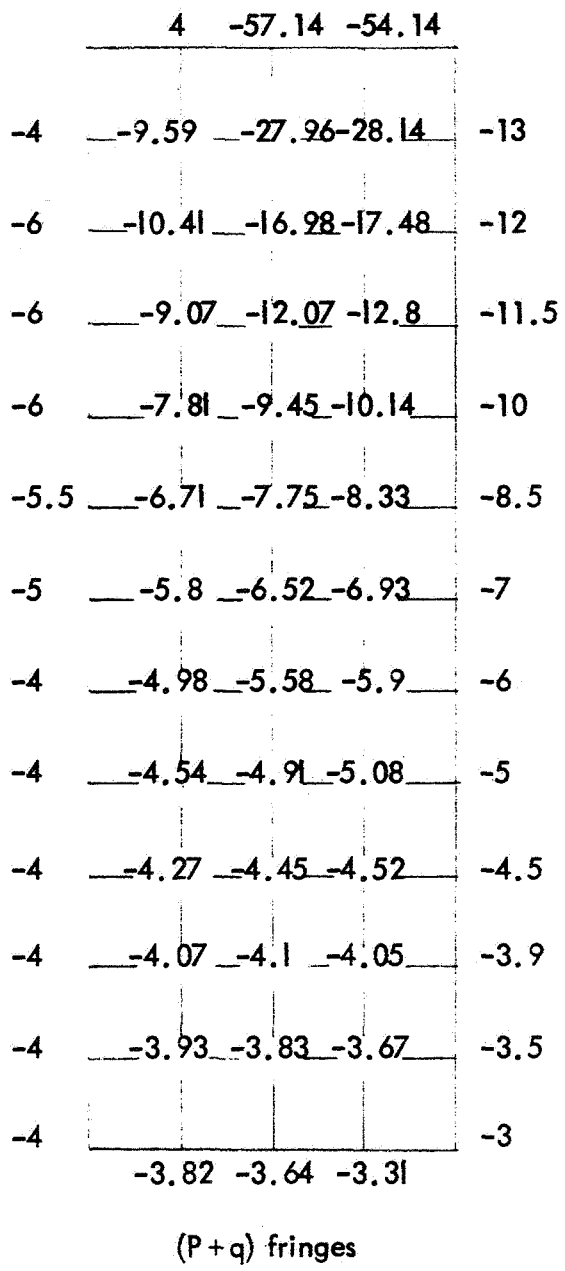


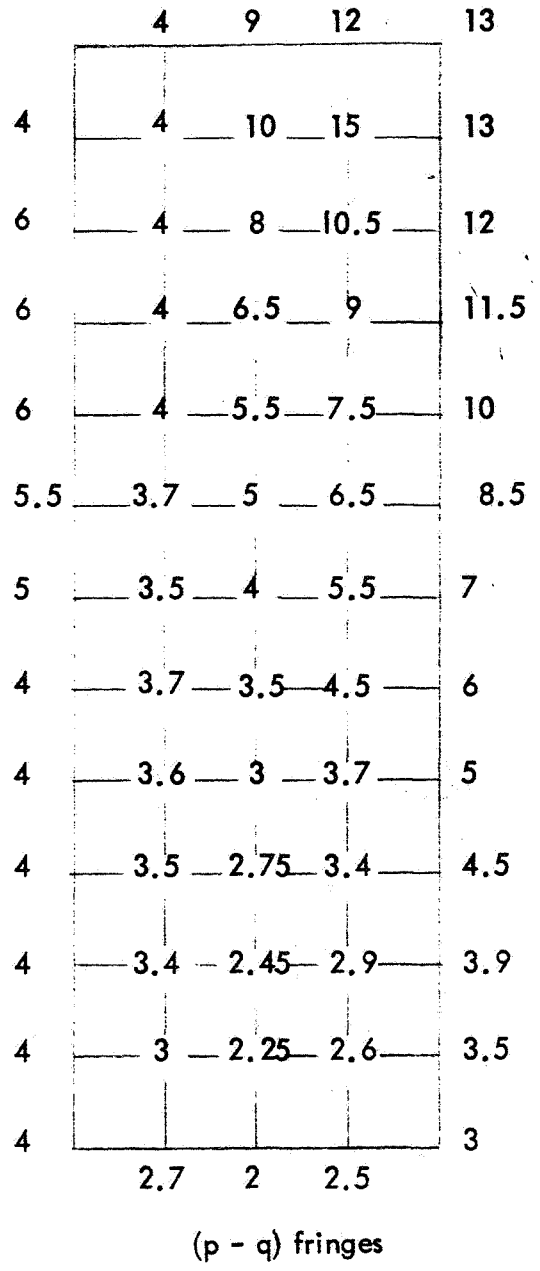


FIGURE 43. PHOTOELASTIC EVALUATION OF AREA ABCD OF SLICE NO. 7 USING FINE GRID

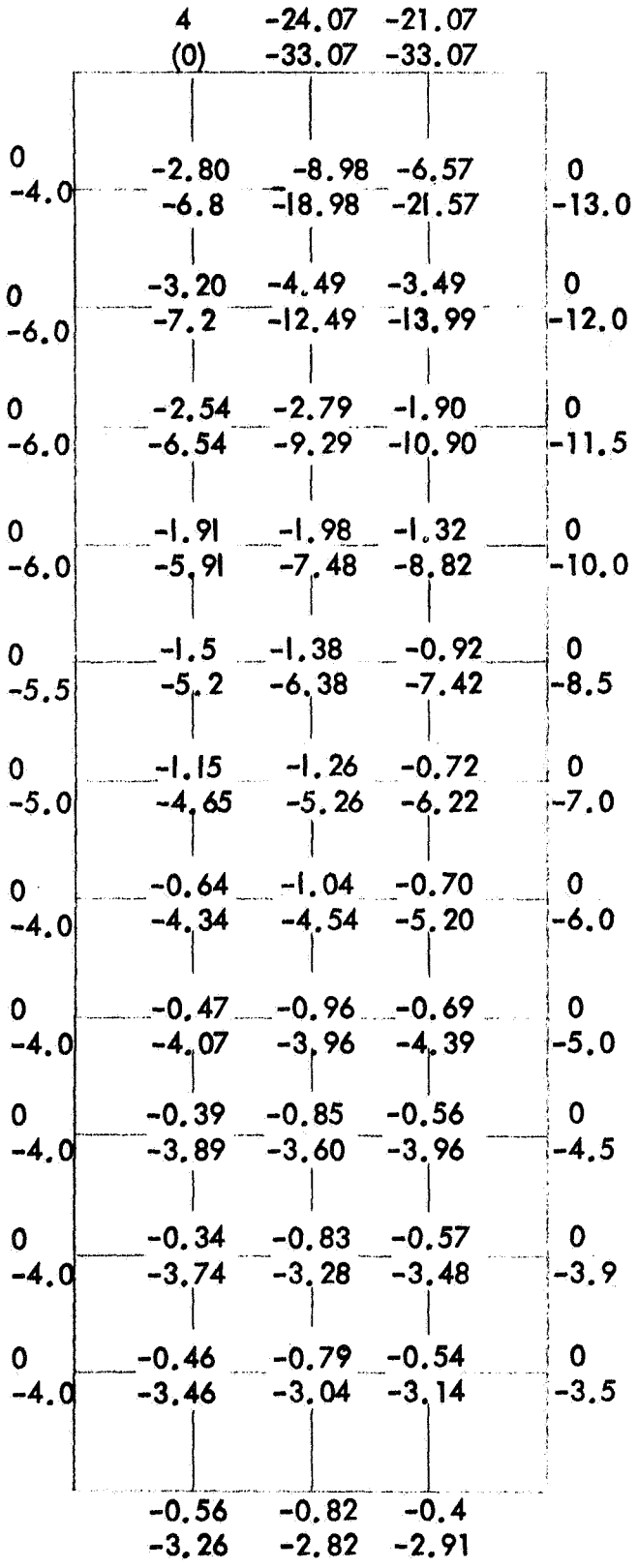


NOTE: SECONDARY PRINCIPAL STRESSES ARE OBTAINED BY MULTIPLYING THESE FRINGE VALUES BY A FACTOR OF 2F = 3.84

FIGURE 44. SEPARATED STRESSES (FRINGES) FOR AREA ABCD OF SLICE NO. 7

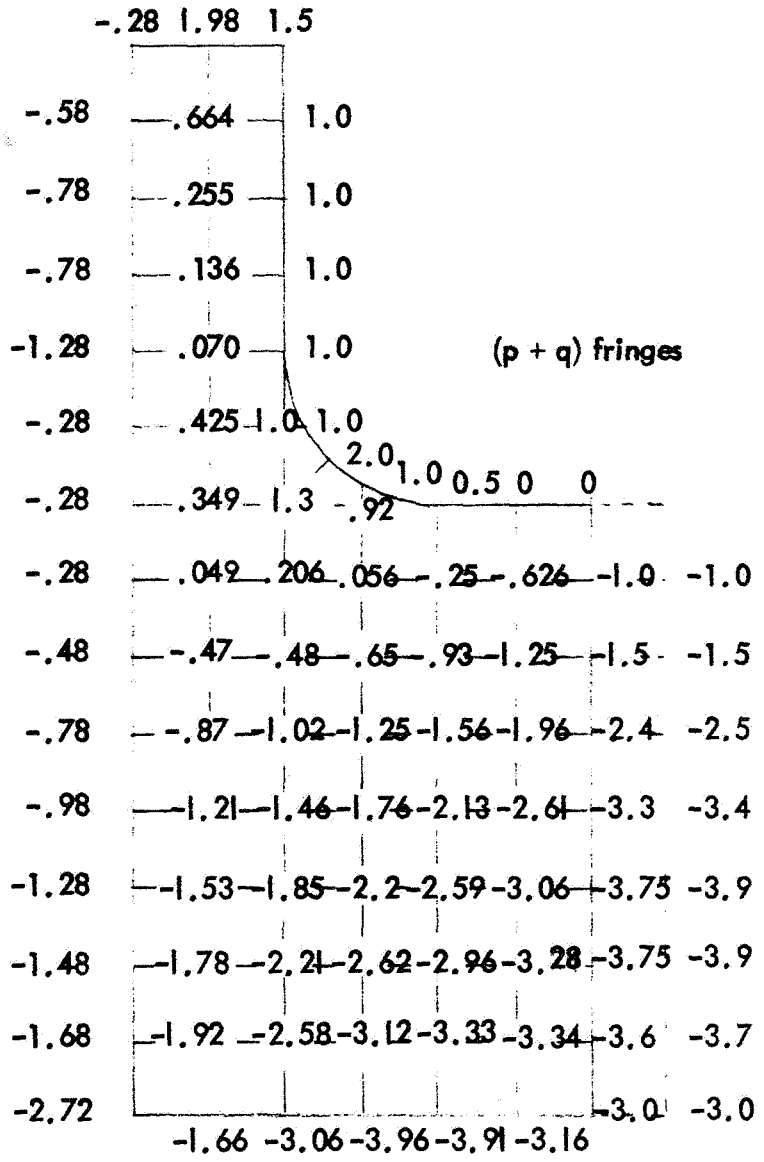


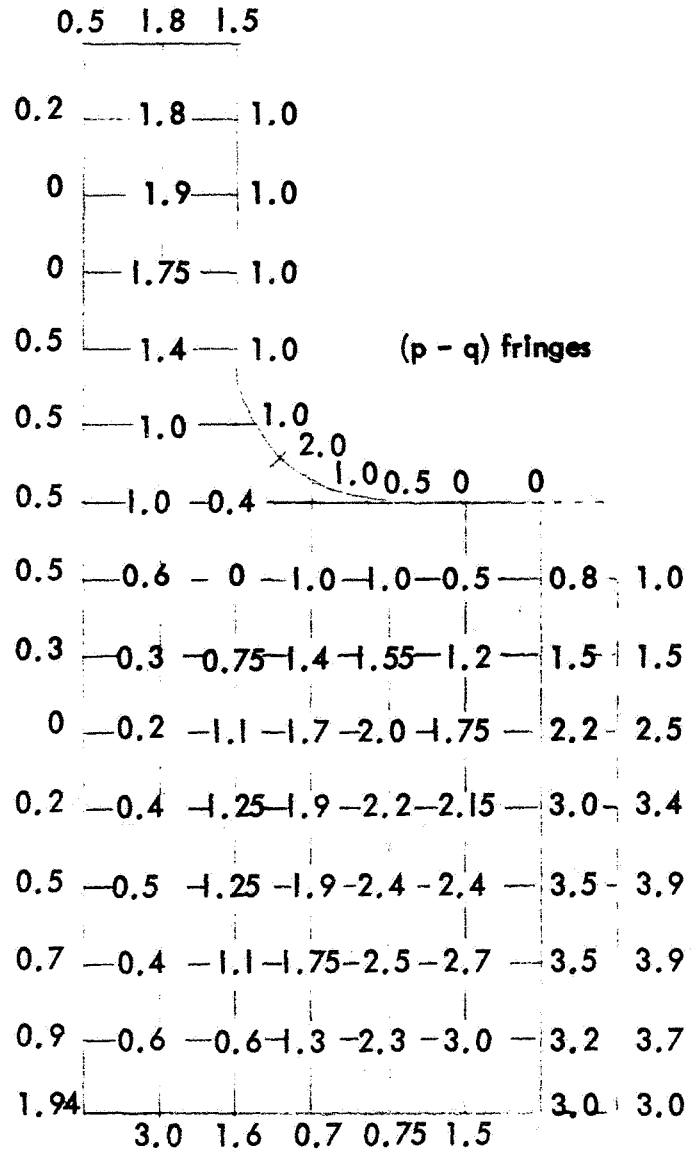


FIGURE 45. PHOTOELASTIC EVALUATION OF SLICE NO. 8

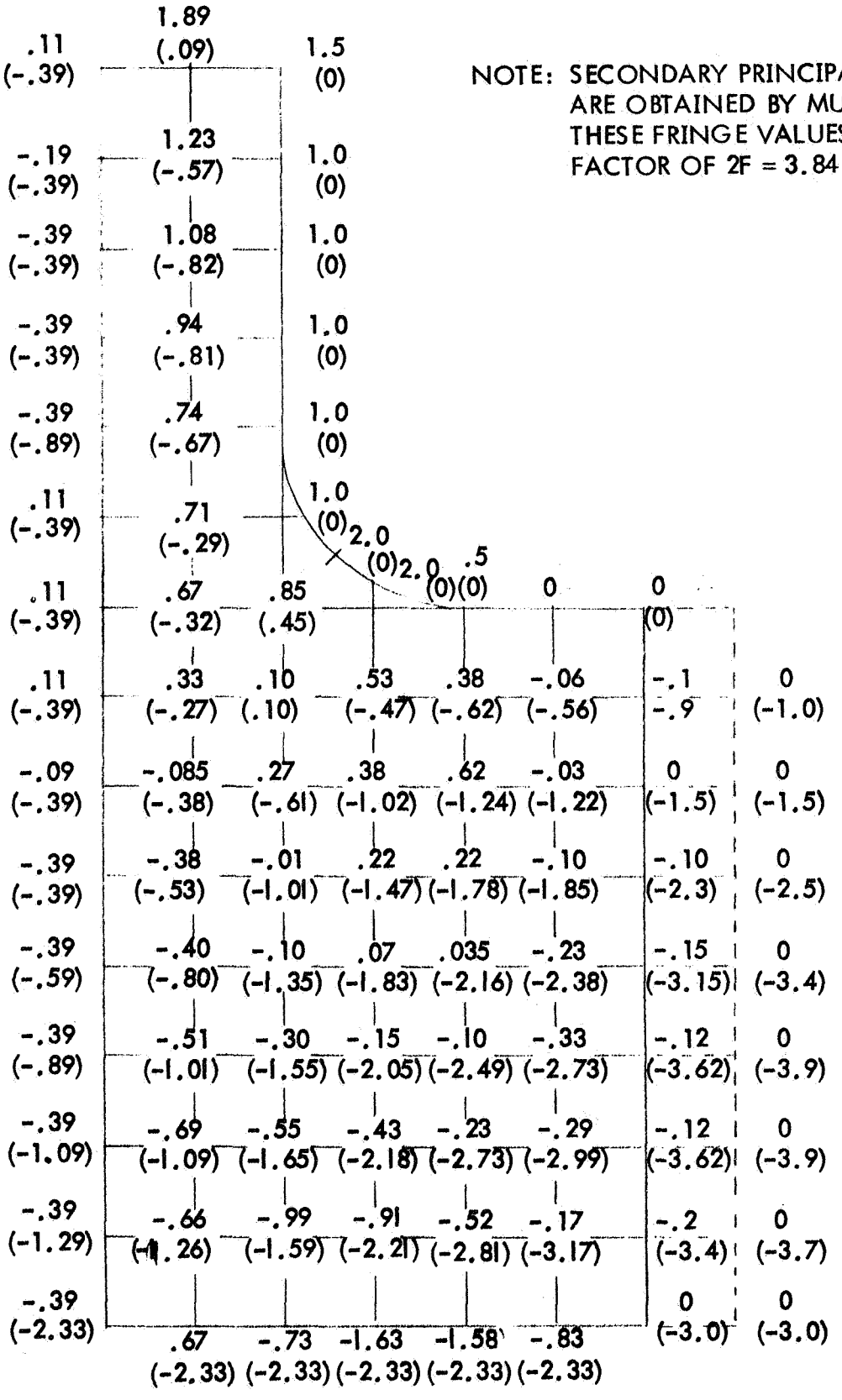


FIGURE 46. SEPARATED STRESSES (FRINGES) FOR SLICE NO. 8

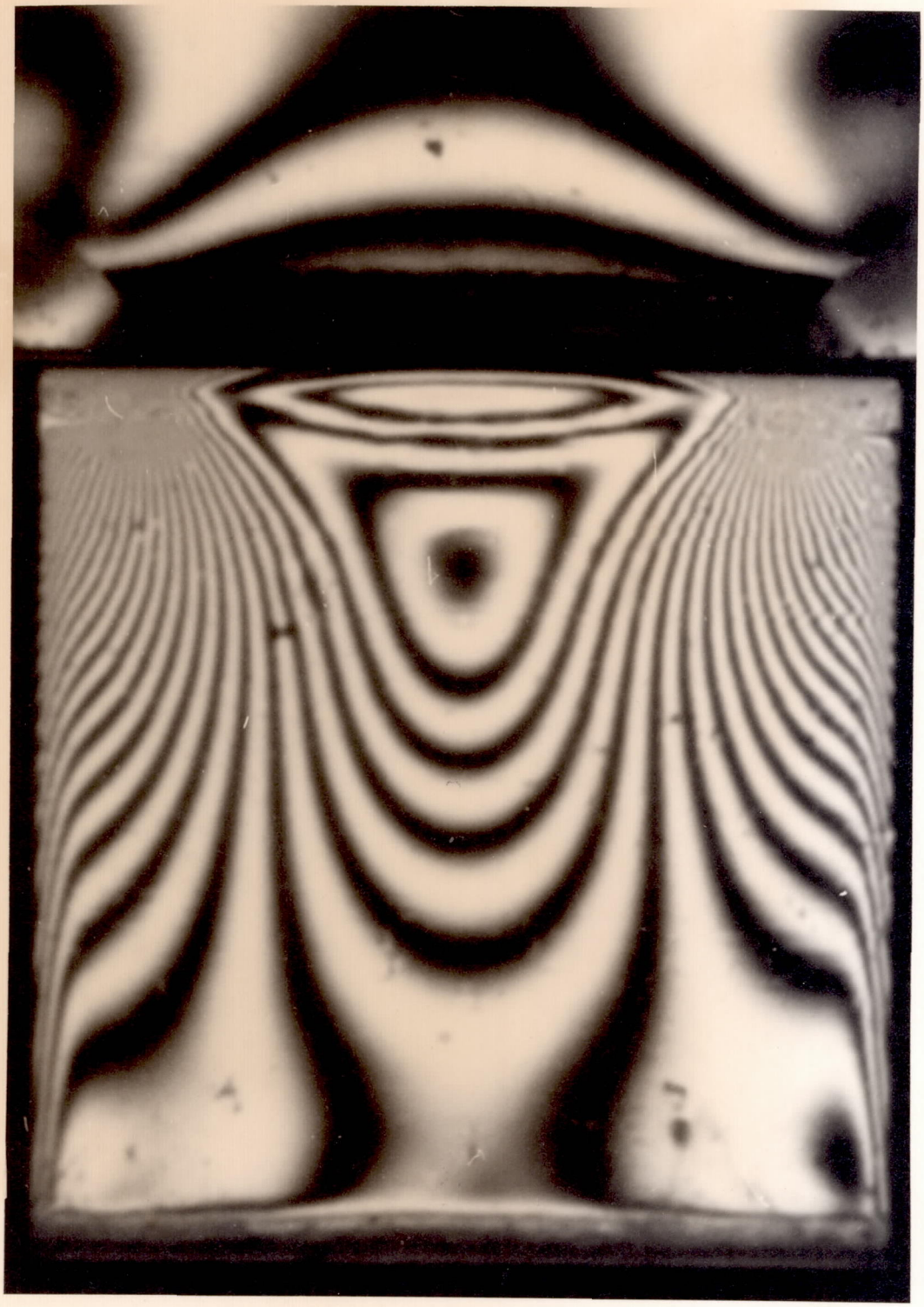

FIGURE 47. RADIAL VIEW OF FLANGE SHOWING ISOCHROMATICS